Fatigue crack growth in Aluminium Alloys

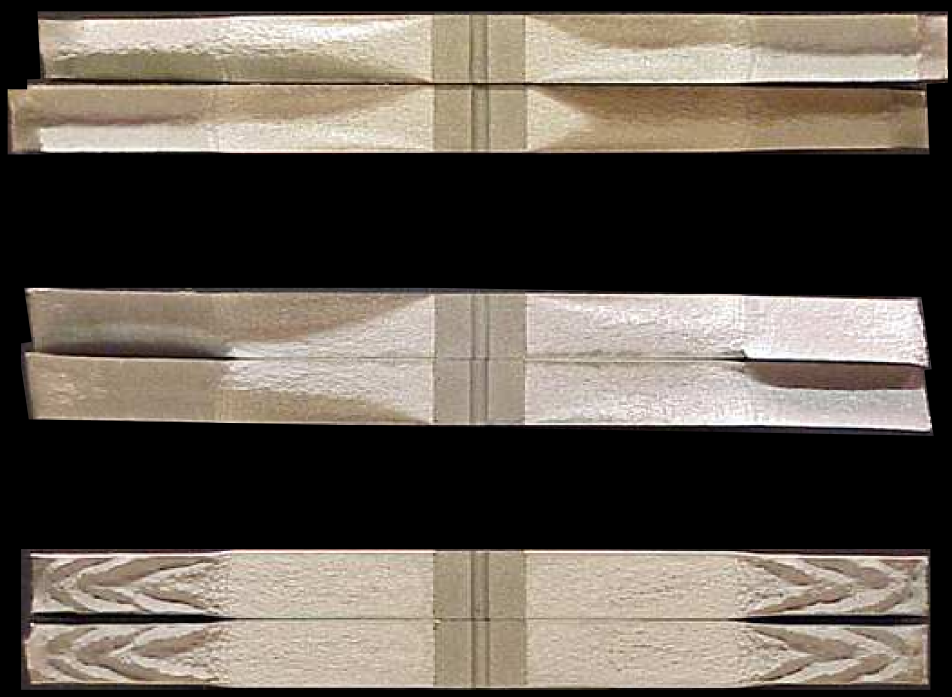

C. van Kranenburg

Cover: The effect of side grooves on shear lip development:
normal shear lip development (above)
suppressed on one side (in the middle)
suppressed on both sides (below)

Fatigue crack growth in Aluminium Alloys

Proefschrift

ter verkrijging van de graad van doctor
aan de Technische Universiteit Delft,
op gezag van de Rector Magnificus Prof.ir. K.C.A.M. Luyben,
voorzitter van het College voor Promoties,
in het openbaar te verdedigen op 9 maart 2010 om 10.00 uur

door

Cornelis VAN KRANENBURG
bouwkundig ingenieur
geboren te Rotterdam

Dit proefschrift is goedgekeurd door de promotor:

Prof.dr. I.M. Richardson,

copromotor: Dr.ir. J. Zuidema, Technische Universiteit Delft

Samenstelling promotiecommissie:

Rector Magnificus	voorzitter
Prof.dr. I.M. Richardson	Technische Universiteit Delft, promotor
Dr.ir. J. Zuidema	Technische Universiteit Delft, copromotor
Prof.dr. A. Bakker	Technische Universiteit Delft
Prof.ir. L. Katgerman	Technische Universiteit Delft
Prof.dr. J. Rots	Technische Universiteit Delft
Prof.dr. G.P.A.G. van Zijl	Stellenbosch University, Zuid-Afrika
Dr.ir. M. Janssen	Technische Universiteit Delft

ISBN 978-90-9025170-7

Samenvatting

Vermoeiing is een geleidelijk proces van lokaal sterkteverlies. Het fenomeen wordt vaak in verband gebracht met een opeenstapeling van beschadigingen, veroorzaakt door spanningswisselingen. In metalen resulteert dit in micro-scheurtjes. Deze scheurtjes groeien onder voortdurende wisselende belastingen tot er bezwijken optreedt.

Vermoeiing is in essentie een scheurgroeiproces. De schadeopeenstapeling (de scheurgroei) begint in eerste instantie langzaam, maar het proces versnelt tot aan bezwijken. Bijna elk constructiemetaal is gevoelig voor vermoeiing.

Dit proefschrift behandelt een aantal aspecten van de vermoeiingscheurgroei in aluminium legering AA5083, van het drempelwaarde gebied tot instabiele scheurgroei.

Hoofdstuk 1 geeft een historisch overzicht en achtergrond van vermoeiingsonderzoek. Hoofdstuk 2 richt zich op de test opstelling die is gebruikt voor dit werk en de nauwkeurigheid hiervan, en berekeningsmethoden worden besproken.

De cyclische spanningsintensiteit wordt sinds 40 jaar gezien als de belangrijkste parameter om scheurgroeisnelheid te beschrijven.

Het effect van de spanningsverhouding (= de minimale gedeeld door de maximale cyclische spanningsintensiteitfactor) op de scheurgroeisnelheid wordt toegeschreven aan plastische deformatie die met de scheurgroei gepaard gaat.

Bij een gelijke cyclische spanningsintensiteit is de scheurgroeisnelheid voor hogere spanningsverhoudingen hoger dan voor lagere spanningsverhoudingen.

Er wordt aangenomen dat dit effect veroorzaakt wordt door “crack closure”. Dit is het vroegtijdige contact van plastisch vervormde scheurflanken, nog voordat de minimale cyclische belasting is bereikt. Bij hogere spanningsverhoudingen

treedt er geen contact op tussen de scheurflanken en kan de volledige cyclische spanningsintensiteitsfactor gebruikt worden als drijvende kracht voor de vermoeiingsscheurgroeisnelheid. Bij lagere spanningsverhoudingen kan alleen de effectieve spanningsintensiteitsfactor, namelijk het deel waar de scheur niet is gesloten, worden gebruikt voor de scheurgroei.

Het is mogelijk om over een groot scheurgroeisnelheidstraject de vermoeiingsscheurgroeisnelheid en de spanningsintensiteitsfactor middels een machts-functie lineair te correleren op dubbel-logaritmische schaal.

Echter, er treden vijf hellingsveranderingen op in de log(da/dN)-log(ΔK curve), namelijk T1-T5. Hierdoor ontstaan er min of meer verschillende rechte stukken, met elk hun eigen helling. De hellingsveranderingen kunnen gekoppeld worden aan verandering in scheurgroeimechanismes.

Vermoeiingsscheurgroeisnelheid per belastingwisseling versus de spanningsintensiteitsfactor bij verschillende spanningsverhoudingen is het onderwerp van hoofdstuk 3. Scheursluitingniveaus zijn gemeten door gebruik te maken van kracht- verplaatsingsmetingen en door scheurgroeisnelheidsmetingen aan verschillende proefstuk geometrieën. Doel is te onderzoeken wat de invloed van de spanningsverhouding is op de scheurgroeisnelheid en om na te gaan of de hellingsveranderingen in de vermoeiingscurve het gevolg zijn van veranderingen in het crack closure mechanisme.

Een vermoeiingsscheur groeit in het algemeen loodrecht op de belastingsrichting. In aluminium legeringen treedt vaak schuine scheurgroei op. Deze zogenaamde shearlipvorming treedt op, onder een hoek van 45 graden met de belastingsrichting, zodra er een bepaalde scheurgroeisnelheid is bereikt. Het transitiepunt T3 in AA 2024 en AA 5083 wordt algemeen in verband gebracht met de start van shearlipvorming en het transitiepunt T4 met de voltooiing ervan.

In hoofdstuk 4 wordt aangetoond dat side grooves, in dit geval kleine krasjes over de volle breedte van een proefstuk ter plaatse van het scheurgroeipad, de vorming van shear lips verhinderen. Echter, dit onderdrukken van shear lips heeft geen effect op de scheurgroeisnelheid. Verder blijkt dat de hellingsverandering bij het transitiepunt T3 ook optreedt bij het (partieel) onderdrukken van de shear lip.
De hellingsverandering ter plaatse van T3 in de scheurgroeicurve kan niet langer toegeschreven worden aan de start van de shear lip vorming, nu blijkt dat de ontwikkeling van de shear lip hier geen invloed op heeft. Experimenten aan proefstukken met en zonder side grooves en experimenten uitgevoerd bij verschillende temperaturen en milieus tonen aan dat de shear lip een omgevingseffect is.

In hoofdstuk 5 worden de resultaten besproken van experimenten waarin het scheurgroeipad middels gekromde side grooves is gedwongen in een voorgeschreven richting. Hierdoor treedt er een verlenging van het scheurgroeipad op, waardoor er mogelijk een verlenging van de vermoeiingslevensduur optreedt.
Om dit te onderzoeken zijn er side gooves met verschillende kromtestralen aangebracht op proefstukken van AA 2024. De eerste side groove heeft een kromtestraal die vrijwel het pad volgt van de te verwachten ontwikkeling van de shear lip. De tweede curve, met een kleinere kromtestraal, dwingt de scheur te groeien in een kleinere kromming dan de normale ontwikkeling van een shear lip. Er is een verband gevonden tussen de mate van vertraging in scheurgroei en de mate van “dwingen” van het scheurgroeipad.

Hoofdstuk 6 richt zich op vermoeiingsscheurgroei in het drempelwaardegebied.
De drempelwaarde is, naar de ASTM E 647, gedefinieerd als de cyclische spanningsintensiteit waarbij de vermoeiingsscheuruitbreiding niet hoger is dan

10^{-10} meter per belastingswisseling. Omdat het grootste gedeelte van de vermoeiingslevensduur van een groeiende scheur plaatsvindt in het drempelwaardegebied, is dit gebied van groot belang voor scheurgroeivoorspellingsmodellen.

Drempelwaarden bij hogere spanningsverhouding, dus theoretisch vrij van crack closure, zijn gemeten middels de ASTM E 647 methode en middels een alternatieve methode. De gevonden resultaten zijn niet met elkaar in overeenstemming.

Met behulp van elektronen microscopie zijn de breukvlakken voor de verschillende testmethodes onderzocht. Het gladde breukvlak, gevonden op proefstukken die verkregen zijn middels de ASTM methode, contrasteren met het ruwere oppervlak van de andere samples. Het verschil in gemeten drempelwaarde wordt toegeschreven aan het feit dat er verschillende condities heersen bij de scheurtip.

Summary

Fatigue is a gradual process of local strength reduction. It is a phenomenon of damage accumulation at stress concentrations caused by fluctuating stresses and/or strains. In metals this results in microscopic cracks. These will start to grow under continued cyclic loading until final failure occurs.

The process of fatigue is essentially a process of crack growth. In general the damage accumulation, i.e. crack growth, is slow in the early stages and at the end of fatigue life it accelerates very quickly towards failure. All engineering metals are sensitive to fatigue.

This dissertation deals with several aspects of fatigue crack growth in aluminum alloy AA 5083 from the threshold regime to final instability.

Chapter 1 gives a historical review and background of fatigue research. Chapter 2 focuses on the test configuration which was used for the experiments in this dissertation and discusses the accuracy of the system and the related calculations.

The variation in stress intensity factor, the stress intensity range, has been considered to be the most important parameter to describe the fatigue crack growth rate for the last fourty years. There is an effect of the load ratio (= minimum stress intensity factor divided by maximum stress intensity factor) on the fatigue crack growth rate, which is generally ascribed to the effects of plastic deformation that accompanies fatigue crack growth. At the same stress intensity range, the crack growth rate is higher at higher load ratios than at lower load ratios.

This effect is often assumed to be due to crack closure. This is premature contact of the plastically stretched crack flanks before the minimum load is reached. At large load ratios no such contact can occur and the total applied stress intensity

range will be the driving force for crack growth. At lower load ratios, only the effective part of the stress intensity range, i.e. where the crack is not closed, can provide a driving force.

Over several decades of crack growth rates it is possible to linearly relate fatigue crack growth rate and driving stress intensity range on a log-log scale by using a power law relation. However five changes in the slope of the log(da/dN) as a function of log(ΔK) curve, called the transitions T1-T5, can be observed. This leads to several linear parts with different slopes. The different slopes can be associated with changes in the crack growth mechanism.

The fatigue crack growth rate as a function of the stress intensity range at different load ratios is the topic of Chapter 3. Crack closure levels, measured using the compliance method, are compared with those determined by the crack growth rate method, i.e. using the similitude concept, for different specimen geometries. The aim is to explain the influence of the load ratio on the fatigue crack growth rate and also to determine if the slope changes in the fatigue crack growth curves are a result of changes in crack closure mechanisms.

A fatigue crack often grows with a flat fracture surface perpendicular to the loading direction. In aluminum alloys the crack front often becomes slanted at higher crack growth rates. Shear lips are formed, at about 45° with the loading direction, when a critical value of crack growth rate is exceeded.

Transition T3 in both AA 2024 and AA 5083 is associated with the start of shear lip growth and transition T4 is approximately associated with the completion of the shear lip to full thickness.

In Chapter 4 it is shown that side grooves, in this case small scratches along the whole crack growth trajectory, suppress the development of shear lips. However, the suppression of shear lips has no effect on the fatigue crack growth rate. Furthermore, a change in the slope of the crack growth rate curve near transition point T3 occurs even when the shear lip is (partially) suppressed.

Since the crack growth rate dependence on the stress intensity range of a specimen with a suppressed shear lip does not differ from that of a specimen with a normally developing smooth shear lip, the origin of the change in slope of the fatigue crack growth rate curve, can not be attributed to the start of the growing shear lip.
The results of tests with and without side grooves and in different environments and/or at different temperatures strongly suggest that the shear lip is sensitive to the environment.

Chapter 5 looks at the results of tests where the crack path is forced in a pre-described direction by introducing curved side grooves. This lengthens the crack path and can thus increase fatigue life. To investigate this, side grooves along curves with different radii were applied on centre-cracked tensile specimens of AA 2024.
The first curve, with a large radius, more or less follows the expected development of the natural shear lip. The second curve, with a small radius, forces the crack to grow at an angle higher than found in the natural shear lip causing an overdrawing effect.
A relation is found between the degree of overdrawing and the resulting decrease in crack growth rate.

Chapters 6 focuses on fatigue crack growth in the threshold regime. The value of the threshold stress intensity factor range is defined in accordance with ASTM E 647, which means that the stress intensity factor range does not produce a fatigue crack propagation rate larger than 10^{-10} m per loading cycle. Because in many cases most of the lifetime of a growing crack is spent in this regime of very low crack growth rate, evidently near threshold fatigue crack growth is one of the important factors in development of materials and in the design and lifetime assessment of structures.

Threshold values at higher load ratios, which by definition should be crack closure free, were determined using the ASTM E 647 method and an alternative method. The two sets of results do not agree. Scanning electron microscopy was used to study the resulting crack surfaces near threshold for both testing methods. The observed smooth fracture surface obtained in the ASTM E 647 specimens contrasts with the rougher crack surface for the other samples. The difference in threshold values is believed to be the consequence of dissimilar conditions near the crack tip.

Contents

NOMENCLATURE

FCP/FCG	= fatigue crack propagation /fatigue crack growth
CTOD	= Crack Tip Opening Displacement
COD	= Crack Opening Displacement
CCT	= Centre-Cracked Tension specimen
CT	= Compact Tension specimen
SENB	= Single Edge-Notched Bend specimen
a	= crack length (mm)
a_0	= initial crack length (mm)
Δa	= crack length interval (mm)
B	= thickness (mm)
C	= normalized K gradient, $C= (1/\Delta K)\ (d\Delta K /da) \geq -0.08\ mm^{-1}$
c	= Paris coefficient
c_r	= distance between reference and forced crack path (mm)
E	= Young's modulus
da/dN	= fatigue crack growth rate (the amount of crack extension per loading cycle)
f	= cyclic frequency (Hz)
f_{delay}	= delay factor
K	= stress intensity factor (MPa√m)
K_{IC}	= plane strain fracture toughness
$K_{closure}$	= the value of K where the crack just starts closing
K_{max}	= maximum level of stress intensity factor
K_{max}^*	= critical maximum stress intensity, minimum peak stress intensity needed to break open the bonds in a cyclically damaged region
K_{min}	= minimum level of stress intensity factor
K_{open}	= the value of K where the crack just is fully open
ΔK	= cyclic stress intensity range
ΔK_{eff}	= effective cyclic stress intensity range
ΔK_{th}	= stress intensity range at a crack growth rate $\leq 10^{-10}$ m/cycle
ΔK^*	= critical driving stress intensity, minimal cyclic stress intensity range that is needed to establish a cyclic damage at a certain crack growth rate
ΔK_{th}^*	= critical driving stress intensity, minimal cyclic stress intensity range that is needed to establish a cyclic damage at threshold level
m	= Paris exponent
N	= number of cycles
N_f	= number of cycles to failure
ΔN	= number of delay cycles
P	= load (N)
P_{max}	= maximum level of load (N)
P_{min}	= minimum level of load (N)
R	= load ratio ($P_{min}/P_{max} = S_{min} /S_{max} = K_{min}/K_{max}$)
R_c	= critical value of R above which no closure can be detected
R_{th}	= value of R at threshold
$2r_p$	= monotonic (plane stress) plastic zone size
$2r_p^c$	= reversed or cyclic plastic zone size
S_{max}	= maximum level of stress (MPa)

S_{min}	= minimum level of stress (MPa)
ΔS	= S_{max}-S_{min}
t	= specimen thickness (mm)
t_{forced}	= width of a forced developed shear lip (mm)
$t_{natural}$	= width of a natural developed shear lip (mm)
t_s	= shear lip width (mm)
$t_{s,z}$	= shear lip width in the z direction
U	= crack closure factor = $\Delta K_{eff}/\Delta K$
V_s	= signal voltage
V_m	= measured voltage
V_g	= ground voltage
W	= specimen width (mm)
σ	= stress (MPa)
σ_{ys}	= yield strength
ν	= speed of increase of K_{min} ($\nu = dK_{min}/da$ in MPa√m/mm)

Chapter 1
Introduction

1.1 Historical review

1.1.1 Industrial revolution-1960

Introduction

Fatigue is a process of local strength reduction. The phenomenon is often referred to as a process of damage accumulation in a material undergoing fluctuating loading. This process occurs in engineering materials such as metallic alloys, polymers and composites. To describe the mechanical fatigue process as a result of a repeated load working on a (part of a) structure, different parameters are used, like: cyclic load, stress intensity and crack growth rate. The maximum load is P_{max}, the minimum P_{min} [kN] and the ratio between the minimum and maximum load (P_{min}/P_{max}), that is often used as a measure of the mean stress, is called the load ratio R. Crack growth rate da/dN is the crack increment da per loading cycle increment dN. The stress intensity factor K [MPa√m], working on the crack tip is calculated from the applied load P and actual crack length and direction in a construction. The maximum stress intensity is K_{max}, the minimum K_{min} and the difference between both is ΔK, see figure 1.1.

Fluctuating loads can lead to fluctuating local high stresses and microscopic small cracks may appear. Once a crack exists in a structure, it will tend to grow under cyclic loading. Even if the maximum of the cyclic load on a construction is below the elastic limit of the material, fatigue may lead to failure.

Fatigue is a progressive process, the damage develops slowly in the early stages and near the end of a structure's life it accelerates very quickly towards failure.

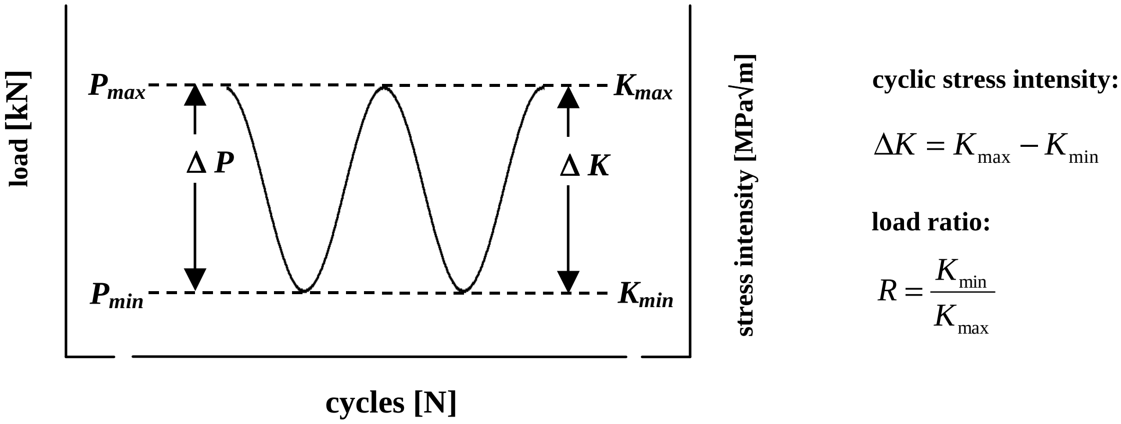

Figure 1.1. Mechanical parameters to describe the fatigue loading system.

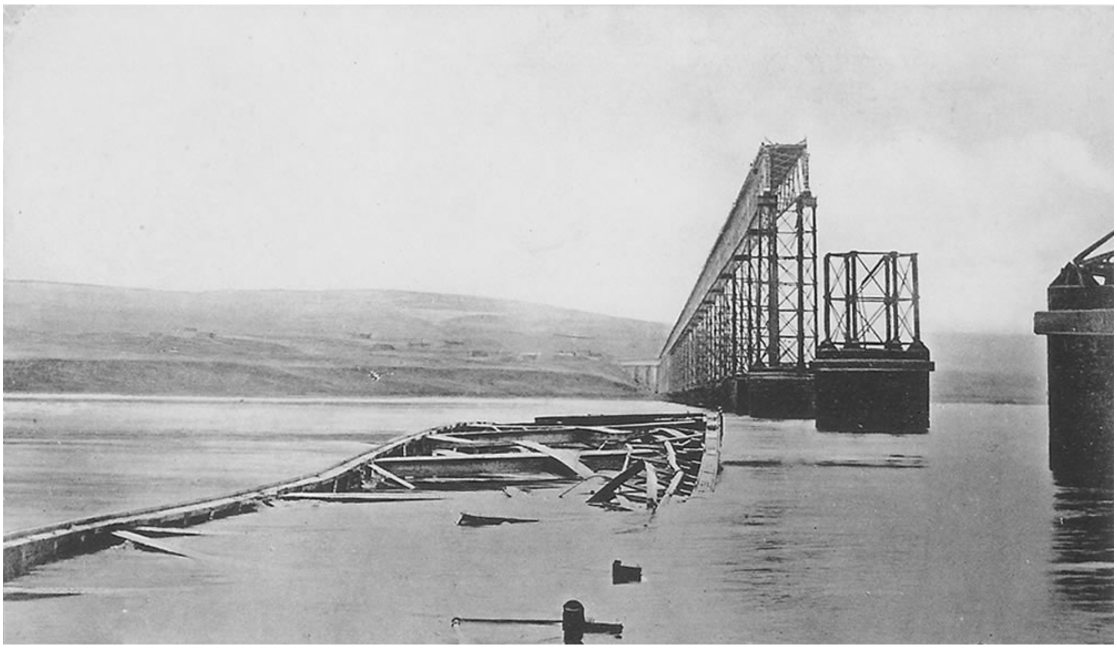

Figure 1.2. Tay Bridge
One of the most famous bridge failures is the Tay Bridge disaster. Some researchers claim that maybe fatigue caused failure of the 19 month old bridge. The evidence is based on the eyewitness reports that the high girders piers oscillated from side to side each time a train crossed the bridge. These dynamic effects on the cast iron lugs, connecting piers and deck, resulted in fatigue cracks and finally in dramatically failure December 28th 1879, the bridge collapsed taking with it a train and killing 75 people [1].

However, details of the fatigue process may differ between materials. The fatigue process can be defined generally as [2]:

> “The process of the cycle-by-cycle accumulation of local damage in a material undergoing fluctuating stresses and strains.”

First steps: description of the phenomenon

Fatigue of metals in structures has been studied since the beginning of the 19th century. Railroads, bridges, steam engines: a whole gamut of new structures and machines were developed, which were made of steel in the times of the industrial revolution. Many of them were exposed to cyclic stresses during service life and many of them failed, see figure 1.2.
The origin of failure was unknown, until Albert [3] made the first report about failure caused by fatigue, in 1829. He observed failure of iron mine-hoist chains, caused by repeated small loads. Ten years later, in 1839, Poncelet, a professor of mechanics at the école d'application, Metz, introduced the term fatigue in his lectures. Rankine [4] recognized the importance of stress concentration in 1843. He noted that fracture occurs near sharp corners. However, until then the phenomenon was described qualitatively only.

Systematic experiments and microscopic observations

A major step was made by Wöhler [5] in 1860. Wöhler, a railroad engineer, started performing systematic experimental research on railroad axles. He observed that steel would rupture at stress below the elastic limit if a cyclic stress was applied. However, there was a critical value of cyclic stress, the fatigue limit, below which failure would not occur. He found a way to visualize “time to failure” for specific materials. In this S-N-curve approach the stress amplitude, σ_a, is plotted as function of the number of cycles to failure, see figure 1.3 [6].

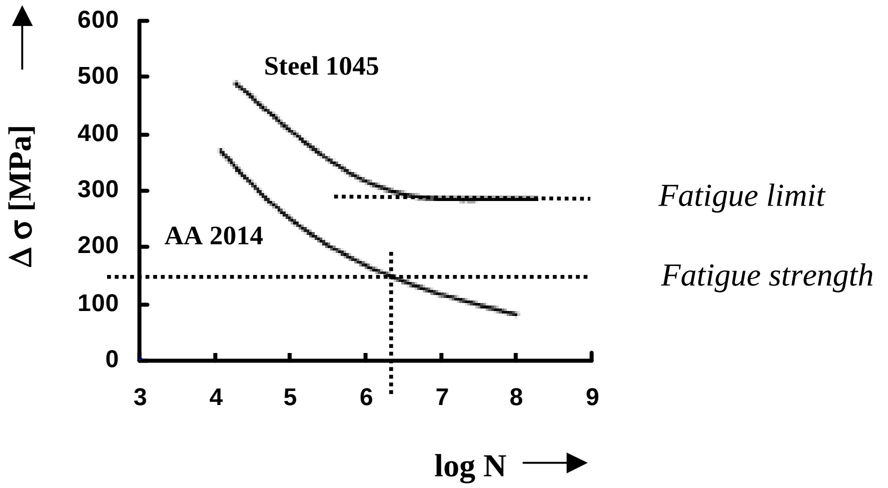

Fatigue limit: *the stress below which a material can be stressed cyclically for an infinite number of times without failure.*

Fatigue strength: *the stress at which failure occurs for a given number of cycles.*

Figure 1.3. S-N curves for low-carbon steel (fatigue limit) and AA 2014 (no fatigue limit).

A logarithmic scale is used for the horizontal axis, while the stress is plotted using either a linear or logarithmic scale.

The first crack surface investigations where made by Ewing [7] in 1903. He showed the nature of fatigue cracks, using a microscope, see figure 1.4.

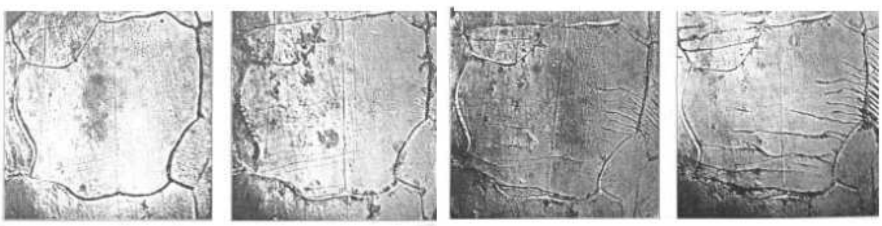

Figure 1.4. Crack surface showed by Ewing & Humfrey, 1903 [7].

Explanations and predictions

Around 1920 Griffith investigated the discrepancy between the theoretical strength of a material, and the true value, sometimes 1000 times less than the predicted value. He discovered that many microscopic cracks and/or other imperfections exist in every material. He assumed that these small cracks lowered the overall strength. Because of the applied load, high stress concentrations are expected near these small cracks, which magnify the stresses at the crack tip. These cracks will grow more quickly, thus causing the material to fail long before it ever reaches its theoretical strength. Any voids, corners, or hollow areas in the internal area of the material also result in stress concentrations. Mostly fracture will begin in one of these areas, simply because of this phenomenon [8].

Miner [9] understood that accumulation of damage leads to failure and he proposed a useful law, especially for engineering. Miner's law says that if a material is exposed to a spectrum of k different stress magnitudes, each contributing n_i cycles at stress S_i, and N_i is the number of cycles to failure of a constant stress S_i, failure occurs when:

$$\sum_{i=1}^{k}\frac{n_i}{N_i}=C \text{, where C is assumed to be 1.} \qquad (1.1)$$

In 1954, Coffin and Manson [10,11] made an important step to describe a system in which fluctuating temperature leads to fatigue. They assumed that plastic strains cause fatigue. In the late 1940s Irwin started to make studies on the impact of plasticity on metallic materials [12]. He suspected that a plastic zone around the crack tip, influencing the fatigue process, would be responsible for several effects, such as under-and overloading effects.

Summarising; in the first half of the 20th century, fatigue research was able to describe the phenomenon fatigue with increasing accuracy and predictive models became more and more reliable. However, crack tip actions as a result of applied load were not well understood.

1.1.2 After 1960: Paris and Elber

An important push to understand the fatigue process was made by Paris and Elber. In 1961, Paris found a more or less linear correlation on double logarithmic scales between crack growth rate da/dN and cyclic stress intensity factor ΔK for some part of the fatigue curve, see figure 1.5 [13]. This well-known Paris' law reads:

$$da/dN = C\Delta K^{m} \tag{1.2}$$

where $\Delta K = K_{max}-K_{min}$ and C and m are experimentally determined scaling constants.

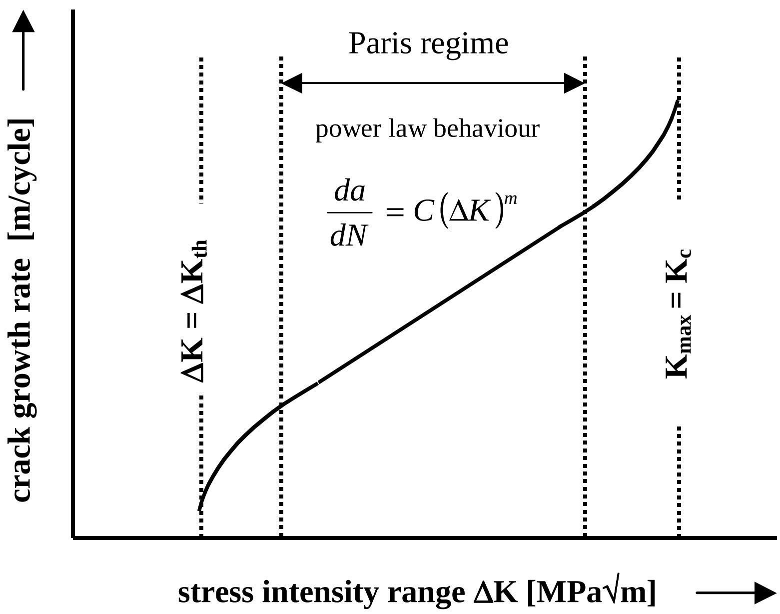

Figure 1.5. Paris' Law: linear correlation between crack growth rate da/dN and stress intensity factor ΔK on log-log scale.

Paris' law is generally accepted for a wide range of different materials, however the physical meaning is limited. The major issue at that time was how to explain stress ratio effects. In 1970, Elber published a famous article titled "Fatigue Crack Closure under Cyclic Tension" [14]. In this article he assumed crack closure to be the cause of stress ratio-effects. By crack closure he meant contact of the crack surfaces, at a load above the minimum load. Elber assumed that, when crack closure occurs, the effective cyclic stress intensity range ΔK_{eff} that works on the crack tip, is lower than the expected or applied ΔK-range, see figure 1.6. The crack growth rate is no longer a result of the whole ΔK magnitude, but only of a part of it.

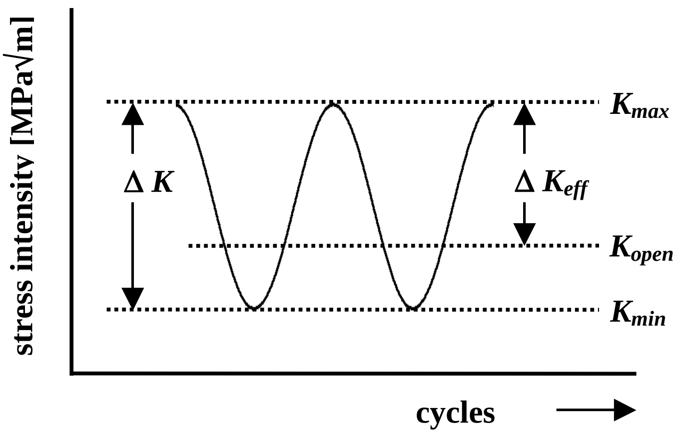

$$\Delta K = K_{\max} - K_{\min}$$

$$\Delta K_{eff} = K_{\max} - K_{open}$$

Figure 1.6. Principle of Elber's crack closure theory.

1.1.3 State of the art

During the last century, the philosophy of design shifted from a material defect-free one to a defect-tolerant one. Development of accurate crack growth prediction models for economical and safety reasons became more and more important. However in some areas of fatigue research, the focus just moved from crack growth to the initiation phase.

Nowadays, both initiation phase and threshold fatigue crack growth are studied intensively all over the world. Research is pushed forward with the release of increasingly accurate equipment and new measurement techniques. Computer simulations, finite element method (FEM) calculations and scanning electron microscope observations (SEM) are leading to a deeper understanding of material behaviour. Not only pure mechanical fatigue, but also fatigue interacting with the environment is subject by considerable researche today. To simulate service life conditions, fatigue experiments are made in different environments applying complex loading spectra. Establishment of new crack growth parameters are developments that may be expected in the near future.

1.2 The fatigue process

1.2.1 Fracture modes

The driving force of fatigue crack growth is cyclic loading leading to the cyclic stress intensity range ΔK. All stress systems near a crack tip can be divided into 3 basic types, see figure 1.7. Each type is associated with a local mode of crack surface displacement [15]. In Mode I, the tension mode, the crack surfaces are pulled apart normal to the plane of the crack. Crack surfaces slide over each other normal to the crack front in Mode II, the shearing mode. In Mode III, the tearing or anti-plane shear mode, the crack surfaces move parallel to the crack front.

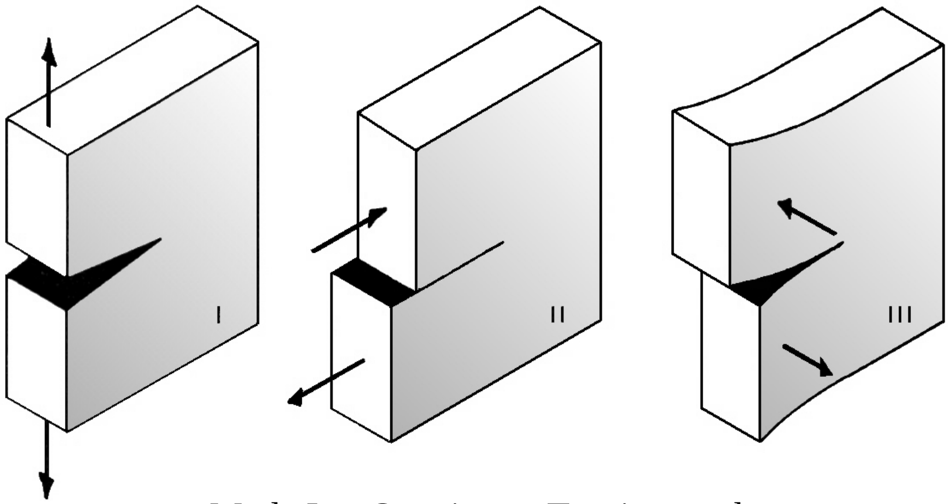

Mode I: Opening or Tension mode
Mode II: Shearing or sliding mode
Mode III: Tearing

Figure 1.7. Different modes of crack surface displacements.

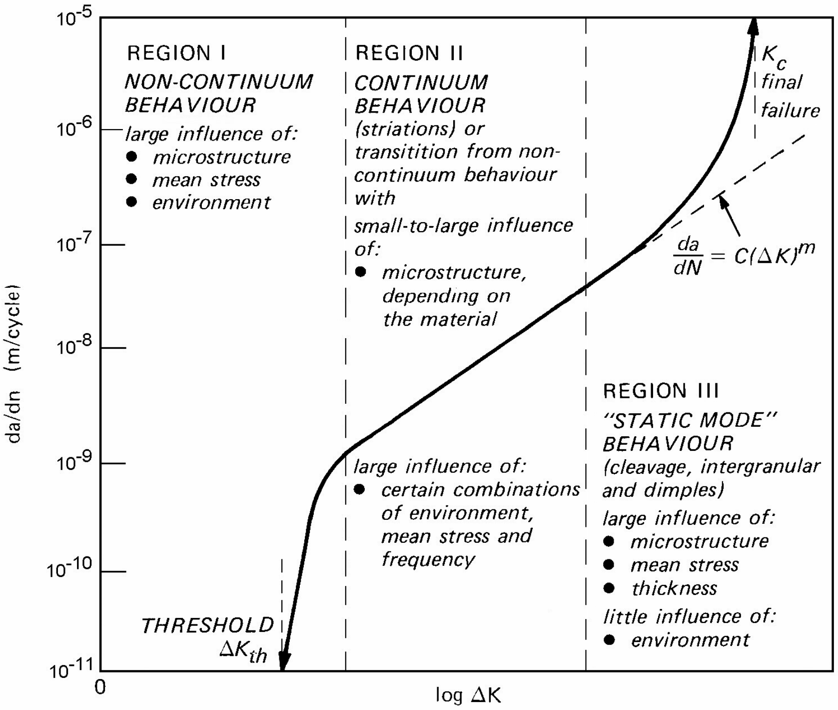

Figure 1.8. Characteristics of the fatigue crack growth rate curve da/dN-ΔK [15].

1.2.2 Different regions

For a better understanding of the causes and processes of fatigue, an exposition is necessary. Fatigue life can be divided into fatigue crack initiation and three main regions. The crack increment rate per cycle da/dN versus stress intensity range ΔK for these regions, i.e. da/dN-ΔK curve on a double logarithmic scale, has a characteristic sigmoidal shape, see figure 1.8. The following characteristics are common to fatigue in all metallic materials:

Region I: (Fatigue crack initiation and) threshold region
Region II: Stable crack propagation, more or less linear on a log-log scale
Region III: Unstable crack propagation

Region I: Fatigue crack initiation and threshold region

The fatigue process starts with the development of microscopically small cracks, which is referred to as the initiation phase. During initiation microcracks appear near a discontinuity in the material e.g. sites of relative high stress concentrations, such as particles or voids, scratches, indents and corners. Microstructurally short cracks, as they are commonly termed, propagate by shear mode (Mode II) and are typically of the order of one or a few grains in length. The fatigue life of aluminium alloys is governed by crack initiation: depending on the stress variation more than 90% of life duration is spent in this phase. Some materials, for example steel and titanium exhibit a fatigue limit. Below this limit repeated stress does not lead to failure. Most other materials, for example aluminium alloys, exhibit no such limit and even infinitesimally small stress amplitudes will eventually cause failure.

Near-threshold fatigue crack propagation takes place at crack growth rates generally less than 10^{-9} m/c, see figure 1.8.

Region II: Stable crack propagation

Stage II cracks propagate by Mode I. Figure 1.9 is a schematic illustration of a typical fatigue crack maturing from a Stage I to a Stage II crack [16]. The crack path in Stage II is now essentially perpendicular to the tensile stress axis. Crack propagation in Region II can be described by a linear relationship between da/dN-ΔK on a log-log-scale, the well-known Paris' Law.

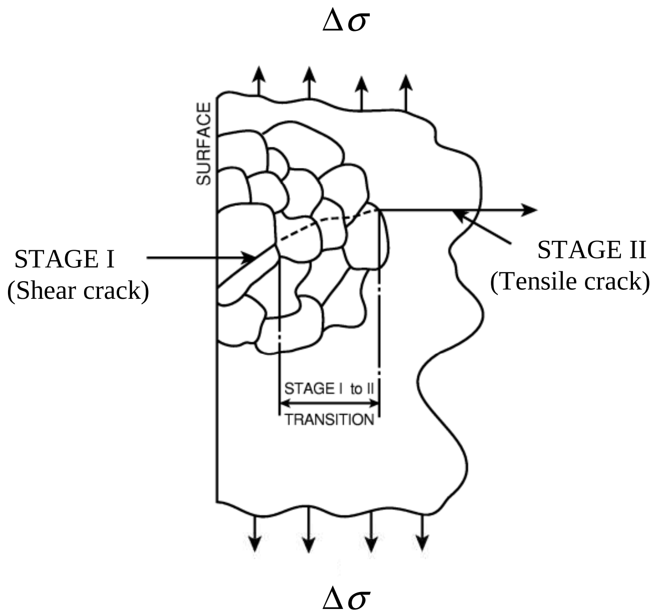

Figure 1.9. Stage I and stage II fatigue crack growth.

On a microscopic scale the most characteristic features of fatigue are the striations that occur during Region II crack growth. The striations represent successive positions of the crack front. Each striation is formed during one load cycle. [15]

Region III: Unstable crack propagation

For stable fatigue crack growth, like Region II, the material's crack resistance should be larger than the crack driving force. In Region III, the material resistance can no longer withstand the increased driving force. The crack growth is no longer a pure fatigue process, but accelerates rapidly, due to interaction between fatigue and static processes. The crack growth direction is now often at an angle to the tensile stress axis. Total fatigue life is a summation of the cycles spent in different regions, see figure 1.10. The duration of Region III growth is short compared to the total fatigue life. For this reason, Region III can be neglected in fatigue life estimations without significant loss of accuracy. Once the maximum stress intensity factor K_{max} reaches the fracture toughness, K_C, failure occurs.

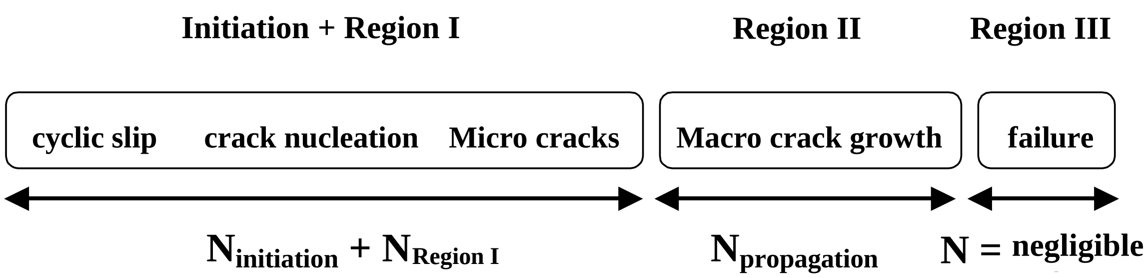

Figure 1.10. Fatigue life duration.

1.2.3 Fatigue crack growth mechanisms

As described in section 1.1, failure by fracture of structures is caused by cracks that extend beyond a safe size. Cracks are always present in all structures, as a result of manufacturing defects, or as localized damage formed in service. A crack can grow by different mechanisms such as creep, stress corrosion and fatigue or combinations. A scheme for the mechanism of fatigue crack growth under constant amplitude loading is given in figure 1.11 [17]. According to this plastic blunting process, crack opening (b), crack advance and blunting (c) are associated with the loading or tensile part of the load cycle, while re-sharpening of the crack tip (d) occurs during the unloading or compressive part of the cycle. Figure 1.11a shows a picture of a sample with an unloaded crack. Loading causes plastic deformation to occur in a region close to the crack tip, the monotonic plastic zone. Plastic deformation occurs by movement of crystallographic planes relative to each other (slip), see figure 1.11b. This slip is caused by dislocation movements. Dislocations are line defects in a crystalline material, which can move and multiply as result of shear stresses. The effect of dislocation movement is a permanent deformation and hardening of the metal.

If the stresses at the crack tip are high, crack propagation will occur, see figure 1.11c. At maximum load, a certain amount of blunting has occurred due to the plasticity. In the unloading part of the cycle, figure 1.11d, the crack tip re-sharpens. During unloading, a reversed or cyclic plastic zone appears within the monotonic plastic zone.

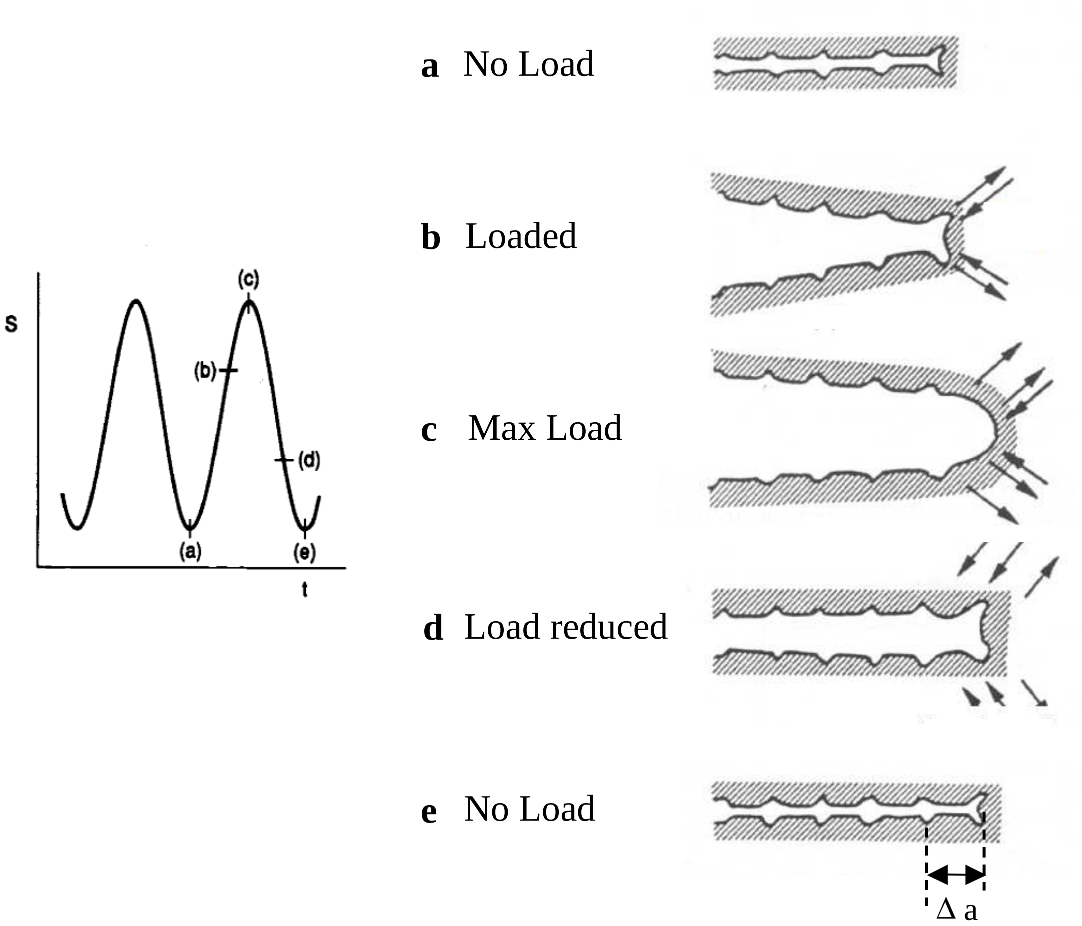

Figure 1.11. Fatigue crack growth mechanism.

1.3 Mechanics and Physics

1.3.1 Introduction

At this moment, the cyclic stress intensity range ΔK is believed to be the dominant mechanical parameter to describe fatigue crack propagation. However, crack growth rate is also assumed to be affected by several other parameters [18], see figure 1.12. These parameters can be divided into intrinsic and extrinsic factors. The influence of intrinsic parameters, e.g. the material's mechanical properties, and extrinsic parameters, such as environmental effects and the loading system are discussed in the next subsections.

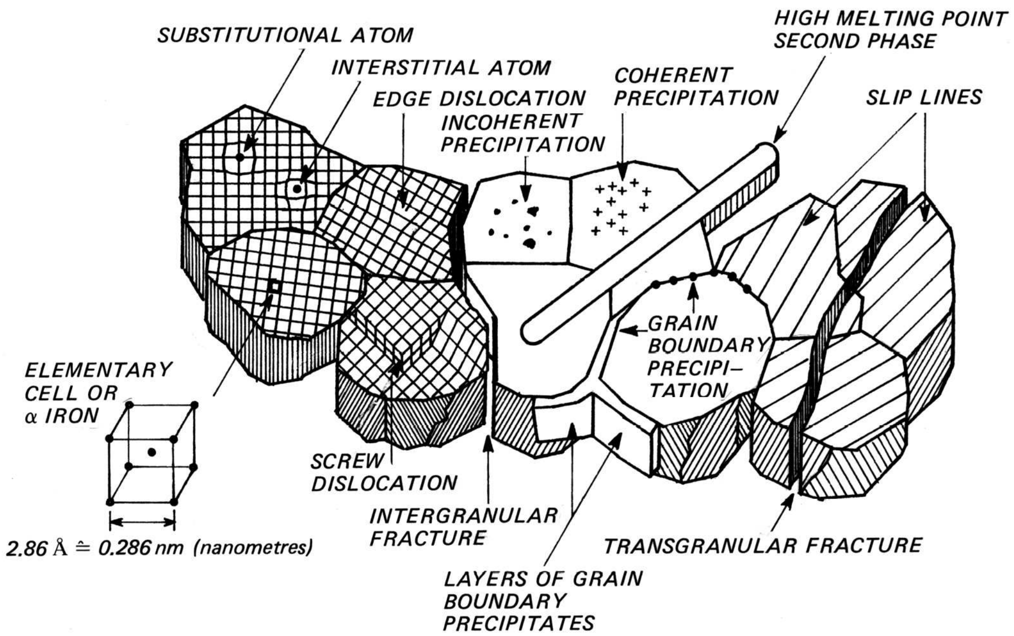

Figure 1.12. Micro structural features in metals [18].

1.3.2 Influence of mechanical properties

Microstructure

The fatigue crack growth mechanisms and the effect of microstructure on these mechanisms are both localized near the crack tip. For example, environmental interaction, surface roughness and corrosion-induced closure are related to the microstructure. The environment and loading system interact with micro-structural features, which make fatigue properties in relation to the microstructure difficult to understand. In general, microstructure has a stronger effect on fatigue crack growth at lower crack growth rates. Explanations to understand these effects are as diverse as the effects themselves. But in general the high K at larger da/dN is dominant over all other mechanisms.

Grain size

The effect of grain size on fatigue crack growth resistance and the occurrence of crack arrest at grain boundaries has been studied by many researchers [19-20]. It was observed that a change in crack growth mechanism sometimes occurred when the monotonic plastic zone size is approximately equal to that of the grain size [21]. Grain boundaries can act as barriers and many times, a decrease of fatigue crack growth rate is observed in the threshold region, as illustrated in figure 1.13 [22].

Grain refinement can be used to increase the fatigue limit. But often the threshold ΔK is larger for larger grains. Grain size variations in a material are in general the result of prior heat treatment and deformation. Not only grain size and shape vary with such processing, but other microstructural changes, for example texture and yield strength, occur simultaneously.

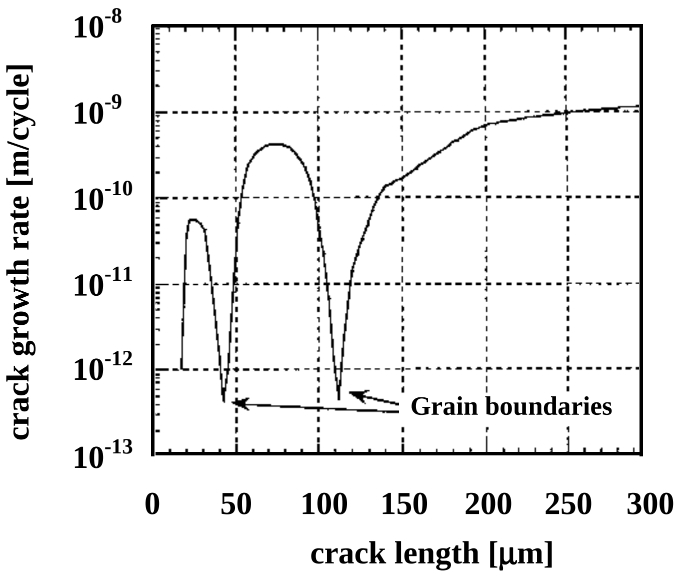

Figure 1.13. Decrease in crack growth rate near grain boundaries in the threshold region [22].

Due to these complex temperature-related and deformation-related changes, it becomes difficult to assess the underlying mechanisms controlling the crack growth behaviour for materials having different grain sizes.

Effect of yield strength

In general, agreement exists on the influence of strength of the material on fatigue crack propagation in the threshold region. A higher yield strength leads to less plasticity and lower threshold values for steel but to higher threshold values for non-ferro metals. Ritchie [23] attempted to explain the effect in steels through hydrogen embrittlement. He assumed the existence of a small area affected by hydrogen near the crack tip. Hydrogen weakens the metal and results in lower threshold values.

1.3.3 Influence of the environment

Influence of moisture

Experiments conducted under very low water vapour pressure have clearly demonstrated that residual moisture, corresponding to very low partial pressures, is sufficient to induce a significant effect on crack growth rates, especially in combination with higher frequencies [24-27]. For aluminium alloys, the formation of hydrogen atoms and oxide layers on a freshly created fracture surface at the crack tip during the fatigue process are described by the following reaction:

$$2Al + 4H_2O \rightarrow Al_2O_3 \bullet H_2O + 3H_2$$

Hydrogen atoms may diffuse into the plastic zone and be transported by dislocation movements. The influence of moisture on fatigue crack growth in AA 2024 is illustrated in figure 1.14 [26]. This figure shows crack growth rates for constant load amplitude tests in the near threshold region in different environments or different water vapour pressure conditions at ultrasonic frequencies in ambient air (dots), dry air (circles) and in a vacuum (triangles) at a load ratio R = –1. The difference in crack growth can be explained by the mechanism of surface diffusion of water vapour molecules into the crack tip.
Water vapour of ambient air is transported to the crack tip by diffusion where chemical processes with newly created fracture surfaces lead to the formation of hydroxide, hydrated oxides and the release of hydrogen. The cycling frequency and the partial pressure of water vapour controls the surface reaction at the crack tip. Embritteling effects are explained by adsorption of hydrogen at the surface or in the first few atomic layers which facilitates dislocation nucleation or by diffusion of hydrogen ahead of the crack tip [27, 28].

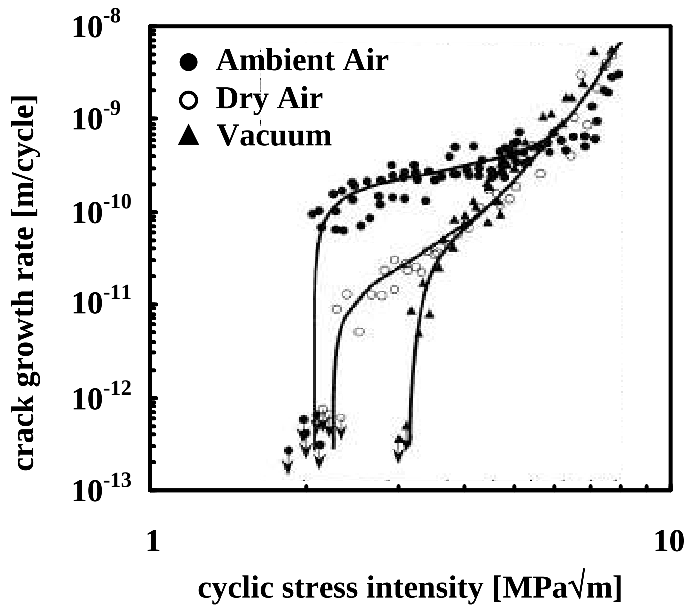

Figure 1.14 Fatigue crack growth in different environments in threshold region for AA7075-T6 [27].

Influence of temperature

A change in temperature often leads to a change in fatigue behaviour. The rate of a chemical (corrosion) reaction is temperature dependent. In general, a corrosion reaction will be faster with increasing temperature. Corrosion products on the crack surfaces may lead to extra crack closure.

1.3.4 Influence of the loading system

Influence of stress ratio

Crack growth is strongly affected by the load ratio R. Crack growth curves show a shift to lower ΔK values with increasing R, see figure 1.15 [28]. To provide a physical explanation for such load ratio effects, a crack closure theory has been developed by Elber. This theory, based on the assumption of “early contact of the crack flanks before the minimum load is reached”, can give a qualitative explanation for stress ratio effects. Besides that, it can be calculated that the crack tip opening at for example R = 0.7 is higher compared to those at R = 0.1. In the case of R = 0.7, the crack opens more widely. The influence of distortion of crack surfaces, for instance in the form of surface roughness, will be small at R = 0.7 and increases with lower R-values.

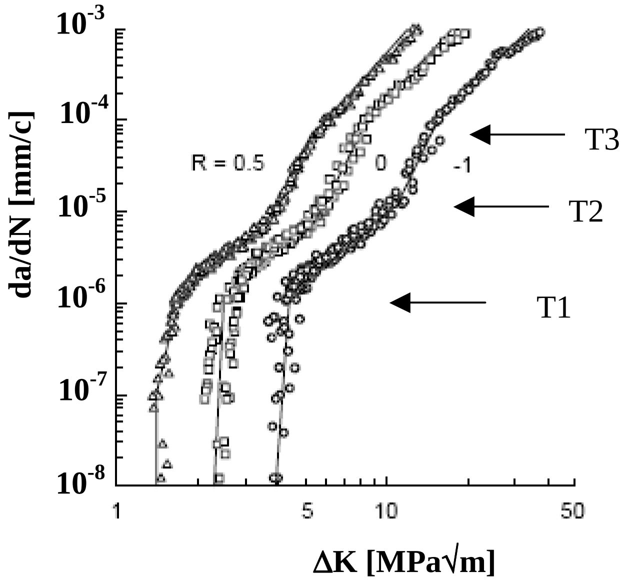

Figure 1.15. Stress ratio effect in AA 7075.

Influence of load frequency

The crack growth rate da/dN, is the result of a collection of mechanisms operative at the crack tip. Some of these mechanisms are related to time dependent chemical processes, such as corrosion, hydrogen absorption and diffusion. High frequency fatigue tests in corrosive fluids frequently lead to longer lifetimes (expressed in cycles) compared to experiments at lower frequencies [29]. Crack growth rate, expressed as da/dN, decreases with higher frequencies, while the reaction time for chemical processes is believed to be frequency independent. If a time dependent mechanism is involved and dominates in the collection of mechanisms, different crack growth behaviour is expected with different frequencies. In general, frequency effects are more pronounced at lower crack growth rates.

Influence of loading history

The effect of an overload is related to the formation of a large plastic zone. An overload produces more plastic deformation ahead of the crack tip. This large plastic zone can result in compression ahead of the crack tip and in crack closure behind the crack tip. Because of the higher crack resistance of the material in the plastic zone, and the lower ΔK_{eff} due to increased closure, crack growth retardation can be expected, see figure 1.16.

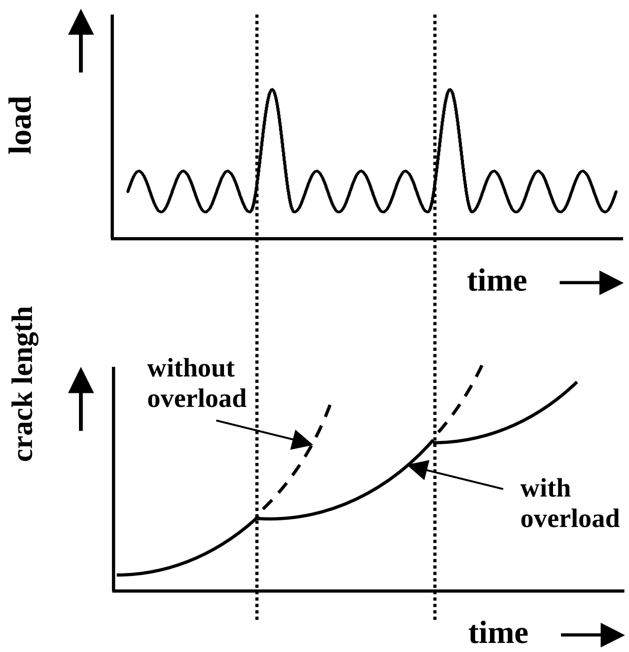

Figure 1.16. Effect of overload on da/dN.

The effect of an overload normally acts over a small distance: after a certain crack increment, the effect disappears and the crack growth rate returns to its original value. An underload can reduce the effect of an overload. The underload leads to compression and the plastic deformation will be (partly) reversed. An overload followed by an underload shows only a marginal effect on crack growth, while an underload followed by an overload leads to retardation [30].

1.4 Crack Closure

Elber discovered the phenomenon of crack closure under cyclic loading in 1970. He proposed that crack closure occurs as a result of crack-tip plasticity. The plastic zone develops around the crack tip as the yield strength of the material is exceeded there. As the crack grows, a wake of plastically deformed material develops while the surrounding body remains elastic. This plastically deformed material, stretches perpendicular to the plane of the crack, causes the crack surfaces to contact each other during the unloading part of the cycle. Elber assumed that crack growth is not driven by the full ΔK range, but only by the effective part. He postulated that this closure effect lowers the effect of the applied stress intensity range ΔK and causes a decrease of the fatigue crack growth rate, see figure 1.6. He introduced a new stress intensity range: the effective stress intensity range ΔK_{eff}.

$$\begin{aligned} \Delta K_{eff} &= K_{\max} - K_{open} \\ &= U \times \Delta K \qquad \text{where U = f (R) and U} \leq 1 \end{aligned} \tag{1.3}$$

Five mechanisms of crack closure have been proposed: plasticity-induced crack closure, roughness-induced crack closure, oxide-induced crack closure, viscous fluid-induced crack closure and transformation-induced crack closure, see figure 1.17 [31]. It has been shown that crack closure plays an important role in the effect of the stress ratio on crack growth and on the near-threshold crack growth behaviour [32, 33].

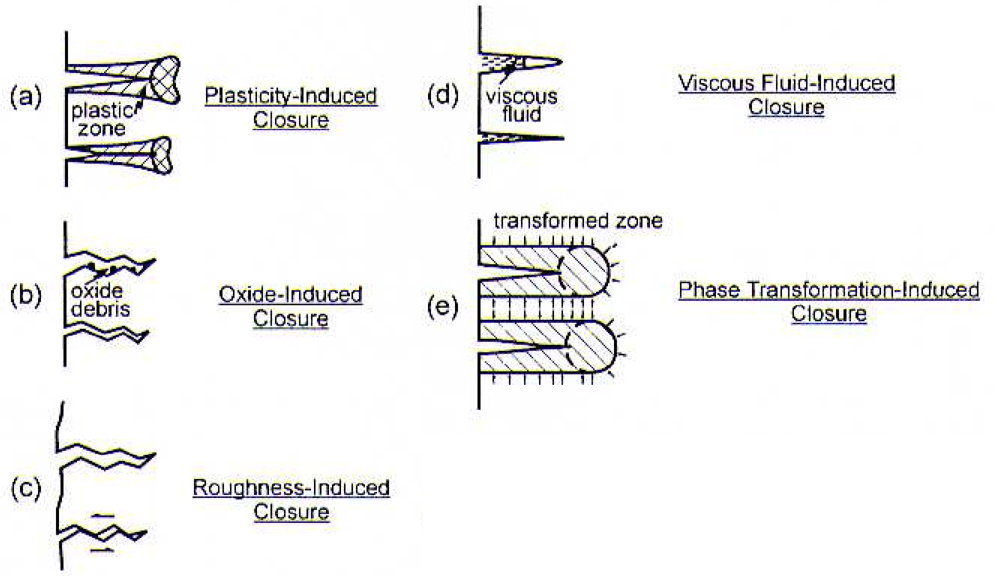

Figure 1.17. Different types of crack closure.

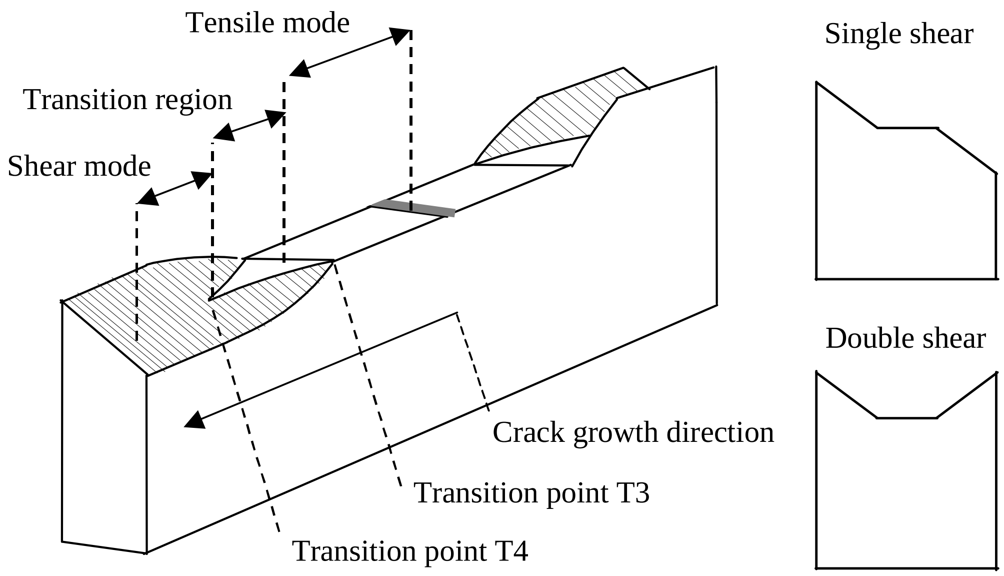

Figure 1.18. Shear lip.

1.5 Shear Lips

In aluminium alloys, the crack surface changes from flat to slant at higher crack growth rates or ΔK-levels, and a so-called shear lip arises, see figure 1.18. The shear lip initiates at the plate surface and grows as the stress intensity ΔK (and thus the crack growth rate) increases. By reducing the cyclic load level the transition can be reversed [34, 35]. The start of the shear lip can be found in the da/dN-ΔK diagram of a constant load amplitude test as a change of slope in the crack growth curve. When the development of the shear lip is completed, the slope of the da/dN-ΔK curve changes again. These two points, i.e. the start and completion of the shear lip, are marked respectively as transition point T3 and T4. The da/dN-ΔK relation between T3 and T4 is about linear on log-log scale and has the form of the Paris relation. Much has been written about the origin of the shear lip. Summarizing this, the development of shear lips is only possible if three conditions are satisfied simultaneously [36]:

1: there must be a material texture with a slip possibility near 45º with the plate surface.
2: there must be a plane stress situation, leading to shear stresses at about 45°.
3: ΔK_{eff} or da/dN must be high enough for initiation of the shear lip.

It has been shown that test frequency has a significant influence on the morphology of shear lips [30, 37]. In AA 2024 shear lips are rough at higher frequencies and smooth at lower frequencies. A rough shear lip results in more scatter in the da/dN-dK curve, while a smooth shear lip results in a smooth curve.

References

[1] Peter R. Lewis, *Beautiful Railway Bridge of the Silvery Tay: Reinvestigating the Tay Bridge Disaster of 1879*, Tempus, 2004

[2] A. Almar-Næss, Tapir, *Fatigue Handbook*, Trondheim, Norway, 1985

[3] W. A. J Albert, *Über treibseile am Harz*, Archive für Mineralogie Geognosie Bergbau und Hüttenkunde, Volume 10, pages 215-34, 1838

[4] W. J. M. Rankine, *A Manual of Applied Mechanics*, Charles Griffin and Company, Glasgow, 1858

[5] A. Wöhler, *Über die Festigkeitsversuche mit Eisen and Stahl*, Zeitschrift für Bauwesen, Volume 20, pages 83, Berlin, 1870

[6] H.W. Hayden, W.G. Moffatt and J. Wulff, *The structure and properties of Materials*, Volume III, John Wiley, United Kingdom, 1965

[7] J.A. Ewing, Classic *historic discovery of role of microscopic cracks in fatigue of metals,* Philosophical Transactions of the Royal Society, 1903

[8] A.A. Griffith, *The phenomena of rupture and flow in solids*, Philosophical Transactions of the Royal Society of London, Series A, 221, pages 163-198, 1920

[9] M.A. Miner, *Cumulative Damage in Fatigue*, Journal of Applied Mechanics, Volume 12, Trans. ASME Volume 67, pages A159-A164, 1945

[10] L.F. Coffin, *Study of the effects of cyclic thermal stresses on a ductile material*, American Society of Mechanical Engineers, Volume 76, pages 931-950, 1953

[11] S.S. Manson, *Behaviour of materials under conditions of thermal stress*, National Advisory Commission on Aeronautics: Report 1170. Lewis Flight Propulsion Laboratory, Cleveland, Ohio, 1954

[12] G. Irwin, *Fracture Dynamics, Fracturing of Metals*, American Society for Metals, Cleveland, Ohio, pages 147-166, 1948

[13] P.C. Paris, M.P. Gomez and W.E. Anderson, *A rational theory of fatigue*, The Trend in Engineering, Volume 13, pages 9-14, 1961

[14] W. Elber, *Fatigue Crack Closure Under Cyclic Tension*, Engineering Fracture Mechanics, Volume 2, pages 37-45, 1970

[15] M. Janssen, J. Zuidema and R.J.H. Wanhill, *Fracture Mechanics*, ISBN 90-407-2221-8, Delft, Second edition, 2002

[16] Y.K. Wong, X.Z. Hu, and M.P. Norton, *Plastically elastically dominant fatigue interaction in 316L stainless steel and 6061-T6 aluminium alloy*, Fatigue and Fracture of Engineering Materials and Structures 25 (2), pages 201-213.

[17] C. Laird, *The influences of Metallurgical structure on the mechanisms of fatigue crack propagation*, Fatigue crack propagation, ASTM STP 415, Society for Testing and Materials, Philadelphia, PA, USA, 1967

[18] A.K. Vasudévan, P.E. Bretz, *Near-threshold fatigue crack growth behaviour of 7xxx and 2xxx alloys: A brief review,* Proceedings of the International symposium on fatigue crack growth threshold concepts, Philadelphia, 1983

[19] J. Petit, *Some aspects of near-threshold crack growth: Micro-structural and environmental effects*, Proceedings of the international symposium on fatigue crack growth threshold concepts, Philadelphia, 1983

[20] L. Lawson, E.Y. Chen, M. Meshii, *Near-threshold fatigue: a review,* International Journal of Fatigue 21, S15-S34, 1999

[21] R.J.H. Wanhill, *Microstructural influences on fatigue and fracture resistance in high strength structural materials*, Engineering Fracture Mechanics, Volume 10, pages 337-357, 1978

[22] A.E. Blom et all, *Short fatigue crack growth in Al 2024 and AL 7075,* symposium, Sheffield, EGF 1, Sept 1985

[23] R.O. Ritchie, *Near threshold fatigue crack propagation in steels,* International Metals Review, No 5-6, pages 205-230, 1979

[24] J. Petit, C. Sarrazin-Baudoux, G. Henaff, *An overview on environmentally-assisted fatigue crack propagation*, Proceedings of the 7th International Fatigue Congress, Beijing, China, 1999

[25] R.P. Wei, P.S. Gao, *Fracture mechanics and surface chemistry studies of fatigue crack growth in an aluminium alloy*, Metallurgical and Materials Transactions A, pages 51-85, 1980

[26] S.P. Lynch, *Environmentally assisted cracking: overview of evidence for an adsorption-induced localised-slip process*, Acta Materialia, Volume 36, pages 2639-2661, 1988

[27] S.E. Stanzl, *The influence of air humidity on near – threshold fatigue crack growth of 2024-T3 aluminum alloy*, Materials Science and Engineering, A147, pages 45-54, 1991

[28] J.C. Newman, X.R. Wu, S. Venneri and C. Li, *Small-Crack effects in High-Strength Aluminium Alloys*, NASA RP-1309, 1994

[29] M. Papakyriacou , H. Mayer , U. Fuchs , S.E. Stanzl-Tschegg , R.P. Wei, *Influence of atmospheric moisture on slow fatigue crack growth at ultrasonic frequency in aluminium and magnesium alloys*, Fatigue and Fracture of Engineering Materials and Structures, September 2002

[30] J. Zuidema, *Square and Slant Fatigue Crack Growth in Al 2024*, ISBN 90-407-1191-7, 177 pages, Dissertation, Delft University Press, Delft, The Netherlands, 1995

[31] S. Suresh, *Fatigue of Materials*, 2nd ed., Cambridge University Press, NY, 1998

[32] P.K. Liaw, *Overview of Crack Closure at Near-Threshold Fatigue Crack Growth Levels*, Mechanics of Fatigue Crack Closure, ASTM STP 982, Philadelphia, pages 62-92, 1998

[33] A.J. McEvily, R.O. Ritchie, *Crack closure and the fatigue-crack propagation threshold as a function of load ratio*, Fatigue and Fracture of Engineering Materials and Structures; 21, pages 847-855, 1998

[34] J. Schijve, *Fatigue Damage Accumulation and Incompatible Crack Front Orientation*, Engineering Fracture Mechanics 6, pages 245-252, 1974

[35] J. Zuidema, J.P. Krabbe, *The effect of Regular and Irregular Shear Lips on Fatigue Crack Growth in AA 2024*, Fatigue and Fracture of Engineering Materials and Structures, 20, pages 1413-1422, 1997

[36] J. Zuidema, F.A. Veer and C. van Kranenburg, *Shear lips on fatigue fracture surfaces of aluminium alloys*, Special Issue of “Fatigue and Fracture of Engineering Materials and Structures” 28, pages 159-167, 2005

[37] F.A. Veer, *The effect of shear lips, loading transitions and test frequency on constant ΔK and constant load amplitude fatigue tests*, Dissertation, Delft University Press, Delft, The Netherlands, 1993

Chapter 2
Fatigue Crack Growth: Measurement and Data Analysis

2.1 Introduction

As explained in Chapter 1, the cyclic stress intensity factor ΔK is believed to be the most suitable parameter to study fatigue crack growth. In this work specimens are fatigued with a sinusoidal load and a fixed frequency on a servo-hydraulic fatigue test system. As a result of this cyclic load, the crack tip is exposed to a maximum and minimum stress intensity. If the difference in stress intensity is large enough, crack propagation will occur. This chapter focuses on the test configuration on which fatigue experiments have been conducted. Moreover, the accuracy of the system and data analysis will be discussed here. Almost all tests have been carried out at TU Delft, The Netherlands, although some tests have been performed at the Karpenko Institute, Lviv, Ukraine.

2.2 Experimental techniques

2.2.1 Specimen

Three specimen geometries have been used in this research, namely centre-cracked tension (CCT), compact tension (CT) and single edge-notched bend (SENB) specimens. The shape and dimensions of these are shown in figure 2.1 a-c.

Standard centre-cracked tension specimens have been manufactured according to ASTM standard E 647 [1] using a length l = 340 mm, a width W = 100 mm and a thickness t, varying from 4.8 up to 10.4 mm. A starter notch perpendicular to the rolling direction is introduced at the center of the specimens. This starter notch with a length $2a_0$ = 10 mm is made by electrical-discharge machining.

Besides centre-cracked tension specimens, experiments have been performed on specimens with compact tension and single edge-notched bend geometry. These two types of specimens were cut out of the larger, original centre-cracked tension specimens. All specimens of the same alloy are taken from the same batch.

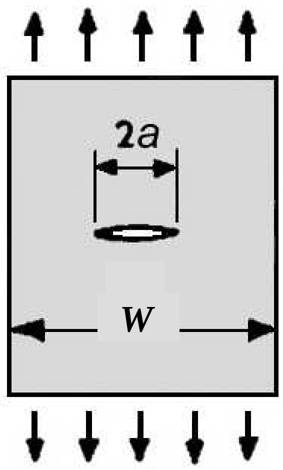

Figure 2.1a. CCT-specimen.

width *W*: 100 mm
thickness *B*: varying from 4.8 to 10.4 mm

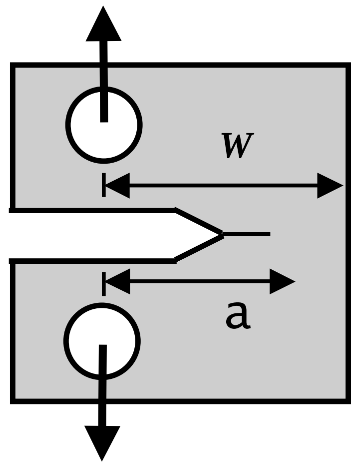

Figure 2.1b. CT-specimen.

width *W*: 32 mm
thickness *B*: varying from 4.8 to 10.4 mm

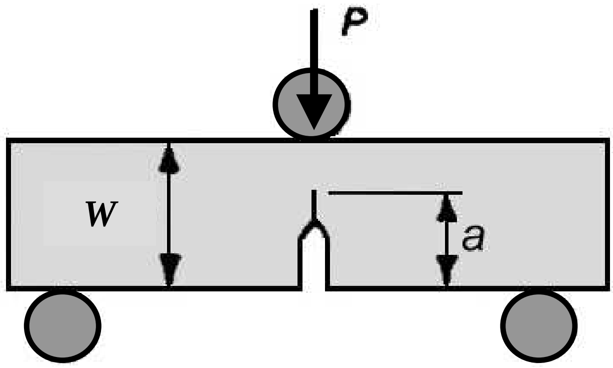

Figure 2.1c. SENB-specimen.

width *W*: 30 mm
thickness *B*: varying from 4.8 to 10.4 mm

The yield strength and chemical composition of the three different alloys investigated are shown in table 2.1.

Table 2.1: Yield strength (MPa) and chemical composition (wt.%) of AA 2024, AA 5083 and AA 7075 [2]

	σ_{ys} [MPa]	Mg	Mn	Si	Fe	Cr	Cu	Zn	Ti
AA 2024	345	1.2-1.8	0.3-0.9	max 0.5	max 0.5	max 0.1	3.8-4.9	max 0.25	max 0.15
AA 5083	228	4-4.9	0.4-1	max 0.4	max 0.4	0.05-0.25	max 0.1	max 0.25	max 0.15
AA 7075	462	2.1-2.9	max 0.3	max 0.4	max 0.5	0.18-0.28	1.2-2	5.1-6.1	max 0.2

2.2.2 Type of experiments

Four types of experiments are performed in this research:

- I constant load amplitude test
- II constant ΔK test
- III ΔK threshold test (recommended by ASTM E 647)
- IV constant K_{max}- increasing K_{min} test

Figure 2.2 schematically shows the maximum and minimum load P and the stress intensity factor K respectively, versus crack length a [mm] for these four different experiment types.

Characteristic for experiment I, the constant load amplitude test, is the constant maximum and minimum load. In this test, both K_{max} and K_{min} and thus ΔK increase with increasing crack length. The load ratio R, defined as the ratio of minimum and maximum load, remains constant.

In experiment II, the constant ΔK test, both K_{max} and K_{min} are kept constant. To achieve this, the load must decrease with increasing crack length. This type of experiment has mainly been used in this work to create a pre-crack from the starter notch.

Loads P_{max} and P_{min} versus crack length a

Stress Intensity Factors K_{max} and K_{min} versus crack length a

I: Constant ΔP test

II: Constant ΔK test

III: Δ K threshold test (ASTM)

IV: Δ K_{th} test (Constant K_{max}- increasing K_{min})

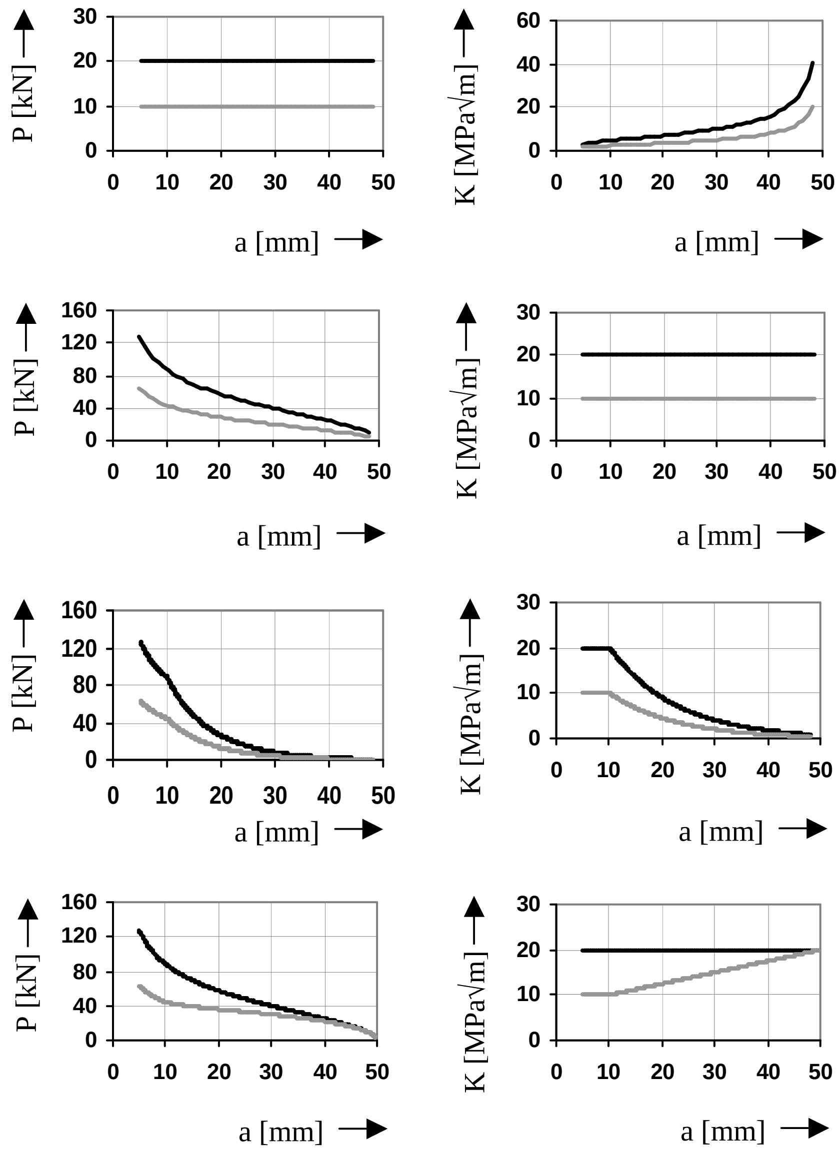

Figure 2.2. Different types of fatigue crack growth experiments.

In experiment II, the constant ΔK test, both K_{max} and K_{min} are kept constant. To achieve this, the load must decrease with increasing crack length. This type of experiment has mainly been used in this work to create a pre-crack from the starter notch.

Examples of such pre-crack procedures can be seen in the first parts of the diagrams of experiment types III and IV.

The accepted method for testing fatigue crack propagation in the threshold region according to standard ASTM E 647, requires R to be constant and ΔK to decrease with increasing crack length, see figure III. The ASTM recommends (1/K) (dK/da), known as the normalized K gradient, is constant. K_{max} and K_{min} both decrease with increasing crack length. The applied load also decreases continuously, in order to compensate for crack growth.

Experiment type IV, the constant K_{max}-increasing K_{min} test procedure, allows ΔK to be decreased with constant K_{max}, see IV.

The usage of the load ratio R is different in test types I-III on the one hand and test type IV on the other hand. For the first three types R is constant, while in type IV, R increases with crack growth.

2.2.3 Test configuration

The test configuration is schematically shown in figure 2.3. The main parts of the test configuration are:

-the fatigue test machine, brand Schenck
-the pulsed direct current potential drop equipment, brand Howden
-the control computer and software

The specimen is clamped in the fatigue machine by grips and connected to the potential drop apparatus which is used for crack length measurement.

The functioning of the test configuration is subdivided into two parts. In the first part a potential drop signal is generated, which is a measure for the crack length. The potential drop signal (voltage) is sent to the control computer, where this signal is converted to a crack length (mm) using a calibration polynomial.

The second part actually controls the fatigue machine. It is a closed-loop system, thus including a feedback signal. The output of the control computer, the load command signal, is fed back into the input of the control computer, the load feedback signal.

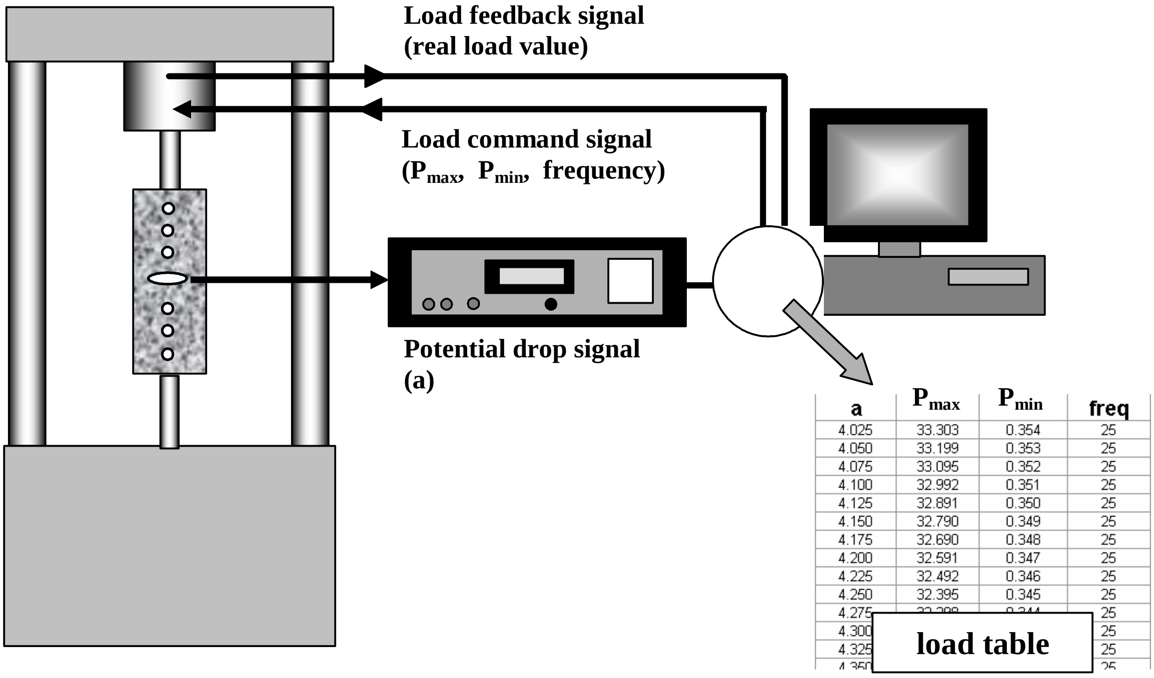

Figure 2.3. Test configuration, containing fatigue test machine, pulsed direct current potential drop equipment and the control computer.

Almost all tests, except constant load amplitude tests, are crack-length controlled. This means that the actual crack length determines the load. Because of this dependence, before starting the experiments, a load table must be made. This load table includes four columns. The first column contains the control parameter i.e. the crack length (mm). The second and third column contain the maximum and minimum load respectively (kN). The fourth column specifies the frequency (Hz).

A command signal, containing the pre-defined maximum load, minimum load and frequency, is sent from the computer to the fatigue machine. The fatigue machine carries out the task and returns a feedback signal to the control computer. Afterwards the control computer checks this response, with the values found in the pre-stored load table. If there is a mismatch between the current feedback signal and the desired combination in the load table, the command signal is adapted in the direction of the values in the load table. The control computer not only ensures a correct implementation of the load table, but also stores all relevant data. This loop process is repeated until the end of the test. The control software has been developed at TU Delft, the Netherlands, in coorporation with CIT, a software house.

2.2.4 Control program in detail

A correct signal handling of the control program is of vital importance in view of the required accuracy and reliability of the measurement results.

The data flow diagram, shown in figure 2.4, illustrates how data is processed by the system in terms of inputs and outputs. Incoming signals, i.e. potential drop and feedback signals, are continuously recorded as received. The incoming signals are buffered. Data is captured from the buffer in order to perform a detailed analysis. The analysis is performed on a block of captured data of the feedback signal. The sample rate is defined as the number of data points that is sampled by the data acquisition hardware per second. The software allows the user to choose both the capture duration and the sample rate. For a correct analysis of the feedback signal, a captured block must contain at least 4 cycles. Each cycle must be built up of at least 400 points, in order to analyze the frequency, P_{max} and P_{min}. These two conditions, 4 cycles and 400 points per cycle, determine the minimum size of the capture duration and the minimum sample rate of the data acquisition hardware.

The received potential drop signal is converted to a crack length, using a calibration polynomial. The data set “actual crack length-feedback signal” is compared to the corresponding combination “crack length-desired load” found in the load table. Once the data set deviates from the desired combination, the command signal is adapted.

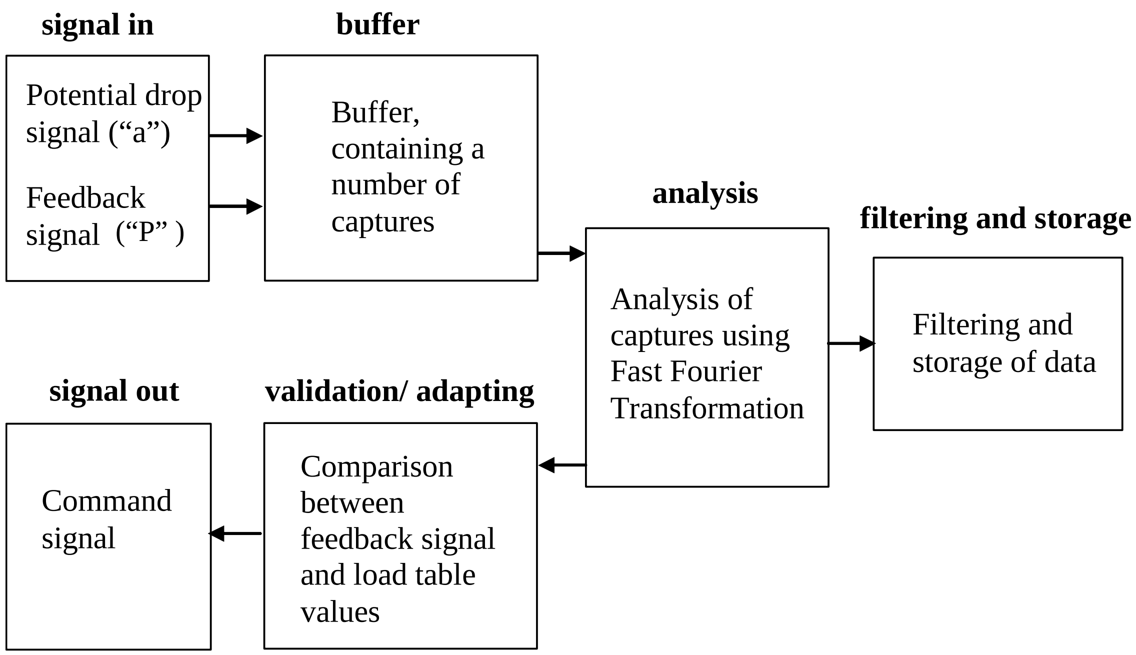

Figure 2.4. Data flow diagram. Illustrated is how data is processed by the system in terms of inputs and outputs.

The potential drop signal, i.e. crack length, is influenced by many factors. In order to smooth the potential drop signal, the control program provides three types of crack length filtering. The following methods may be used to restrict the range of stored data:

-no filtering; in this case the actual crack length is used

-average of a number of captures

-highest value in a number of captures

Both the type of experiment and the test frequency determine the capture duration, what kind of filtering is applied and how frequently a signal is stored.

2.2.5 Environment

It is believed that environment and/or test frequency have a marked influence on the fatigue crack growth rate behaviour and threshold levels for most engineering materials. Tests with a simulated (changing) environment allow investigating of such effects on the crack growth rate. The majority of tests are performed in room temperature air. Some tests in this work were conducted at different temperatures, using argon as a shielding gas or in an artificial seawater environment.

A climate chamber was used to test specimens at different temperatures. This chamber provided temperature control for low and high temperature tests. With this set-up a stationary state was reached with fluctuations in a range of ± 2 degrees.

To create a marine environment, a specially designed Perspex cell was clamped around the specimen. The cell covers the part of the test specimen where the crack grows. To ensure that the load is not affected by this corrosion cell, only the lower cell wall was attached to the specimen. The upper wall is open. A barrel containing artificial seawater is connected to a pump system to circulate seawater through the cell. The locations for the two inlets and outlets are in the middle of the cell, on the faces opposite to each other. More details about the corrosion cell are described in [3]. Artificial seawater was prepared according to ASTM D 1141 [4].

For tests in a shielding gas, the same Perspex cell was used. Again the cell was clamped round the specimen, but the upper side was sealed with silicon rubber. Two flow meters were built into the pipeline system, one before the inlet and the other one after the outlet. Flow speed was monitored and possible leakage can be detected by these flow meters.

2.2.6 Potential drop technique and calibration

For measuring the crack length the potential drop method has been used. In short this method correlates the crack length to the electrical resistance of the specimen. A pulsed direct current, generated by a potential drop apparatus, is led through a specimen, creating an electric field. Any change in the effective cross sectional area of the specimen leads to a change in this electric field, measured by means of potential drop. If the cross sectional area decreases due to a growing crack, this results in an increase of the electrical resistance, which is measurable as an increase in potential drop.

An advantage of this method is that even very small crack increments can be measured. A disadvantage is that as the crack tips approach the plate edges of the specimen, i.e. at the end of crack growth, the potential drop method is less reliable, due to excessive plasticity [5]. Note that plasticity also increases the electrical resistance.

The potential drop measurement is synchronized with the load signal. The disturbance is measured at the maximum load, thus at the maximum opening of the crack, in order to avoid an influence of (partial) crack closure.

A correct and accurate calibration is essential. The relationship between crack length and corresponding potential drop is not linear. A third order polynomial, see equation 2.1, has been used in order to relate the crack length a and potential drop voltage V:

$$a = P_0 + P_1 V + P_2 V^2 + P_3 V^3 \tag{2.1}$$

The constants P_i of the calibration polynomial can be found in several ways, leading to about the same result.

The first method uses constant ΔK loading. The specimen is clamped in the fatigue testing machine and fatigued with a constant ΔK. To avoid crack closure and shear lip effects on the potential drop signal, typical load parameters are R >

0.5 and $\Delta K < 6$ MPa$\sqrt{m}$ for aluminium alloys. Crack length is optically measured on one specimen surface using a traveling microscope.

The second method uses a milling machine. The specimen is only connected to the potential drop apparatus. An artificial crack is introduced step by step by milling. The crack tip is blunt, caused by the end mill with a radius in the order of 2 mm, while in a real fatigue test a very sharp crack tip is present. Moreover the plastically deformed area at the crack tip can influence the electrical resistance of the material. Because of these two effects, the reliability of this method relative to the method described above can be less. An advantage of mechanically creating a “crack” is that a straight crack front is assured.

The third method uses a saw. The specimen is only connected to the potential drop apparatus. A crack is extended step by step using a small jigsaw, with step sizes in the range of 2 to 3 mm. After each extension the crack length is optically measured using a sliding gauge on both specimen surfaces and the corresponding voltage is listed. This method is useful and fast to determine a calibration polynomial. In real tests, the optical measured crack length deviates less from the electrically measured crack length in the case of the saw cutting technique, compared to the other techniques. However, it is not clear why saw cutting leads to the most accurate calibration polynomial.

For each unique geometry, for example for specimens with side grooves or with a local variation in thickness, an additional calibration was made using the saw cutting technique.

2.3 Calculations

2.3.1 Stress intensity and plastic zone size

The stress intensity factor K defines the magnitude of the local stresses around the crack tip. This factor depends on the load, crack size, crack shape, and geometry, with the general form given by [6]:

$$K = \sigma\sqrt{\pi a}\, f\left(\frac{a}{W}\right) \tag{2.2}$$

where:

σ = applied (remote) stress

a = crack length

W = specimen width

$f\left(\frac{a}{W}\right)$ = a correction factor that depends on specimen and crack geometry

For example for a centre-cracked tension specimen [7]:

$$f\left(\frac{a}{W}\right) = \sqrt{\sec\frac{\pi a}{W}} \tag{2.3}$$

During (cyclic) loading metals show plastic strains near the crack tip because the yield stress is exceeded in that region, as a result a plastic zone develops, see figure 2.5. The shape and size of the plastic zone are not exactly defined. According to Irwin [7], the monotonic plastic zone size, $2r_p^m$, at a stress intensity factor K, is calculated using:

$$2r_p^m = \frac{1}{\pi}\left(\frac{K}{\sigma_{ys}}\right)^2 \tag{2.4}$$

where σ_{ys} is the yield strength. The plastic zone is assumed to be circular in cross- section.

As the nominal tensile load is reduced during the decreasing part of the loading cycle, i.e. the stress intensity is reduced from K_{max} to K_{min}, the plastic region near the crack tip is put into compression by the surrounding elastic body. This compression leads to a reversed plastic zone. This reversed or cyclic plastic zone size, $2r_p^c$, depends on the magnitude of ΔK and twice the yield strength [6]:

$$2r_p^c = \frac{1}{\pi}\left(\frac{\Delta K}{2\sigma_{ys}}\right)^2 \tag{2.5}$$

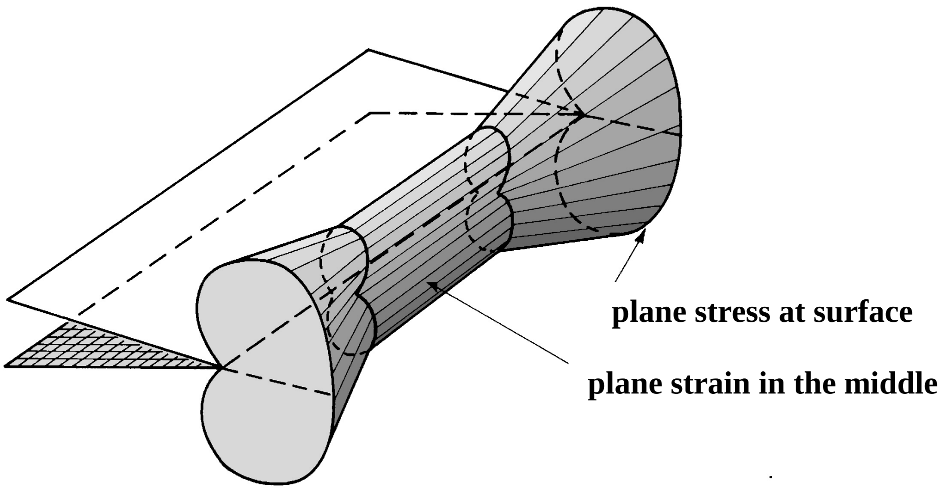

Figure 2.5. Plastic zone: plane stress and plane strain.

2.3.2 Crack growth rate

The rate of fatigue crack growth is to be determined from the crack size *a* as a function of the number of elapsed cycles *N*. The ASTM E 647 recommends two approaches: the secant or the incremental polynomial method [1, section X1].

The incremental polynomial method is mainly used in this work to calculate the fatigue crack growth rate from a-N data. However, for data obtained in the threshold region, a third method is used. The three methods are explained below.

The secant technique

The secant or point-to-point technique for computing the crack growth rate simply involves calculating the slope of the straight line connecting two adjacent data points on the a-N curve. It is more formally expressed as follows:

$$(da/dN) = (a_{i+1} - a_i)/(N_{i+1} - N_i) \tag{2.6}$$

Since the computed da/dN is an average rate over the (a_{i+1} - a_i) increment, the average crack size, $\bar{a} = \frac{1}{2}(a_{i+1} + a_i)$, is normally used to calculate ΔK.

The secant method often results in an increased scatter in da/dN relative to the incremental polynomial method, since the latter numerically "smooths" the data [10, 11].

The incremental polynomial method

The Incremental Polynomial Method for computing da/dN involves fitting a second-order polynomial (parabola) to sets of data points. The form of the equation for the local fit is as follows:

$$a = b_0 + b_1 N + b_2 N^2 \tag{2.7}$$

The regression parameters b_0, b_1, and b_2 are determined by a least squares fit. The rate of crack growth da/dN at (a_i,N_i) is obtained from the derivative of the above parabola, which is given by the following expression:

$$da/dN_{(a_i, N_i)} = b_1 + 2b_2 N_i \tag{2.8}$$

The value of ΔK associated with this da/dN value is computed using the fitted crack size, a_i, corresponding to N_i. The procedure is schematically given in figure 2.6.

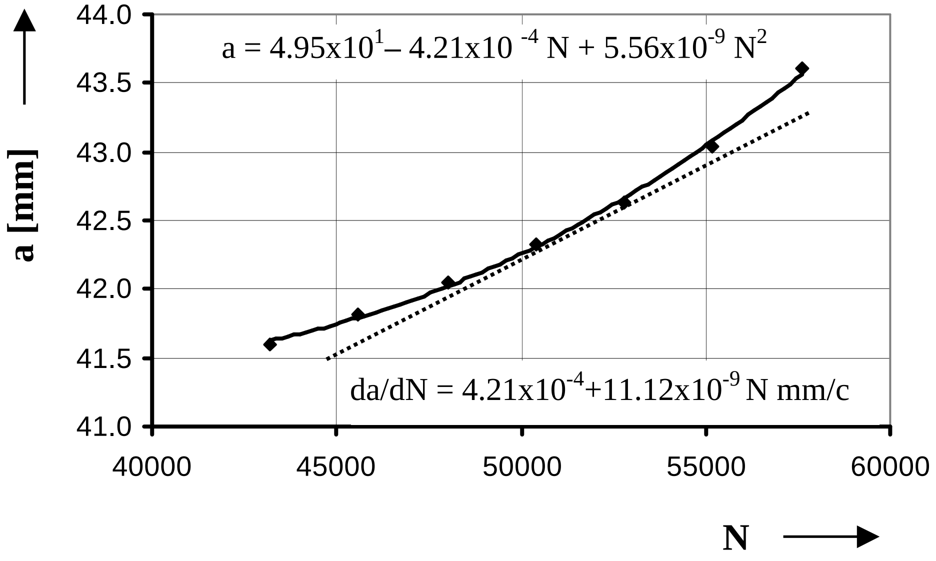

Figure 2.6. The Incremental Polynomial Method for computing da/dN involves fitting a second-order polynomial to sets of successive data points. The rate of crack growth da/dN at N_i is obtained from the derivative of the parabola.

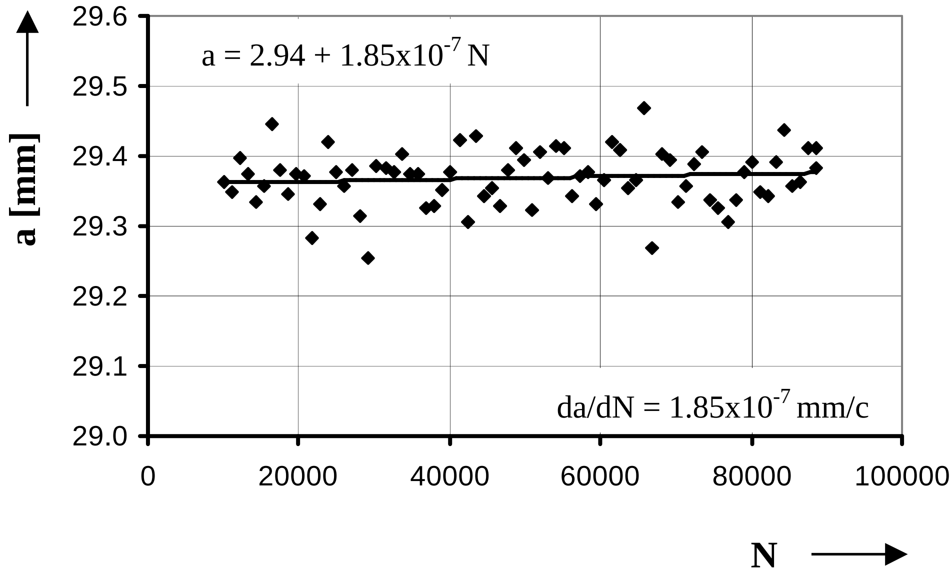

Figure 2.7. For a very small crack increment, crack advance is considered to be linear. The least squares method is used to determine crack growth rates in the threshold region.

The least square line

The ASTM allows the use of a maximum of 9 data points per data set in the case of the incremental polynomial method. However, with tests in the threshold region many data points are acquired over a very small crack increment. In this case the incremental polynomial method leads to a very scattered result.

For a very small crack increment, crack advance can be considered to be linear with the number of cycles. For this reason the least squares method is used to determine crack growth rates in the threshold region [8].

The linear least squares line of the chosen set of data points can be represented as:

$$a = b_0 + b_1 N \tag{2.9}$$

where the b_0 and b_1 can be found using the linear least squares method. The crack growth rate da/dN at N_i is the derivative of equation 2.6, thus equal to b_1.

a-N data, obtained in the threshold region, is processed using the linear least squares method and shown in figure 2.7.

For all methods mentioned, the value of ΔK is determined using the calculated average crack length from the chosen set of data points.

Figure 2.8 schematically shows how to calculate the da/dN-ΔK relation from load and crack length data.

2.4 Overall accuracy

2.4.1 Sources of error

To make an assessment of the accuracy of the test results an analysis of the possible errors should be made. All measurements are affected by systematic and random errors. Random errors are reduced when experiments are repeated many times and the results are averaged; systematic errors are consistent and repeatable. Causes and behaviour of systematic errors are well known and understood. First the errors are discussed individually, after which the impact of the errors on the ultimate result is considered. The most important errors are:

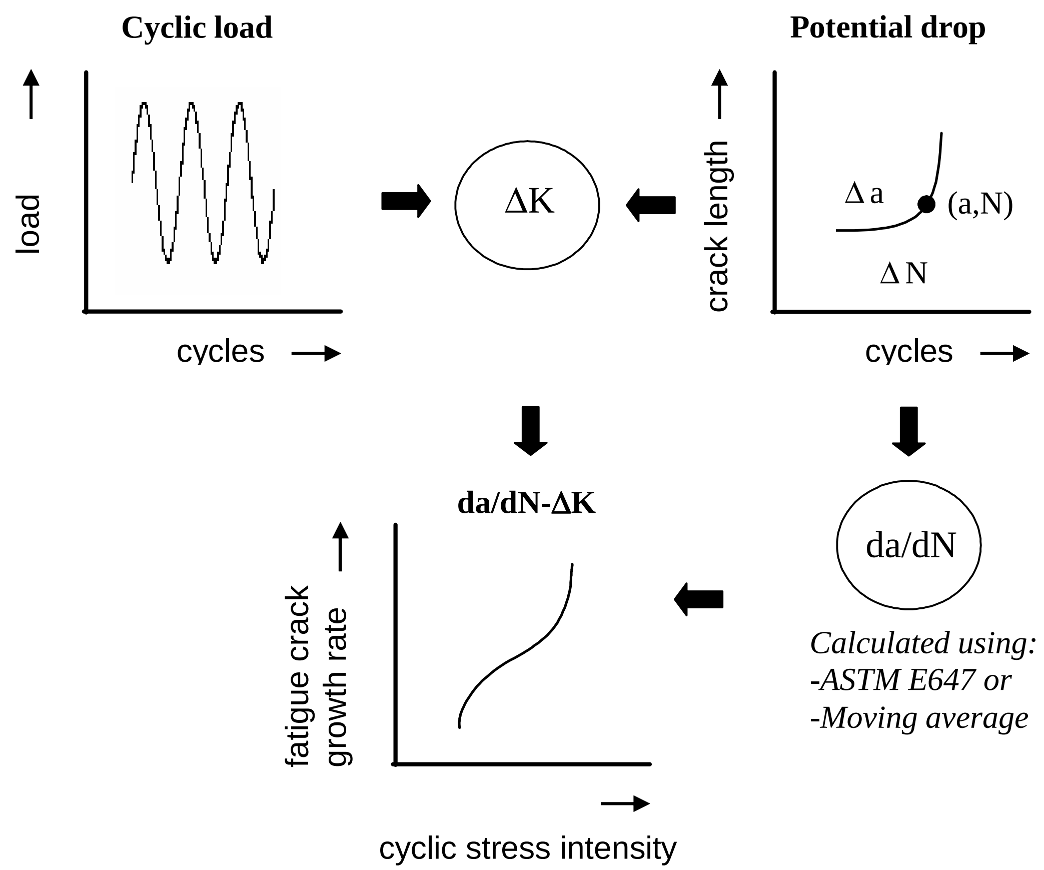

Figure 2.8. Scheme for the calculation of the da/dN-ΔK relation from load and crack length data.

Accuracy of the load cell

The load cell is part of the fatigue machine. It measures the load and provides a representative signal. A typical load cell signal is 0-10000 mV, representing the applicable load range. The accuracy of the load cell is estimated as 1/1000 (10 mV) of the total load range, e.g. corresponding to 250 N in case of a 250 kN load cell.

Crack length

An error in crack length measurement leads to an incorrect interpretation of the load table, which can have large consequences for the applied load and thus for crack growth. The crack length is influenced by both random and systematic errors. The control program buffers the potential drop signal needed for data processing. The filtering technique and the number of data points that are used to calculate an average crack length can be adapted to an experiment. Filtering to reduce the random error in the crack length signal generates a small positive systematic error in the crack length, caused by an increasing crack growth rate during the procedure. However, the systematic error in the average crack length is negligible compared to the systematic error due to the usage of a calibration curve. The systematic error in the calibration polynomial, estimated to be less than 0.1 mm, is related to the method of calibration.

An example of a potential drop signal as funtion of time and the frequency distribution of the corresponding crack length is shown in figures 2.9-2.10.

The data set is obtained under the condition that no filtering is applied and no crack propagation occurs. The shape, as shown in figure 2.10, is typical for a normal distribution, described by a mean value and a standard deviation. The standard deviation sd of the crack length measurement is calculated to be 0.05 mm.

A disadvantage of the potential drop method is that it does not take into account the shape of the crack front. This can also be regarded as an advantage, because it measures the cracked surface area. This surface area may be a good measure for the crack growth resistance.

Close to the plate edges the potential drop method is less reliable, but on the other hand K is also not well defined there, see ASTM E 647 [9]. For this reason nearly all experiments are provided with a pre-crack procedure to avoid effects due to the presence of the starter notch and crack length values obtained close to the plate edges are rejected for calculation.

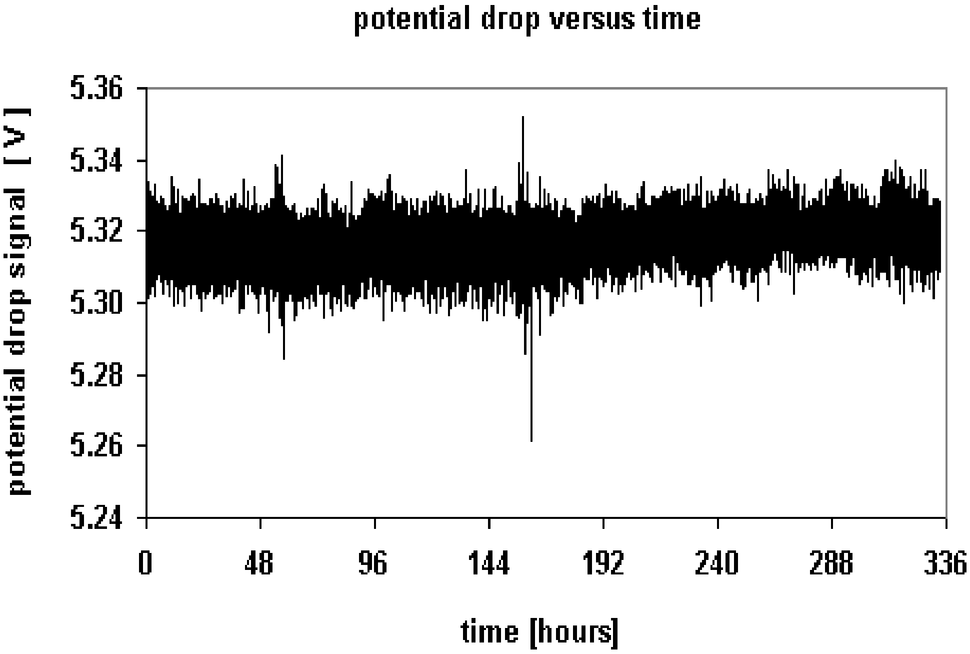

Figure 2.9. Potential drop signal (V) versus time (hours) at a fixed crack length.

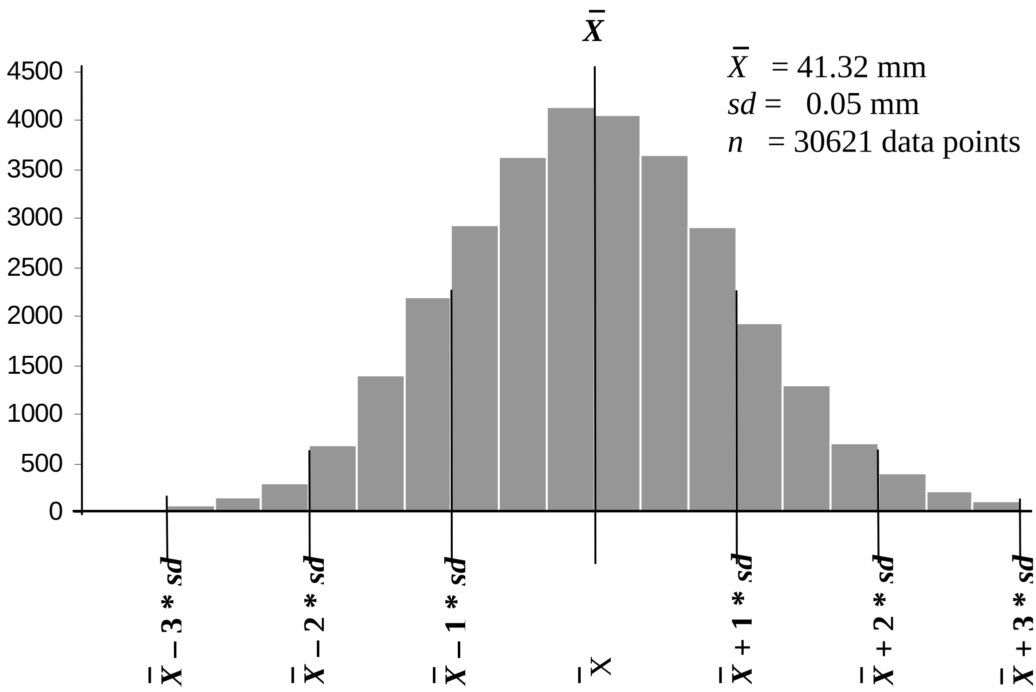

Figure 2.10. Frequency distribution of the corresponding crack length.

External influences

Any voltage signal is measured as the potential difference across two points. However, a measured voltage will almost inevitably include some amount of unwanted signal. Noise or unwanted signal contamination is added to the signal voltage because signal wires act as aerials, picking up environmental electrical activity. Because of this, there are many (random) fluctuations in the measured values and the overall-result is a noisy measurement system.

An ideal crack length measurement system responds only to the potential difference between its two terminals. In order to minimize noise, a measurement system ground can be made, which is also influenced by the same noise too. If both terminals are affected by the same noise, noise is eliminated when the voltage difference is measured, see figure 2.11. A benefit of such a circuit is that even larger distortions, being the same on both terminals, will theoretically have no effect on the measured voltage.

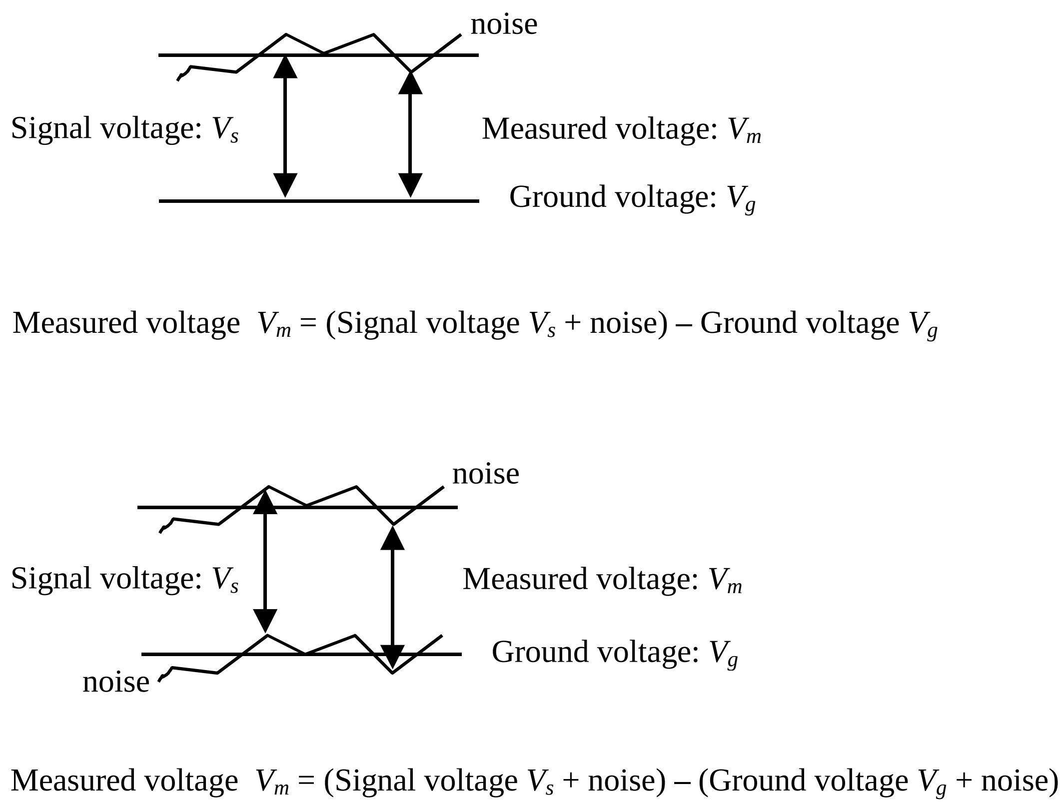

Figure 2.11. Principle of noise reduction/elimination.

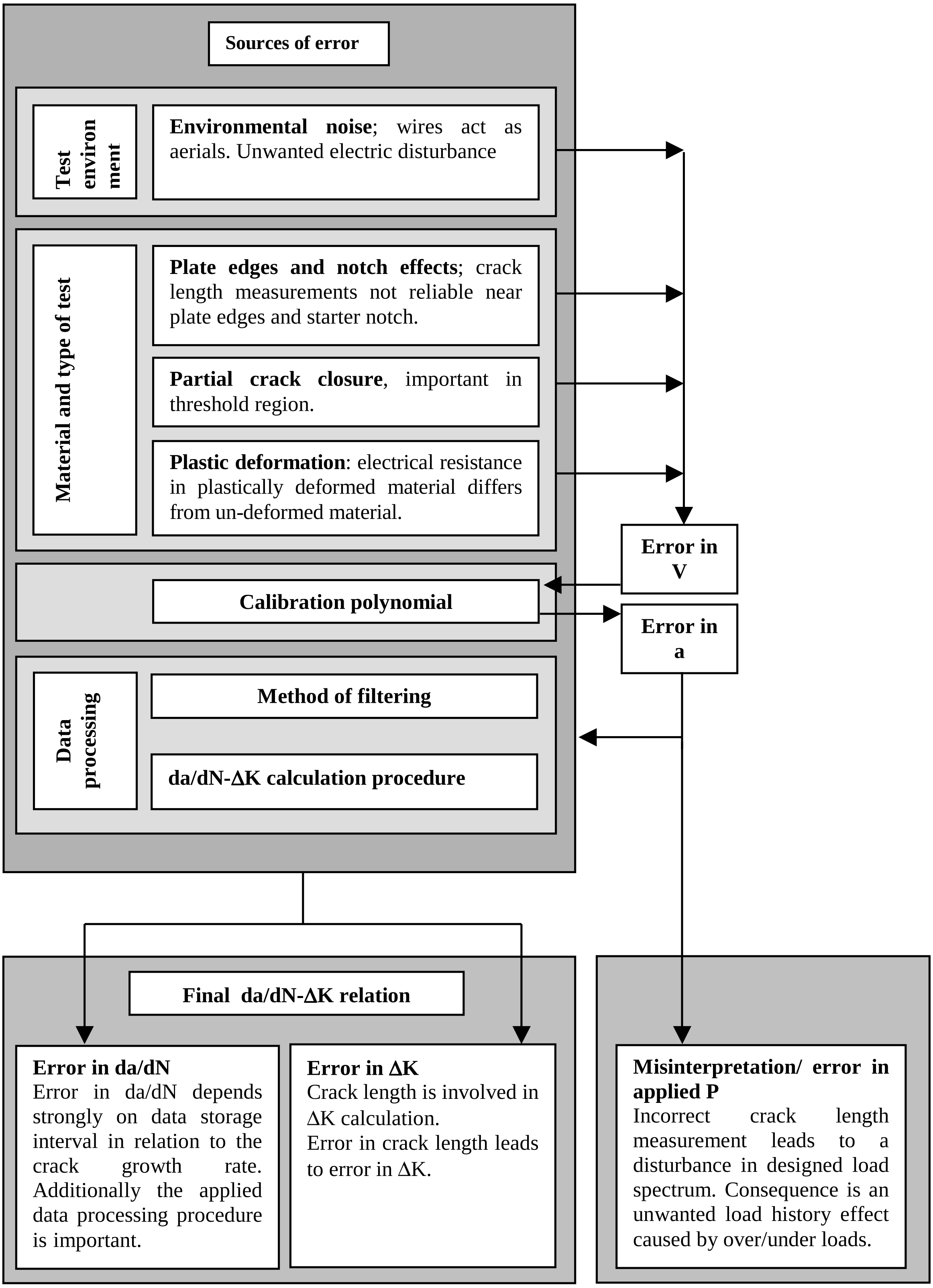

Figure 2.12. Sources of error.

2.4.2 Accuracy

The precision of the test results needs to be considered. It is difficult to give a general conclusion about the accuracy of the test configuration, the data obtained and the finally calculated results. The reason for that is the complex mix of dependent and independent variables, see figure 2.12. First, it is necessary to identify the independent and dependent variables. For example, with a constant ΔK test the crack length precision depends on the calibration accuracy, fluctuations in the measured signal and method of filtering. However, the applied load depends on the crack length precision too. Both applied load and crack length are involved in stress intensity calculations, see figure 2.8. The log(da/dN)-log(ΔK) correlation ultimately calculated is determined by the crack length because ΔK is also crack length dependent. The conclusion can be drawn that only the variable “number of cycles” is a hard, independent variable.

To avoid large errors in the final results, a general strategy to reduce the effect of unwanted noise in crack length measurements is followed. Preceding the experiments, the expected crack growth rate is estimated. The estimated crack growth rate determines the filtering technique. A compromise must be found between the capture duration and the filtering method. For example in tests with a relative high crack growth rate, e.g. at large ΔK, an average crack length based on a large number of captures is not allowed. However, at a low crack growth rate, e.g. in a ΔK threshold-test, filtering is useful. At low crack growth rates, crack length can be measured frequently without the crack length increasing substantially. This gives the possibility to perform very precise crack length measurements. For this reason results in the threshold region generally are highly reliable. Therefore, a crack length error, due to the measurement system itself, is relatively unimportant in the threshold region, provided that the optimal combination of capture duration and filtering method is chosen. However, the situation in the Paris region is different. The relatively large and increasing crack growth rate forces the use of a small capture duration time.

It will be assumed that errors in crack length are due to random noise in the potential drop signal and a systematic error in the calibration polynomial. As much data must be stored as possible. The large number of a-N data can be used to minimise the random error.

Evidently, the higher the voltage (or crack length), the larger the impact of an inaccuracy of this signal on the final error in log(da/dN)-log(ΔK), see equation (2.2).

2.5 References

[1] ASTM E 647, *Standard test method for measurement of fatigue crack growth rates,* American Society for Testing and Materials, Philadelphia, PA, USA, 2000

[2] www.matweb.com

[3] A.P. Hascaryantono, *Effects of load frequency and stress ratio on corrosion fatigue crack growth of aluminium alloy 5083-H321*, Master Thesis, Delft University, The Netherlands, 2002

[4] ASTM D 1141, *Practice for preparation of Substitute Ocean Water,* American Society for Testing and Materials, Philadelphia, PA, USA, 1998

[5] P.C.H. Ament, *Corrosion Fatigue of Structural Steel in Sea Water, Dissertation*, Delft University Press, Delft, The Netherlands, 1998

[6] M. Janssen, J. Zuidema and R.J.H. Wanhill, *Fracture Mechanics*, ISBN 90-407-2221-8, Second edition 2002

[7] Tada, Paris, Irwin, *The stress analysis of cracks handbook*, Del Research Corporation, 1986

[8] Schaum, *Statistics*, McGraw-Hill Book Company, UK, 1972

[9] F.A. Veer, *The effect of shear lips, loading transitions and test frequency on constant ΔK and constant load amplitude fatigue tests*, Dissertation, Delft University Press, Delft, The Netherlands, 1993

[10] W. G Clark Jr. and S. J Hudak Jr., *Variability in Fatigue Crack Growth Rate Testing, Journal of Testing and Evaluation*, Volume 3, No. 6, pages 454-476, 1975

[11] W. G Clark Jr. and S. J Hudak Jr., *The Analysis of Fatigue Crack Growth Rate Data, Application of Fracture Mechanics to Design*, J.J. Burke and V. Weiss, Eds, Volume 22, Plenum, pages 67-81, 1979

Chapter 3
da/dN-ΔK relations in AA 5083 for different specimen geometries

3.1 Introduction

In aluminium alloys fatigue crack growth depends on many factors. The cyclic stress intensity factor ΔK is believed to be the most important parameter to describe the fatigue crack growth rate da/dN. However, besides ΔK, the crack growth rate is influenced by other parameters, such as: the loading system (cycle shape, mean stress, frequency), the fracture mode (mode I, II, III or mixed mode), the load history (multiple and single overloads and underloads) and the environment (for example: temperature, shielding atmosphere and relative humidity) [1-3].

An important factor is the mean load. The mean load is often represented by the load ratio R (= P_{min}/P_{max}). The effect of R on the fatigue crack growth rate is ascribed to plastic deformation that accompanies fatigue crack growth. The effect is probably due to crack closure, i.e. premature contact of crack flanks before minimum load is reached, see Chapter 1, section 1.4 and figure 1.6. At large R-values no contact occurs and the full applied ΔK drives crack growth. At lower R, only part of ΔK (ΔK_{eff}) is available to cause fatigue crack growth. At the same ΔK, da/dN is higher for higher R than for lower R, due to this effect.

This chapter focuses on da/dN-ΔK relations in aluminium alloy AA 5083. The experimental work is divided into three test programs:

Test series 1

In test series 1, described in section 3.2, constant load amplitude tests are performed on AA 5083 using centre-cracked tension specimens. Crack growth rates for a wide range of different load ratios are measured. The da/dN-ΔK curves, presented on logarithmic scales, are found to be dependent on the load ratio R. The aim is to investigate the influence of R on the fatigue crack growth rate and also to determine if the slope changes between more or less linear parts of the log(da/dN)-log(ΔK) curves are a result of changes in crack closure mechanisms.

A so-called similitude approach is applied on the test data to investigate the effect of R. This approach, with ΔK as the similitude parameter, requires that:

"A similar K cycle applied to a crack in a standard specimen and to a crack in a structure of the same material, will induce the same crack length increment in both cases" [5].

Similitude is used here to compare da/dN-ΔK results at different mean stresses, i.e. at different R values. Similar conditions in general also include similar fatigue crack geometry in the same material with the same material structure and heat treatment. If these conditions are not satisfied, the similitude can be adopted only if these variables do not affect the crack extension mechanism. To satisfy these conditions as closely as possible, all tested specimens with a centre-cracked tension geometry are taken from the same batch and fatigued under the same environmental conditions.

The amount of crack closure can be quantified in two ways:

1: The effect of crack closure can be found by shifting log(da/dN)-log(ΔK) curves for different load ratios R, into one single log(da/dN)-log(ΔK_{eff}) curve. A function U of R, with U = ΔK_{eff} /ΔK is used to let the curves for different R values coincide. The principle of this procedure is shown in figure 3.1.

2: Crack closure can be measured directly by determining load-displacement curves. Load values where the crack opens and closes can be found by using this measurement technique.

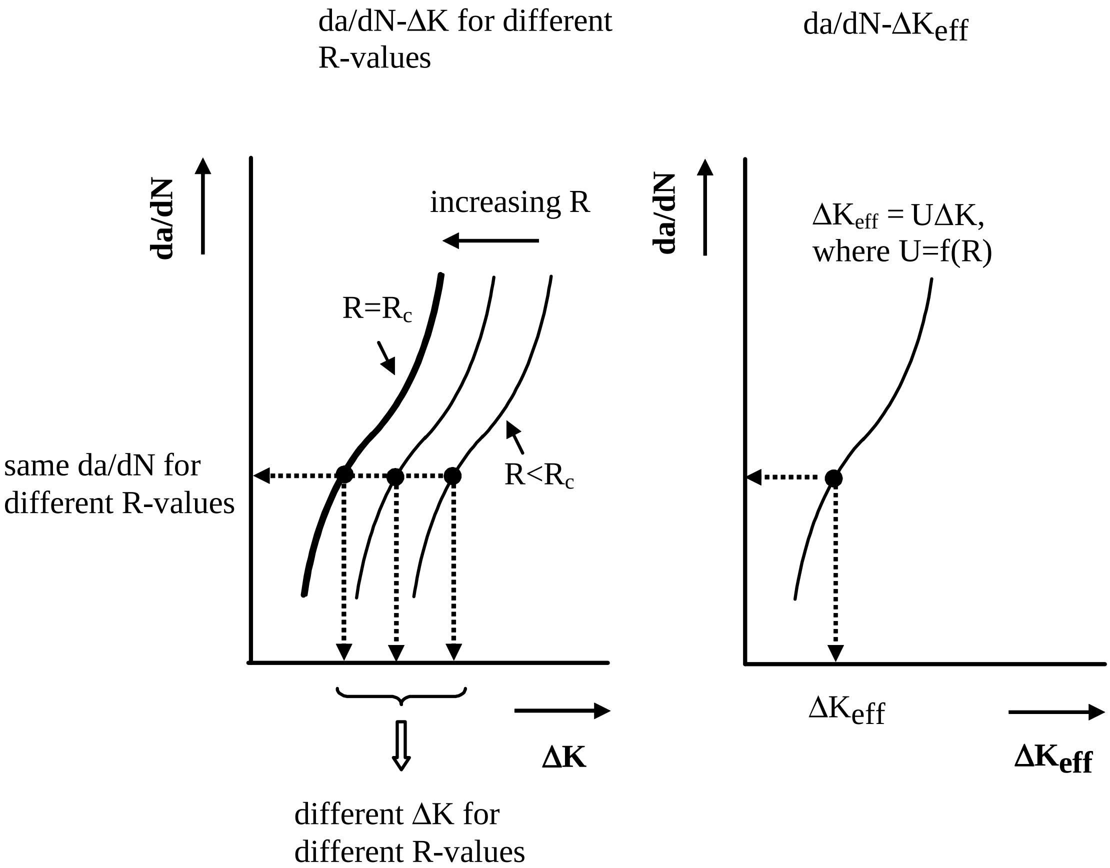

Figure 3.1. Principle of shifting da/dN-ΔK curves into one single da/dN-ΔK_{eff} curve [2]. A function U of R is used to let curves for a range of different R-values coincide into one curve of da/dN-ΔK_{eff}. At high R ($R \geq R_c$) the crack is believed to be always open and not influenced by crack closure. Thus no R effect is observed for $R \geq R_c$.

Test series 2

The amount of crack closure is possibly affected by the specimen compliance, resulting in different crack growth behaviour in specimens with different geometries [6-8]. In test series 2, described in section 3.3, constant load amplitude tests are performed on single edge-notched bend specimens, using three different R values. The results obtained are compared to the results found using the centre-cracked tension specimens.

Test series 3

In test series 3, described in section 3.4, direct crack closure measurements are performed on 3 different specimen geometries: centre-cracked tension, compact tension and single edge-notched bend specimens, in order to find a possible effect of compliance on crack closure. These geometries have been chosen because of the large differences in compliance. Load-displacement curves, or more specifically crack opening/closing loads, are compared at different crack growth rate regimes. An overview of all tests is given in table 3.1.

Table 3.1 Overview of test series 1, 2 and 3

	Measurement type	**Purpose**	**Results**
Test series 1	Constant load amplitude tests on centre-cracked tension specimens, using a range of different R values	To calculate a da/dN-ΔK relation and an R dependent U function	Comparison between U-values obtained from similitude approach and U values obtained from direct crack closure measurements for the centre-cracked tension specimen geometry
	Load displacement / crack closure measurements on centre-cracked tension specimens, using 3 different R values	To obtain $K_{closure}$ levels and U-values for centre-cracked tension specimens at different R-values	
Test series 2	Constant load amplitude tests on single edge-notched bend specimens, using 3 different R values	To obtain (da/dN)-(ΔK) relations for single edge-notched bend specimens	Comparison between U-values and crack growth rate for centre-cracked tension and single edge-notched bend
Test series 3	Load displacement/crack closure measurements on centre-cracked tension, compact tension and single edge-notched bend specimens. Measurements are performed in 3 crack growth rate regimes	To obtain $K_{closure}$ levels for centre-cracked tension, compact tension and single edge-notched bend specimens at different R -values and different crack growth rates	Influence of specimen compliance on da/dN in different crack growth rate regimes

The work presented in this chapter is a joint Dutch, Ukrainian and Japanese cooperation. Part of the experimental work has been performed at TU Delft, department of Materials Science and Engineering, the Netherlands and part at the Karpenko Physico-Mechanical Institute, Lviv, the Ukraine.

3.2 Centre-cracked tension specimen

3.2.1 Experimental set-up for constant load amplitude tests in centre-cracked tension specimens

Different series of constant load amplitude tests are carried out on centre-cracked tension specimens of AA 5083, using a range of different R values. The aim of these tests is to examine the influence of the load ratio R on fatigue crack growth rate da/dN and also to find the critical value of R (= R_c) above which no closure can be detected. The fatigue crack growth measurements are performed on a computer-controlled servo-hydraulic fatigue testing machine.

Crack length was measured using a pulsed direct-current potential drop measurement system. A test frequency of 10 Hz was chosen since no frequency effects on da/dN-ΔK were found in the range of 5-40 Hz [9].
The environment was lab air with a relative humidity of 35-45%. The dimensions of the centre-cracked tension specimens are a length of 340 mm, a width of 100 mm and a thickness of 8 mm. All specimens were fatigued until failure. Data was analyzed using the procedures given in ASTM E647 [10].

3.2.2 Results of constant load amplitude tests in centre-cracked tension specimens

Results of the fatigue crack growth tests are shown in figures 3.2 and 3.3. Figure 3.2 presents the results of the constant load amplitude tests, figure 3.3 shows the da/dN-ΔK curve for R = 0.1 from threshold until failure. For this latter curve, three constant load amplitude tests are combined with a decreasing ΔK test in order to show the da/dN-ΔK behaviour from the near threshold area until the very high value of da/dN near instability. At a crack growth rate of 10^{-4} μm/c, a threshold value ΔK_{th} of about 2 MPa√m is found. On the basis of K_{max} at failure, a critical K value, i.e. K_c, of about 42 MPa√m is found from the test data, which corresponds to data found in the literature [11].

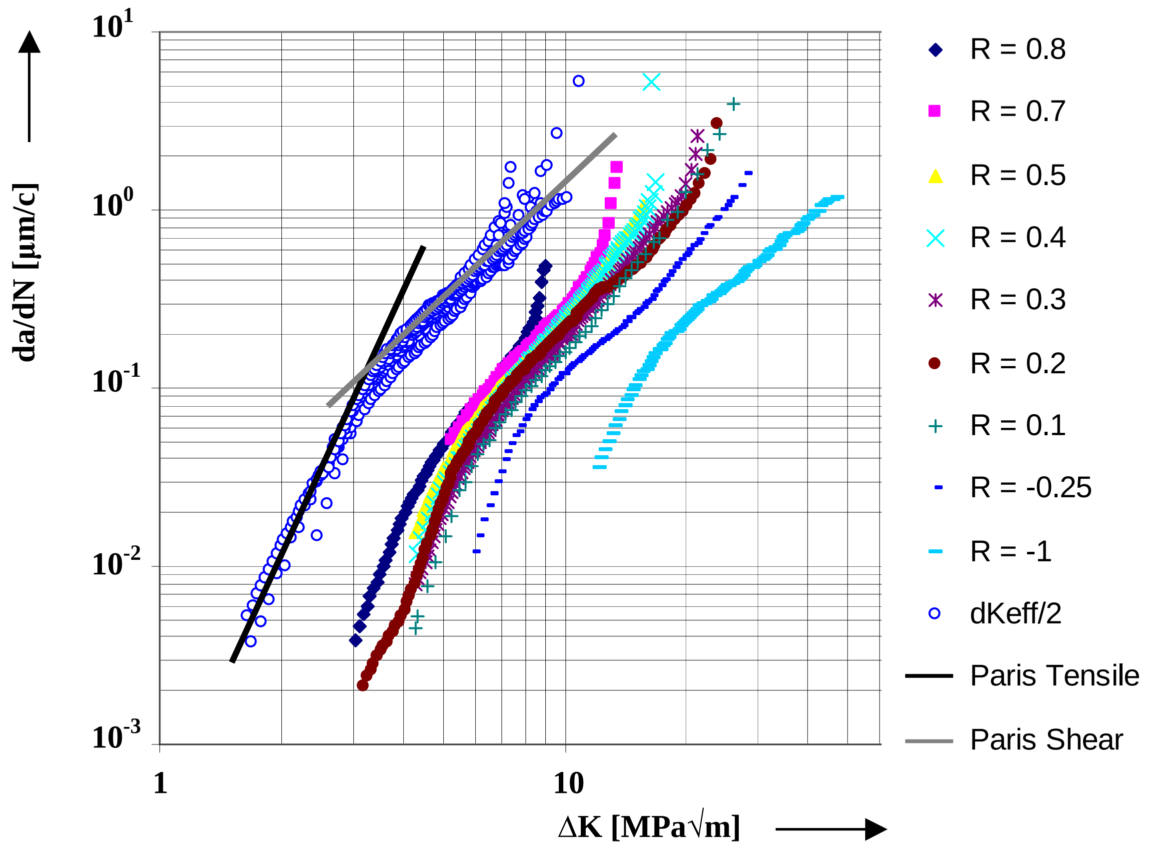

Figure 3.2. Results of constant amplitude tests on AA 5083 at different values of R. A parallel shift by a factor 2 to the left is applied to the ΔK_{eff} curve to show the result better.

It is suspected that a change in slope of the log(da/dN)-log(ΔK) curve, generally indicates a change in crack growth mechanism. In figure 3.3 five slope transitions, T1-T5, in log (da/dN)-log (ΔK) are shown. The first transition point, T1, takes place just above the threshold-value at a crack growth rate of about 10^{-3} μm/c, while T2 takes place at about 0.5 10^{-3} μm/c. The change in slope at about 10^{-1} μm/c, T3, can probably be attributed to a different crack closure situation due to the start of shear lip development. It is believed that besides plasticity induced crack closure the presence of shear lips will lead to an additional amount of closure. In the crack growth range below T3, where the crack shows no shear lips yet and is still flat, the so-called tensile mode, there is only plasticity induced crack closure. Above T3, where shear lips develop, a superposition of two closure mechanisms is assumed; i.e. plasticity induced crack closure plus crack closure due to shear lips.

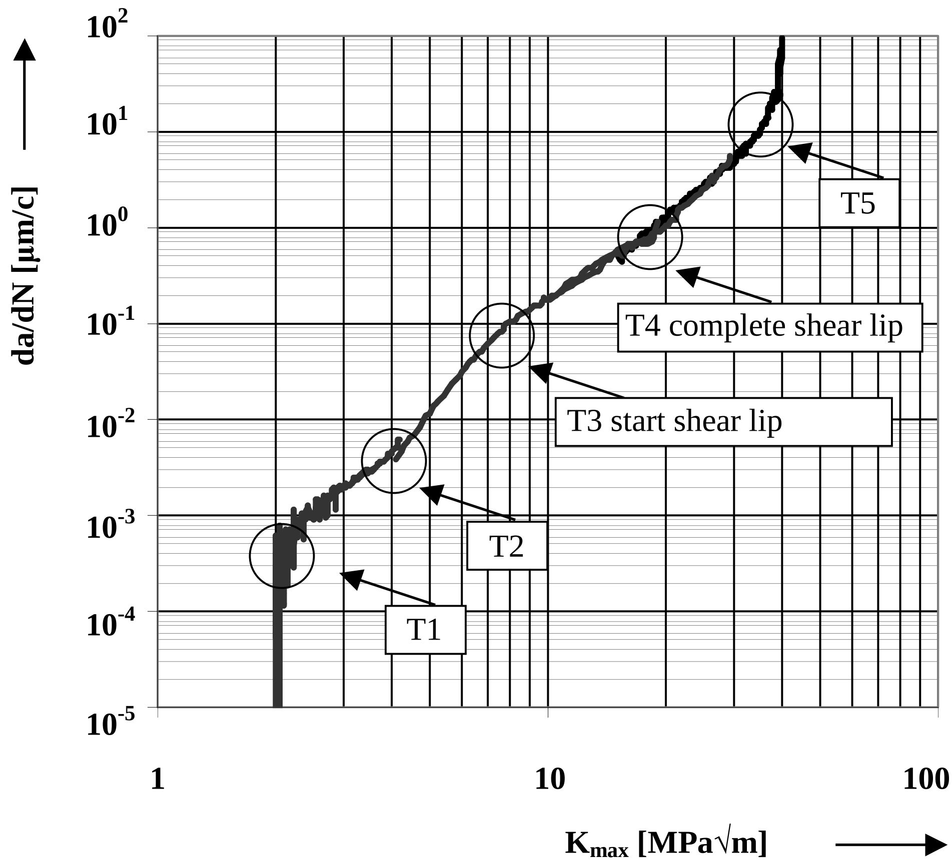

Figure 3.3. Experimental fatigue crack growth rate results for AA 5083 at R=0.1.

The latter can be attributed to a mismatch of shear lips for closing crack flanks. The completeness of the development of shear lips depends on the thickness of the specimen, or on ΔK_{eff} for incomplete shear lips [12]. The shear lip is fully developed at transition point T4. The subject of shear lips will be extensively addressed in Chapter 4. From transition point T5 until failure, crack growth accelerates dramatically. In this high ΔK region crack advance is no longer determined by pure fatigue, but due to high the K_{max} values, static effects, i.e. instable crack growth, becomes important.

3.2.3 Crack closure relation in centre-cracked tension specimens using the similitude approach

Calculation procedure

A special computer program was written in order to let the log(da/dN)-log(ΔK) curves for a range of different R-values coincide into one general curve of log(da/dN)-log(ΔK_{eff}). The effective stress intensity factor, ΔK_{eff} (= UΔK) is obtained by using a quadratic closure function U, as proposed by Schijve [13]. The crack closure function $U = a+bR+cR^2$ is found by taking a large number of combinations of a, b and c, within certain boundaries, and calculating ΔK_{eff} for all measurement points of the tests.

In general more solutions for U are possible. A single solution for U can be found by adding a constraint to the problem. The da/dN-ΔK results in figure 3.2 show that the curves for $R \geq 0.5$ are about the same, except at very high values of K_{max}, where "static" fracture mechanisms are becoming important. This coincidence of curves with $R \geq 0.5$ means that crack closure is not important or does not exist, above R = 0.5. It is thus assumed that $R_c = 0.5$, is the limiting R-value above which no crack closure exists, and thus U = 1 for all $R \geq R_c$. This critical R value was confirmed experimentally by performing more tests in the expected critical R range.

Based on the assumption that U = 1 for $R = R_c$, a constraint is added to the calculation procedure: it is assumed that there is a dependency between coefficients a, b and c. The c value used is considered to be dependent of a and b and taken as $c = (1 - a - R_c \cdot b) / R_c^2$. For each combination on a and b, a power law expression of the type $da/dN = C\Delta K_{eff}^m$ is fitted through all da/dN-ΔK_{eff} points. Using a step size in a and b of 0.01 this has been done 40000 times for all crack growth data and each crack growth regime separately.

Besides using $\Delta K = K_{max} - K_{min}$, the calculations are also performed using $\Delta K = K_{max}$ for R < 0 (ASTM E 647 recommendation [10]).

The combination of a and b that yields a maximum correlation coefficient, based on a linear relation between log(da/dN) and log(ΔK_{eff}), is considered to be the optimal combination. Results are validated occasionally by repeating the calculations with a smaller step size of 0.001.

All data

The results for all da/dN-ΔK curves, i.e. calculated for all data points at different R values, are shown in table 3.2, both in terms of U and da/dN-ΔK_{eff}. The resulting da/dN-ΔK_{eff} points are shown in figure 3.2. A parallel shift by a factor 2 to the left is applied to show the result better. Note that by adopting U = 1 for R = 0.5 means that the da/dN-ΔK_{eff} relation can be found without a crack closure calculation, because it is equal for all coinciding da/dN-ΔK relations for $R \geq 0.5$. The calculation is only needed for finding the U expression, because then the da/dN-ΔK_{eff} relation can be found for all R-values.

Two crack growth regimes: tensile area and growing shear lip area

The computer program can also be used to correlate different crack growth rate regimes of the measured da/dN-ΔK curves separately. The calculation is performed for the tensile mode and the growing shear lip regime of the measured da/dN-ΔK curves separately, see table 3.2 for the results. No result is calculated for data points above 1 μm/cycle, because not enough data were available in this crack growth rate regime. Almost the same U expression is found for the two parts of the da/dN-ΔK_{eff} curves, $U = 0.79+0.4R+0.04R^2$ and $U = 0.81+0.37R+0.02R^2$ for the tensile and growing shear lip regimes respectively, see figure 3.4.

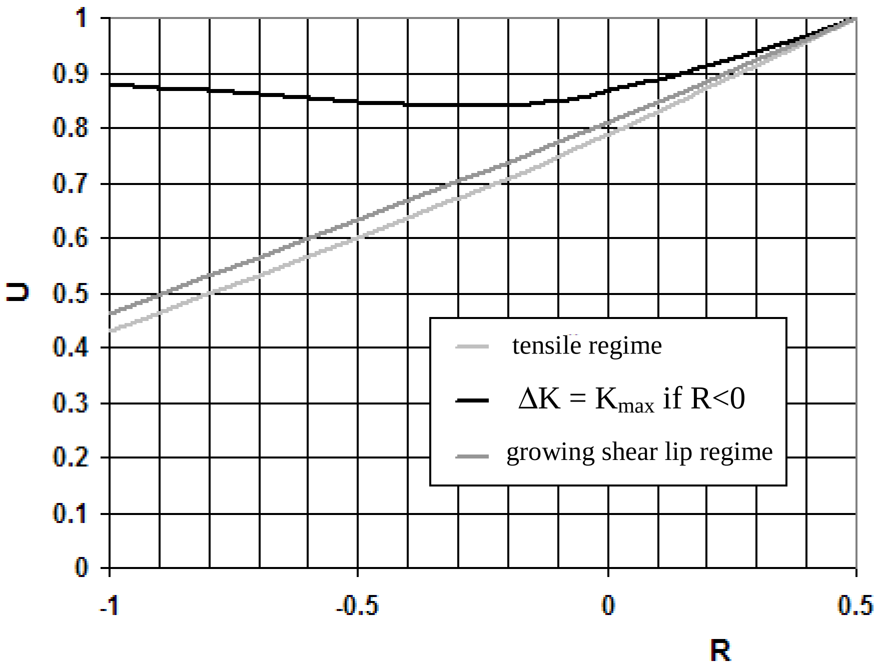

Figure 3.4. U relations in tensile mode and growing shear lip regimes.

Four additional fatigue tests at different R values were performed and data is used for validation of the calculated crack closure relations. When the calculated U (R) relation is used, the resulting da/dN-ΔK_{eff} curves of the 4 additional tests fall into the same scatter band as found by the previous calculations for da/dN-ΔK_{eff}.

All data with $\Delta K = K_{max}$ if $R<0$

In the foregoing calculations the full ΔK is used, also for negative R values. The reason is that a negative K_{min} theoretically can have influence on the resulting crack closure relations. For the sake of completeness the calculations are also performed for the condition that $\Delta K = K_{max}$ if $R < 0$. This implies that the compressive part of the loading cycle has no influence on the crack growth rate. Using all da/dN-ΔK curves, relations for U and da/dN are calculated, see table 3.2. The calculated da/dN-ΔK_{eff} relation is almost the same as without the restriction that $\Delta K = K_{max}$ if $R < 0$, but U is different. For R = 0.1 it is now found that U = 0.89, while without this restriction it was found earlier that U = 0.83. It is not clear which expression for U describes crack closure better. However there is a slight tendency for a better correlation when the full $\Delta K = K_{max}–K_{min}$ is used in the calculation. Probably other types of crack closure evaluation, can give more information. The next section deals with such crack closure measurements.

Table 3.2 da/dN-ΔK_{eff} relations and U (R) relations for AA 5083 in different crack growth rate regimes, da/dN in μm/c, ΔK_{eff} in MPa√m

	U (R) found by similitude =	**"Paris eq." da/dN =**	**U at R = 0.1 (measured)**	**U at R = 0.1 (similitude)**
All data	$0.79+0.40R+0.04R^2$	$0.4\times10^{-4}\,\Delta K_{eff}^{2.81}$	----	0.83
All data with $\Delta K = K_{max}$ if $R<0$	$0.87+0.17R+0.18R^2$	$0.4\times10^{-4}\,\Delta K_{eff}^{2.79}$	----	0.89
Tensile mode regime below T3	$0.79+0.40R+0.04R^2$	$0.3\times10^{-4}\,\Delta K_{eff}^{4.22}$	0.83	0.83 at da/dN = $3\ 10^{-2}$ μm/c
Growing shear lip regime T3-T4	$0.81+0.37R+0.02R^2$	$17.5\times10^{-4}\,\Delta K_{eff}^{2.18}$	0.85	0.85 at da/dN = $1.3\ 10^{-1}$ μm/c
Stabilized shear lip regime above T4	-----	----	0.86	----

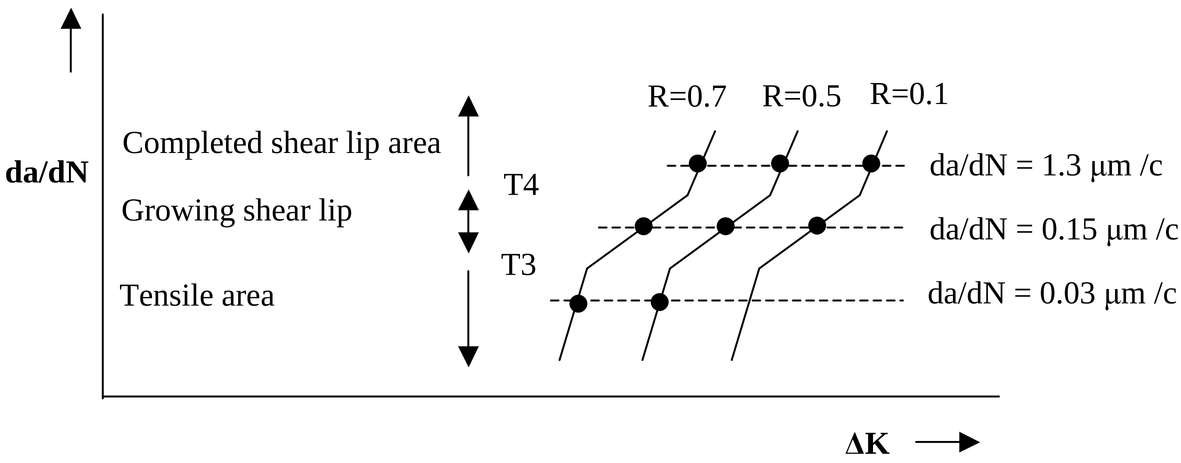

Figure 3.5. Scheme of different crack growth regimes.
Nine specimens are pre-cracked to 3 different crack growth rates at three different R-values.

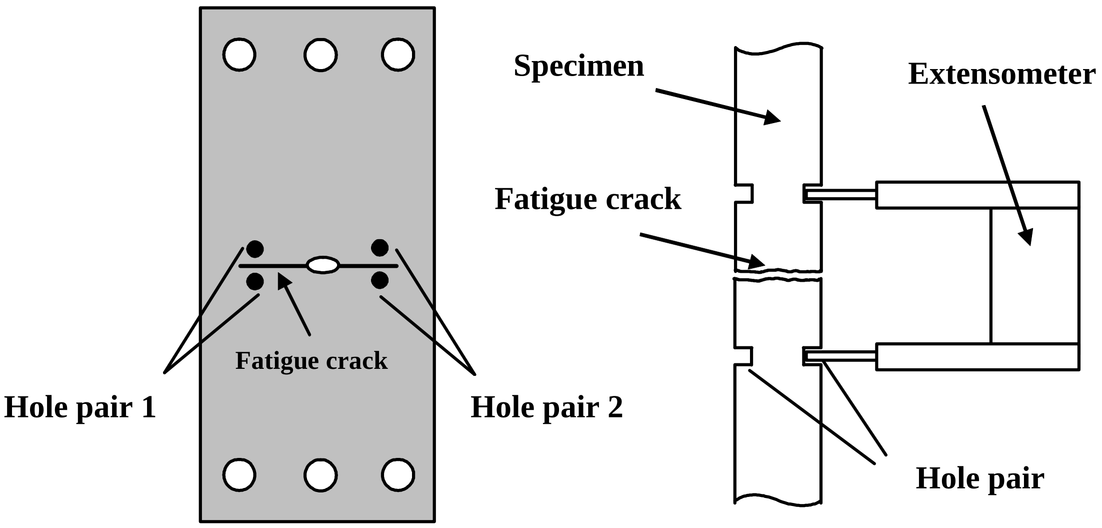

Figure 3.6. Holes of 1 mm diameter are drilled into the specimen to a depth of 0.5 mm. These holes are for fixing the extensometer. The holes are drilled close to both crack tips at both sides of the specimen, i.e. four pairs of holes per specimen.

3.3 Crack closure measurements using load displacement curves

3.3.1 Experimental set-up for load displacement measurement in centre-cracked tension specimen

Nine centre-cracked tension specimens were fatigue loaded with a constant stress amplitude using R values of 0.7, 0.5 and 0.1 respectively. Direct crack closure measurements were performed on these specimens, based on measuring compliance. The fatigue crack growth was interrupted at the moments that crack growth rates of $3x10^{-2}$ μm/cycle (tensile area), $1.5x10^{-1}$ μm/cycle (growing shear lip area) or 1.3 μm/cycle (stabilized shear lip area) were reached, see figure 3.5.

The crack opening or closing load levels were found by measuring displacements as a function of the applied load at both sides of each crack tip, in total 4 per specimen, see figure 3.6. Note that the distribution of crack closure is not necessarily uniform over the entire cross section of the specimen and for this reason the measured opening and closure points have a local character.

An example of a load displacement curve for R = 0.1 is shown in figure 3.7.

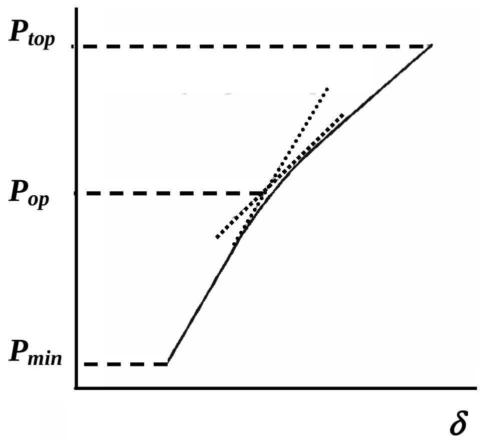

$$U = (P_{max} - P_{op}) / (P_{max} - P_{min})$$

Figure 3.7. Load displacement scheme. The two tangent lines are drawn and the intersection point of these two lines is defined as P_{op}. P_{top} is 15% less than P_{max} for the preceding fatigue crack growth cycle.

During a number of cycles load and displacement were recorded simultaneously. P_{op} is defined as the intersection of the two lines tangent to the load displacement curve at higher and lower load respectively. This corresponds to the load where the crack just becomes fully open at increasing load or starts closing at decreasing load. The maximum load applied during the load-displacement measurements, P_{top}, is kept 15% lower than the maximum value of the preceding fatigue load in order to avoid effects of the measurement on the crack closing load. The calculated values for the crack opening load, P_{op}, are averaged. Characteristic hysteresis loops for three R values are shown in figure 3.8.

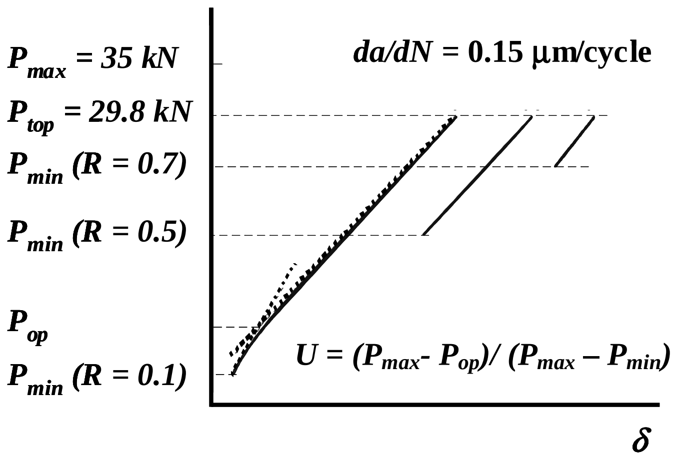

Figure 3.8. Load displacement curves for three R-values.

3.3.2 Results of load displacement measurements for centre-cracked tension specimen

For R values of 0.7 and 0.5 a linear load displacement relation is found between P_{min} and P_{top}. At these R values, the crack does not close before the minimum load is reached, see figure 3.7. This means that crack closure is absent for R ≥ 0.5 in the measured ΔK range. This observation is in agreement with the fatigue test results, see figure 3.2. For R = 0.1, the load displacement curve is not entirely linear; a crack closure effect is found.

The results for U = $(P_{max}–P_{op})/(P_{max}–P_{min})$ are given in table 3.2 for the three crack growth rate regimes tested. The differences between the measured U values for the three crack growth rate regimes are small. This means that the crack closure level is about constant over the whole da/dN-ΔK range tested. Even closure levels that are measured in the growing shear lip regime, do not differ from those found at higher and lower crack growth rates. The shear lips that develop in AA 5083 have a smooth appearance, suggesting that an additional crack closure contribution due to the development of smooth shear lips is absent.

The crack closure levels for the tensile and the shear lip regime, measured using either the compliance method or the crack growth rate method show good agreement, see table 3.2. However this agreement is remarkable. From the literature [14-17], it is clear that crack closure behaviour is influenced by specimen thickness. Closure is suspected to be more important in thin specimens, due to the predominant plane stress state. With increasing specimen thickness or decreasing stress intensity factor, the role of the lateral surfaces becomes less important. The stress state then changes from plane stress to plane strain. Since the distribution of crack closure is not necessarily uniform over the entire cross section of the specimen, the measured opening and closure loads are related to local phenomena. For this reason different U values were expected for direct crack closure measurements using compliance (section 3.3.1) and closure measurements using fatigue crack growth rates (section 3.2.3). In the latter case the crack growth rate da/dN is a measure for the closure. Closure found in this way probably represents an average over the cross section.

3.4 Other specimen geometries

3.4.1 Comparison of fatigue crack growth in centre-cracked tensile and single edge-notched bend specimens

Initial fatigue crack growth experiments were performed on centre-cracked tension specimens at TU Delft. Tests were carried out at a frequency of 25 Hz in lab air, with a relative humidity of 35-45 %. Crack length was measured using a pulsed direct-current potential drop measurement system. After pre-cracking these centre-cracked tension specimens, single edge-notched bend specimens were cut out at the Karpenko Physico-Mechanical Institute, Lviv, Ukraine. Subsequently, fatigue crack growth rates for R = 0.1, 0.5 and 0.7 were measured in these single edge-notched bend specimens. The dimensions of the specimens are given in figure 3.9.

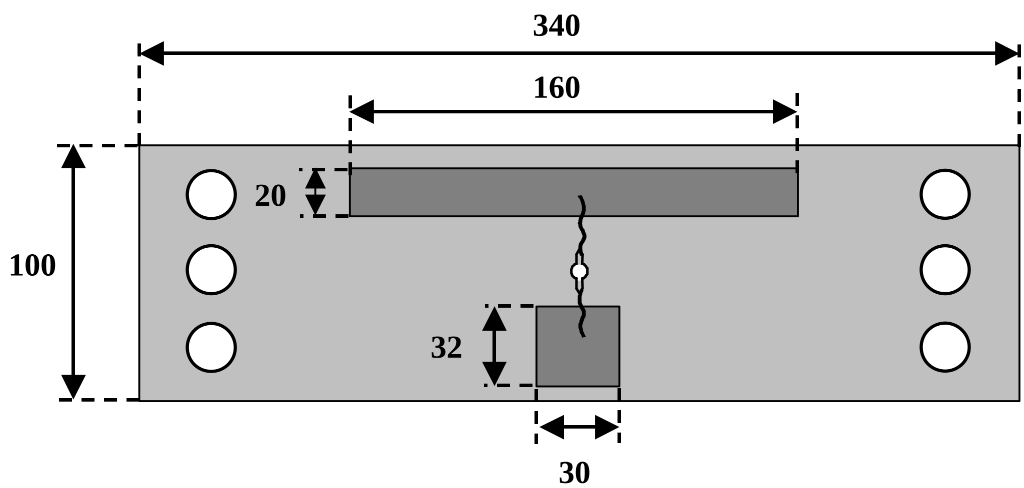

Figure 3.9. Cutting of compact tension and single edge-notched bend specimens. Compact tension and single edge-notched bend specimen geometries are pre-fatigued in centre-cracked tension geometry and afterwards cut out of the original specimen.

The crack length on the single edge-notched bend specimens was measured on both lateral surfaces by using an optical microscope with a resolution of 0.01

mm. An additional calibration of the crack length had to be performed for these single edge-notched bend specimens, because it was observed that the propagating crack front became irregular, i.e. the crack length varied along the thickness. Therefore, for a number of samples the fatigue crack growth was stopped at different crack lengths, and thus different ΔKs. They were subsequently broken and the average crack length along the fatigue crack front was measured. On the basis of these results a crack length correction factor was introduced.

Results of the fatigue tests are shown in figures 3.10a and 3.10b, where ΔK and ΔK_{eff} are plotted for centre-cracked tension and single edge-notched bend geometries respectively. The results for R = 0.5 are not shown: the measured curves coincide with that for R = 0.7. For both geometries a significant effect of the stress ratio on the fatigue crack growth rate is observed. This indicates that crack closure is probably responsible for differences in crack growth rate at R = 0.1 and R = 0.7.

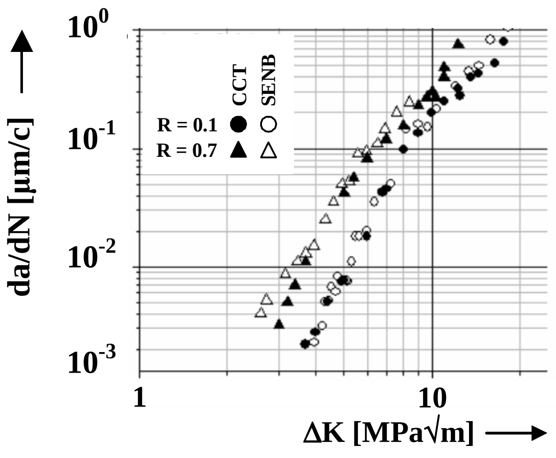

Figure 3.10a. Fatigue crack growth rate da/dN versus ΔK in centre-cracked tension and single edge-notched bend specimens.

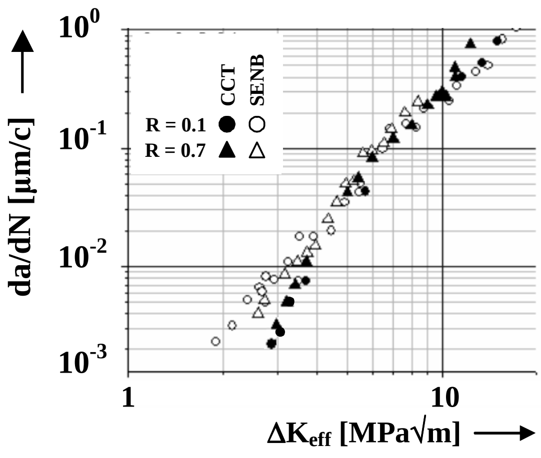

Figure 3.10b. Fatigue crack growth rate da/dN versus ΔK_{eff} in centre-cracked tension and single edge-notched bend specimens.

Comparison of the da/dN – ΔK_{eff} curves for the different geometries, see figure 3.10b, shows no effect in the crack growth rate range between 10^{-1} till 10^{0} μm/c. Near the threshold region, i.e. for da/dN < 10^{-2} μm/c, a tendency towards higher crack growth rates is observed for single edge-notched bend samples. Figure 3.11 provides a closer look at the K_{max} and $K_{closure}$ values in this region. Note that in this investigation the centre-cracked tension samples were tested in lab air at a relative humidity of 35-45 % (in the Netherlands), while the single edge-notched bend specimens were tested at a relative humidity of 70-85% (in the Ukraine).

It is well known from the literature [18-20] that fatigue crack growth in aluminium alloys is sensitive to the environment. Moist air can be considered as an aggressive environment for AA 5083.

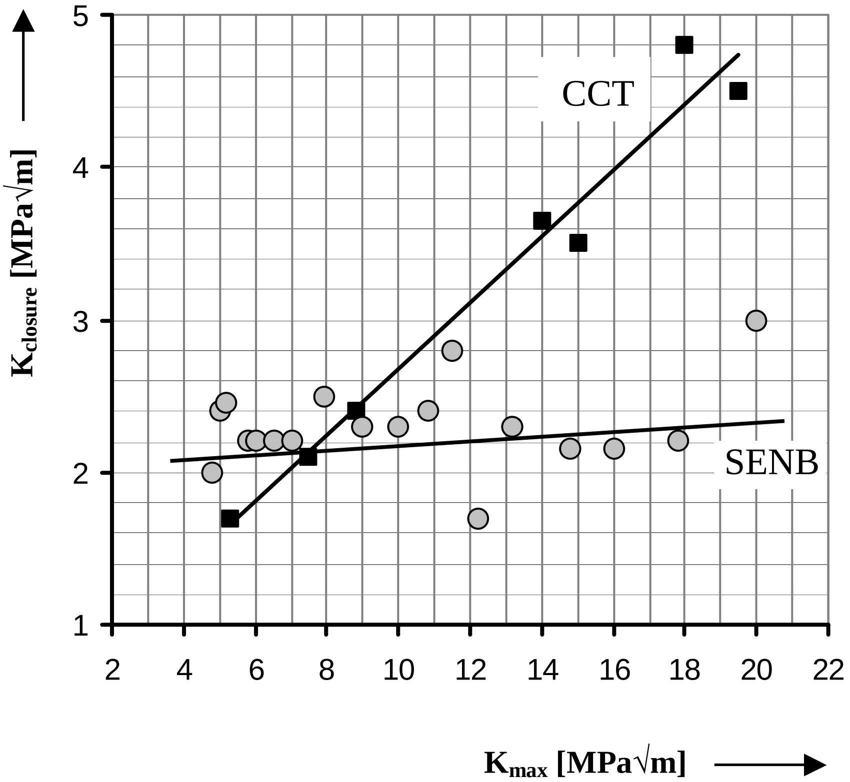

Figure 3.11. K_{max} and $K_{closure}$ values for centre-cracked tension and single edge-notched bend specimen geometry at R=0.1, measured using the compliance method.

The impact of environmental attack, which in general will be more pronounced at relatively low crack growth rates, increases with humidity. A higher relative humidity leads to an increase in fatigue crack growth rate. At higher rates such an effect is not observed.

3.4.2 Load displacement for three different geometries

Direct crack closure measurements using compliance were performed on centre-cracked tension, compact tension and single edge-notched bend samples. All samples were pre-cracked in the centre-cracked tension specimen geometry and afterwards cut out of the original sample according to figure 3.9. P_{op} values were measured for R = 0.1, 0.5 and 0.7 in the 3 crack growth regimes: tensile, growing shear lip and stabilized shear lip, see figure 3.5.

In the cases of R = 0.5 and R = 0.7, the crack did not close before the minimum load used in the preceding crack growth was reached, i.e. $K_{min} > K_{op}$, for this reason P_{op} values were measured below P_{min}.

Figure 3.12 shows the results of the measurements performed on the samples of the three different geometries. A linear dependency of K_{op} on K_{max} is found. K_{op} increases with increasing K_{max}. Results for the crack closure parameter U for R = 0.1 are summarized in table 3.3.

Table 3.3: U values for different specimen geometries at different crack growth rate regimes, measured using compliance, R = 0.1

	centre-cracked tension	compact tension	single edge-notched bend
Tensile mode regime	0.83	0.86	0.83
Growing shear lip regime	0.85	0.87	0.90
Stabilized shear lip regime	0.86	0.87	0.95

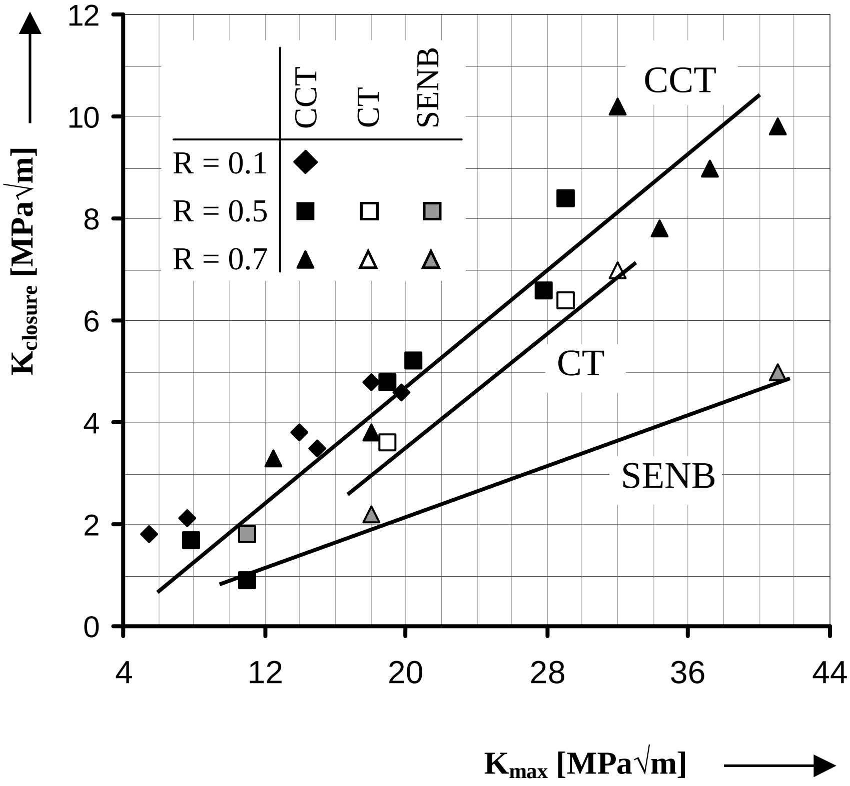

Figure 3.12. K_{max} and K_{closue} – values for centre-cracked tension, compact tension and single edge-notched bend specimen geometry at different R-values.

3.5 Discussion and conclusions

Crack closure relations

The crack closure relation obtained by similitude for the tensile mode regime is $U = 0.79+0.40R+0.04R^2$, as was already indicated in table 3.2. For the growing shear lip regime $U = 0.81+0.37R+0.02R^2$. These U formulae are almost identical, e.g. for R = 0.1 it can be calculated that U = 0.83 and U = 0.85, respectively.

Thus both measurement methods give about the same result for U for R = 0.1 in both crack growth regimes. However the slope of the da/dN-ΔK_{eff} curve (on a double logarithmic scale) is very different for the two regimes, i.e. 4.22 and 2.18 respectively. Both “Paris lines” are also shown in figure 3.2. Because the U functions are almost the same in both regimes, the differences in crack growth behaviour in the tensile and shear lip regimes can not be attributed to differences in crack closure behaviour. This means that shear lips do not have a separate closure contribution. If there is crack closure, then this will be the same in the shear lip and the tensile regimes. The closure mechanism is probably only based on residual plastic deformation along the crack flanks, i.e. plasticity induced crack closure, in both regimes.

This latter conclusion is also confirmed by tests with side grooves along the crack path, see Chapter 4. There it is shown that shear lips in AA 5083 do not have any effect on the crack growth rate. Furthermore, slope changes, as shown in figure 3.2, occurred to an equal extent in fatigue crack growth tests performed on specimens with and without shear lips. Since additional crack closure due to shear lips can be ruled out as a possible cause for the different crack growth rate behaviour in the two crack growth rate regimes, there must be another reason for this behaviour. Because shear lips do not affect the crack growth rate in this alloy, it has to be concluded that shear lips are not the cause of retarded crack growth rate above T3, but that both the occurrence of shear lips and the retarded crack growth rate are the consequence of another (micro) mechanism that has to be found yet.

Specimen geometry

There seems to be a relation between the specimen compliance and the degree in which crack closure depends on the crack growth rate regime, see Table 3.3. The three geometries can be ranked in the order of decreasing compliance according to single edge-notched bend – compact tension – centre-cracked tension. In this same order they show a decreasing closure dependency. For the centre-cracked tension and the compact tension specimens, U is constant over a large ΔK range.

At plane strain conditions, i.e. at lower ΔKs, the da/dN – ΔK curves are invariable for the different geometries. However, at higher ΔK, a difference in U-values is found for the centre-cracked tension and single edge-notched bend geometry. This is thought to be due to the fact that crack closure is determined not only by the situation close to the crack tip, but also by crack face contact at locations behind the crack tip. Crack opening angles at a given K are different for the different specimen geometries, see figure 3.13. Since the faces have contact over a finite distance behind the crack tip, the part of the loading cycle during which the crack is opened, in case plasticity induced crack closure is significant, can expected to be larger for a specimen with a larger compliance. Thus at higher ΔK the amount of crack closure depends on the specimen geometry.

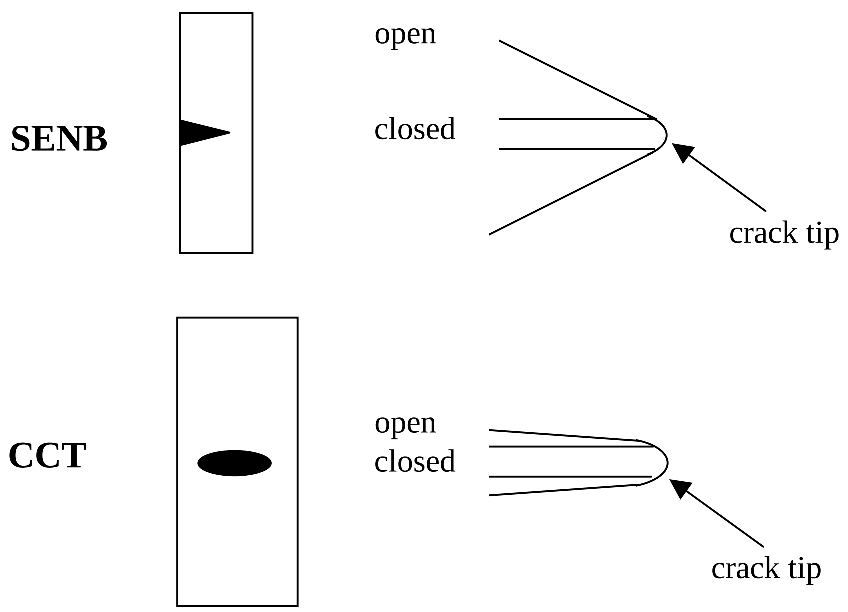

Figure 3.13. Different crack opening angles in single edge-notched bend and centre-cracked tension geometry due to a difference in compliance.

References

[1] M. Janssen, J. Zuidema and R.J.H. Wanhill, *Fracture Mechanics*, ISBN 90-407-2221-8, Second edition 2002

[2] R.C. McClung, J.C. *Newman, Advances in Fatigue Crack Closure Measurement and Analysis*, ASTM STP 1343, ISBN 0-08031-2611-5, Aug 1999

[3] J.C. Newman, Elber, *Mechanics of Fatigue Crack Closure*, ASTM, STP 982, June 1988

[4] J. Schijve, *Fatigue of Structures and Materials*, ISBN10: 0792370147, Kluwer Academic Publishers, The Netherlands, 2001

[5] J. Schijve, *Four Lectures on Fatigue Crack Growth, Part III: Fatigue Cracks, Plasticity Effects and Crack Closure*, Engineering Fracture Mechanics, Volume 11, pages 167-221, 1979

[6] H.M. Nykyforchyn, *On the ambiguities of the parameters of fatigue crack growth and stress corrosion cracking*, Fracture Mechanics, Strength and Integrity of Materials, eds. O.M. Romaniv and S.Ya. Yarema, pages 84-94, 1996

[7] C. K. Clarke and G. C. Cassatt , *A study of fatigue crack closure using electric potential and compliance techniques*, Engineering Fracture Mechanics, Volume 9, Issue 3, pages 675-688, 1977

[8] A. M. Abdel Mageed, R. K. Pandey and R. Chinadurai, *Effect of measurement location and fatigue-loading parameters on crack closure*

behaviour, Materials Science and Engineering A, Volume 150, Issue 1, pages 43-50, 20 February 1992

[9] A.P. Hascaryantono, *Effects of load frequency and stress ratio on corrosion fatigue crack growth of aluminium alloy 5083-H321*, Master Thesis, Delft University, The Netherlands, 2002

[10] ASTM E 647, *Standard test method for measurement of fatigue crack growth rates*, American Society for Testing and Materials, Philadelphia, PA USA, 2000

[11] www.matweb.com

[12] J. Zuidema, *Square and Slant Fatigue Crack Growth in Al 2024*, ISBN 90-407-1191-7, 177 pages, Dissertation, Delft University Press, Delft, The Netherlands, 1995

[13] J. Schijve, *Some Formulas for the Crack Opening Stress Level*, Engineering Fracture Mechanics, Volume 14, pages 461-465, 1981

[14] F.A. Veer, J. Zuidema, P.A. Houdijk, *The effect of specimen thickness during constant fatigue testing of S355 construction steel*, Proceedings of the 8th International Fatigue Conference, Volume 1/5, Stockholm, 2002

[15] J. D. M. Costa and J. A. M. Ferreira, *Effect of stress ratio and specimen thickness on fatigue crack growth of CK45 steel*, Theoretical and Applied Fracture Mechanics, Volume 30, Issue 1, pages 65-73, September 1998

[16] D. S. Dawicke and A. F. Grandt, Jr J. C. Newman, Jr, *Three-dimensional crack closure behaviour*, Engineering Fracture Mechanics, Volume 36, Issue 1, pages 111-121, 1990

[17] W. J. Mills and R. W. Hertzberg, *The effect of sheet thickness on fatigue crack retardation in 2024-T3 aluminum*, Engineering Fracture Mechanics, Volume 7, Issue 4, pages 705-708, 1975

[18] S. Suresh, G.F. Zamiski, R.O. Ritchie, *Oxide-induced crack closure: an explanation for near-threshold corrosion fatigue crack growth behaviour,* Metallurgical and Materials Transactions, Volume 12A, pages 1435-1443, 1981

[19] J. Ruiz and M. Elices, *Effect of water vapour pressure and frequency on fatigue behaviour in 7017-T651 aluminium alloy plate,* Acta Materialia, Volume 45, Issue 1, pages 281-293, January 1997

[20] H. L. Ewalds, *The effect of environment on fatigue crack closure in aluminium alloys*, Engineering Fracture Mechanics, Volume 13, Issue 4, pages 1001-1007, 1988

Chapter 4

Shear Lips in AA 2024 and AA 5083: Linear Side Grooves

4.1 Introduction

A major development in the description of fatigue crack growth was the notion that the fracture mechanics parameter K can be used as a controlling parameter. This resulted in the well-known Paris power-law relation, $da/dN = C\Delta K^m$, where $\Delta K = K_{max} – K_{min}$ and C and m are experimentally determined scaling constants describing the material's crack growth behaviour [1]. Over a large crack growth rate range it is possible to linearly relate the logarithm of fatigue crack growth rate, log(da/dN) with the logarithm of the driving stress intensity range, ΔK. However some changes occur in this linear relation, leading to several parts with different slopes, see figure 4.1. The transitions T1-T5 indicate slope changes, which are associated with changes in the crack growth mechanism.

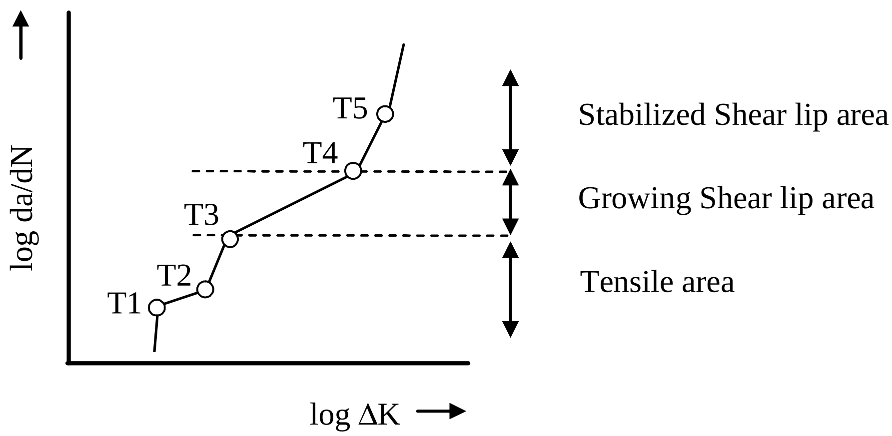

Figure 4.1. Transition points in aluminium alloys.

A fatigue crack often grows with a fracture surface oriented perpendicular to the loading direction. Sometimes the crack front becomes slanted due to the formation of shear lips. These shear lips make an angle of about 45° with the loading direction. In some cases the original crack growth direction is maintained, but also a deviated growth direction can be observed.

With reference to figure 4.1, transition T3 in aluminium alloys AA 2024 and AA 5083 can roughly be associated with the start of shear lip growth and the transition T4 with its completion, see also figure 4.2.

The transition usually starts when a critical value of da/dN, or equivalently ΔK_{eff}, for a given material is exceeded [4.2-4.6]. Investigations on AA 2024 and AA 5083 have shown that the change in crack growth mode (T3) is at a critical rate of crack growth of the order of 0.1μm/cycle. The completion of the transition (T4) occurs at higher values, about 1 μm/cycle [17-19], depending on the material thickness [6, 23], see figure 4.3.

This trend could for example be observed in the experiment presented in figure 3.3, Chapter 3. Note that the transition can be reversed by reducing the cyclic load level [10, 17]. This chapter focuses on the growing shear lip regime between T3 and T4, within the Paris region.

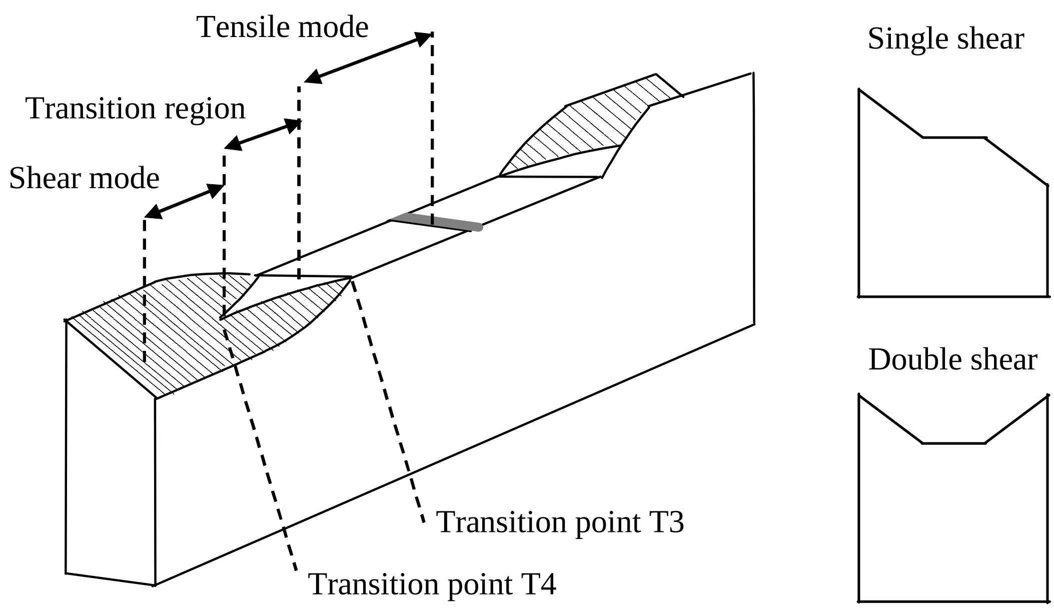

Figure 4.2. Development of shear lips in a constant load amplitude test. At T3 the shear lip starts, at T4 the surface is completely slant.

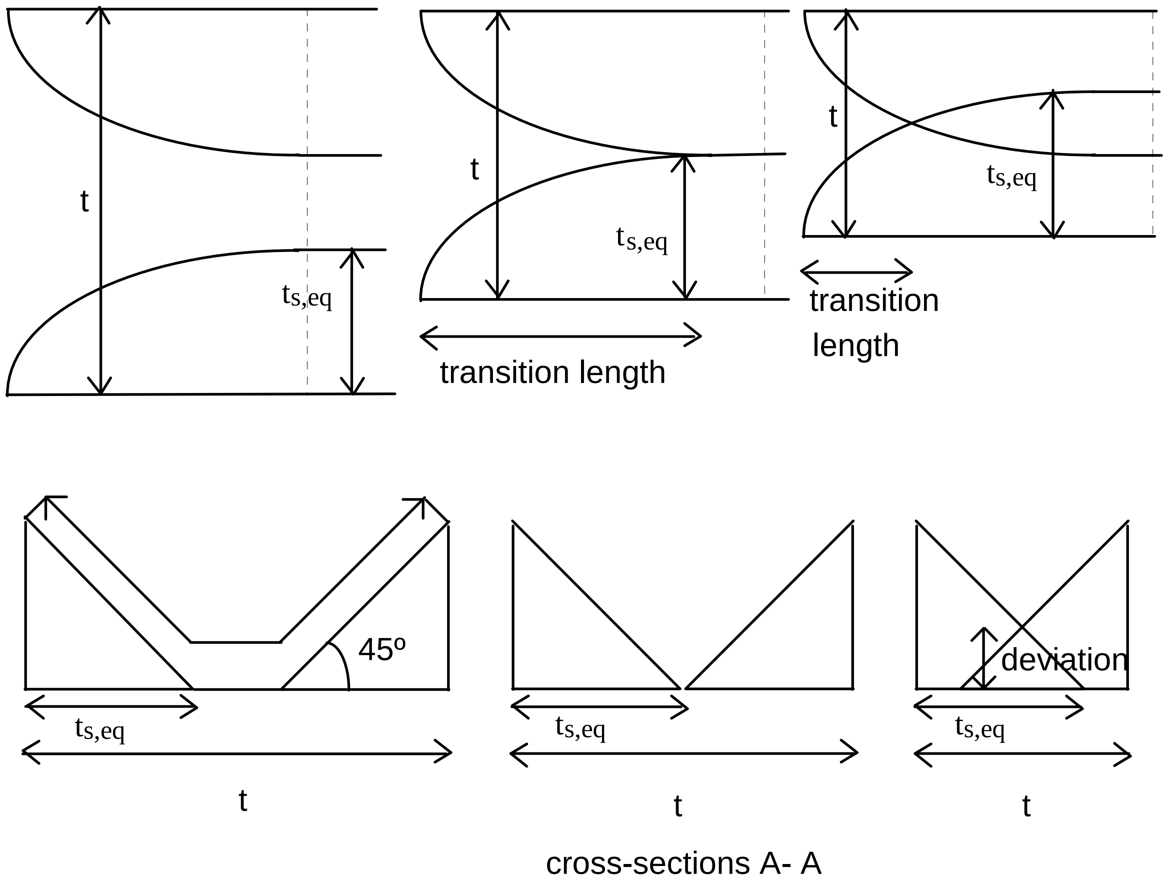

Figure 4.3. Double shear lip width development in a constant ΔK_{eff} test. The specimen thickness and shear lip width are t and $t_{s,eq}$ respectively. The transition length is longer for a thicker specimen.

An important difference between AA 5083 and AA 2024 is the frequency dependency of shear lip behaviour. In AA 5083 smooth shear lips develop over the whole of the frequency range between 5 and 40 Hz [16], while in AA 2024 the appearance of shear lips is frequency dependent. At lower frequencies, < 1 Hz, smooth shear lips are formed, while at higher frequencies, from about 10 Hz, rough shear lips develop [7-9]. Rough shear lips have an enhancing effect on crack closure, while smooth shear lips show no effect on crack closure [10, 11, 21].

In figure 3.2, Chapter 3, a shift to the right of the fatigue crack growth rate curves for decreasing R values is observed. This shift is generally considered to be the result of crack closure. Crack closure is caused by contact of the crack surfaces before minimum load is reached. At higher R values contact of crack surfaces is less, because of the larger average opening of the crack. At very high R, the opening is so large, that no closure at all will occur at minimum load.

The closure effect can be caused by plastic deformation at the crack tip. The effect is not expected to be homogeneous over the specimen thickness. It has a maximum effect near the plane stress surfaces of the specimen, see figure 4.4.

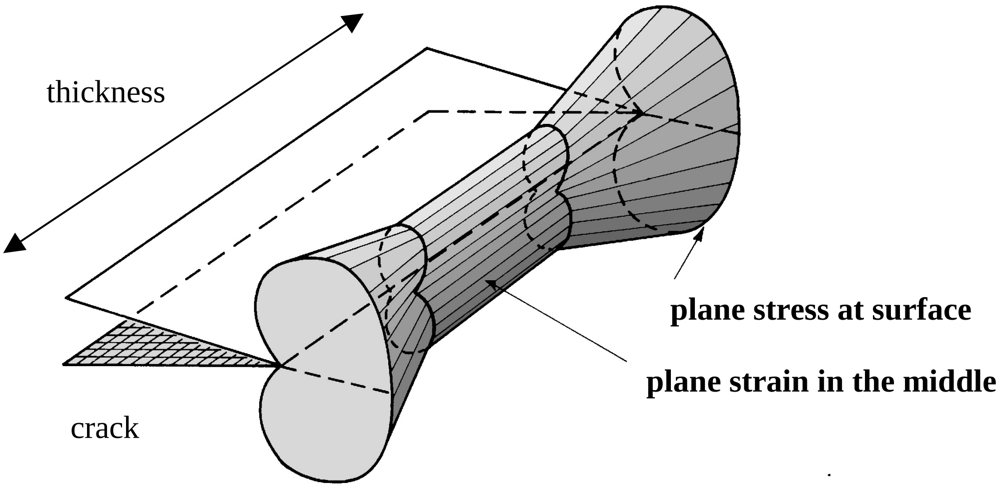

Figure 4.4. Plastic zone in plane stress-plane strain.

It is possible to create a predominantly plane strain situation by using very thick specimens or low K values; in these cases most of the fracture surface is in plane strain, except for the specimen surfaces [12, 13].

To investigate plasticity induced crack closure in the growing shear lip regime, i.e. between T3 and T4, it is essential to be able to measure it. As crack closure has an effect on da/dN, (accurate) measurement of da/dN can be assumed to be a measure of the amount of crack closure.

A first step to measure the influence of crack closure on da/dN is conducting tests on specimens in which closure is reduced as much as possible. An almost crack closure-free status can be expected in a situation where plane strain dominates over plane stress.

In this chapter, the possibility of maintaining a plane strain state at the crack tips in a centre-cracked tension specimen of arbitrary thickness during constant amplitude experiments has been investigated by implementing linear side grooves, involving AA 5083 (section 4.2) and AA 2024 (section 4.3). A linear side groove is a small scratch along the crack growth path over the full width of the specimen. The assumption is made that by introducing side grooves in centre-cracked tension specimens a predominantly plane strain situation is created, because the influence of plane stress plastic deformation in the flanks is diminished, see figure 4.5 [14].

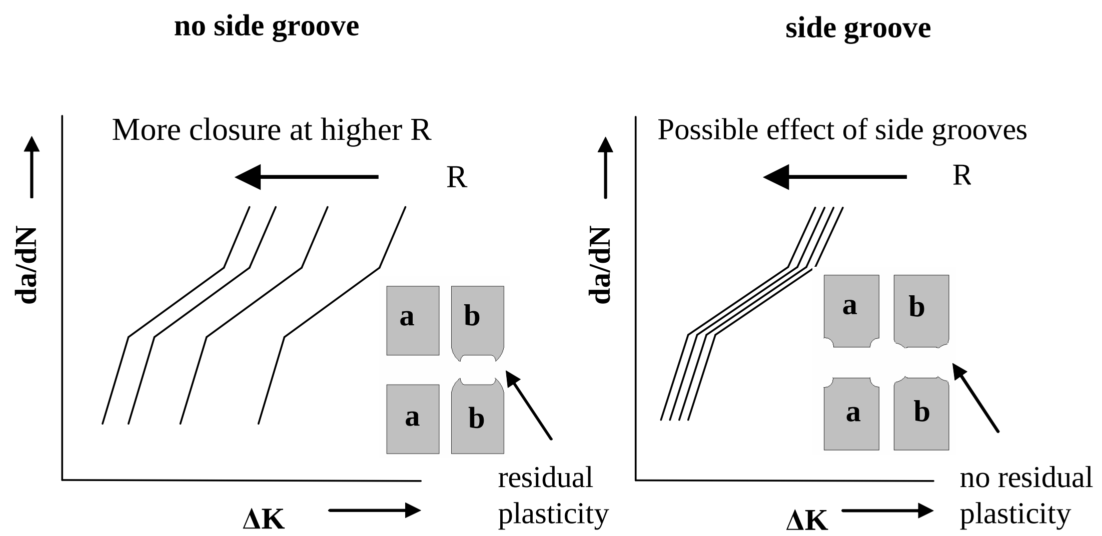

Figure 4.5. Possible effect of side grooves. A cross section is schematically shown of a specimen with and without side grooves:
(a) before deformation at the flanks, (b): after deformation at the flanks
Plasticity induced crack closure is caused by plastic deformation. It has a maximum in the plane stress flanks of the specimen. By introducing side grooves in centre-cracked tension specimen, a predominantly plane strain situation is created: the effect of deformation at the flanks is diminished. In a da/dN-ΔK plot a shift of the curves to the left is expected, in the direction of lower closure levels associated with higher R-values.

This means that plasticity induced closure, due to the extensive plasticity associated with the plane stress edges, will be reduced. If crack closure can be minimized in this way, it is to be expected that the da/dN-ΔK curves at different R values will shift into a narrow scatter band. The curves for lower R values will shift to the left in the direction of high R values.

Besides linear side grooves over the full length of the specimens of AA 5083 and AA 2024, experiments have been conducted on specimens of AA 5083, using side grooves with varying lengths along the crack growth path, see section 4.4. The influence of the environment on shear lip behaviour is also investigated. For this purpose, constant load amplitude tests were performed using different environments and temperatures (section 4.5).

4.2 Linear side grooves in AA 5083

4.2.1 Experiments on AA 5083: different types of side grooves

Side grooves with different depths and geometries were applied to centre crack specimens. The grooves were created by putting a scratch on the surface using the edge of a chisel. Four different types of side grooves were examined (see figure 4.6) these are:

-type A, a sharp groove with a depth of 1 mm

-type B, a rounded groove with a depth of 1 mm

-type C, a very small scratch of 0.1 mm

-type D, specimens reduced in thickness, without side grooves.

In type D specimens, the original thickness of 8 mm was locally milled down to a thickness of 6 mm. The milling was performed over a sufficiently large area, so that the original plane strain/plane stress situation of a test plate with 6 mm thickness and no side grooves was reached.

During the experiments, the crack length was measured using the pulsed direct current potential drop technique. For this purpose, each geometry was calibrated first using the saw cutting method; see Chapter 2, section 2.2.6. Subsequently the specimens were fatigued to failure by constant load amplitude tests in laboratory air at a frequency of 10 Hz.

Three test series were performed. In test series 1 and 2, all linear side groove geometries mentioned above, were applied to centre-cracked tension specimens of AA 5083 and tested at R = 0.5 and 0.1. In test series 3, the fatigue behaviour in the presence of a very small linear side groove, type C, was compared to that of specimens without side grooves, using R = 0.5 and 0.1. For specific load data, see table 4.1. The data were analyzed using the procedures given in ASTM E647 [15].

Table 4.1: Parameters of test series 1,2 and 3

AA 5083	P_{max} [kN]	R	Geometry
Test series 1	40	0.5	All geometries, Types A-D
Test series 2	25	0.1	All geometries, Types A-D
Test series 3	83.5	0.1	No SG / type C
	35	0.5	No SG / type C

4.2.2 AA 5053: results and discussion

Side grooves over the full width of the specimen did not result in an effect on the crack growth rate compared with a specimen without side grooves at the same nominal thickness. Thus introduction of side grooves does not have the intended effect, namely changing the crack closure situation.

However, no shear lips were formed in any of the specimens with side grooves of type A, B or C. The reason for shear lip suppression probably lies in the plane strain situation at the surfaces of the specimens, introduced by the side grooves. Shear lips always initiate and grow from the specimen surfaces towards the centre. A plane stress situation at the specimen surface leads to maximum shear stresses on planes inclined at 45° to the specimen surface. Shear lip formation needs shear deformation on planes oriented about 45° with the plate surface [2]. A plane strain state suppresses this type of deformation.

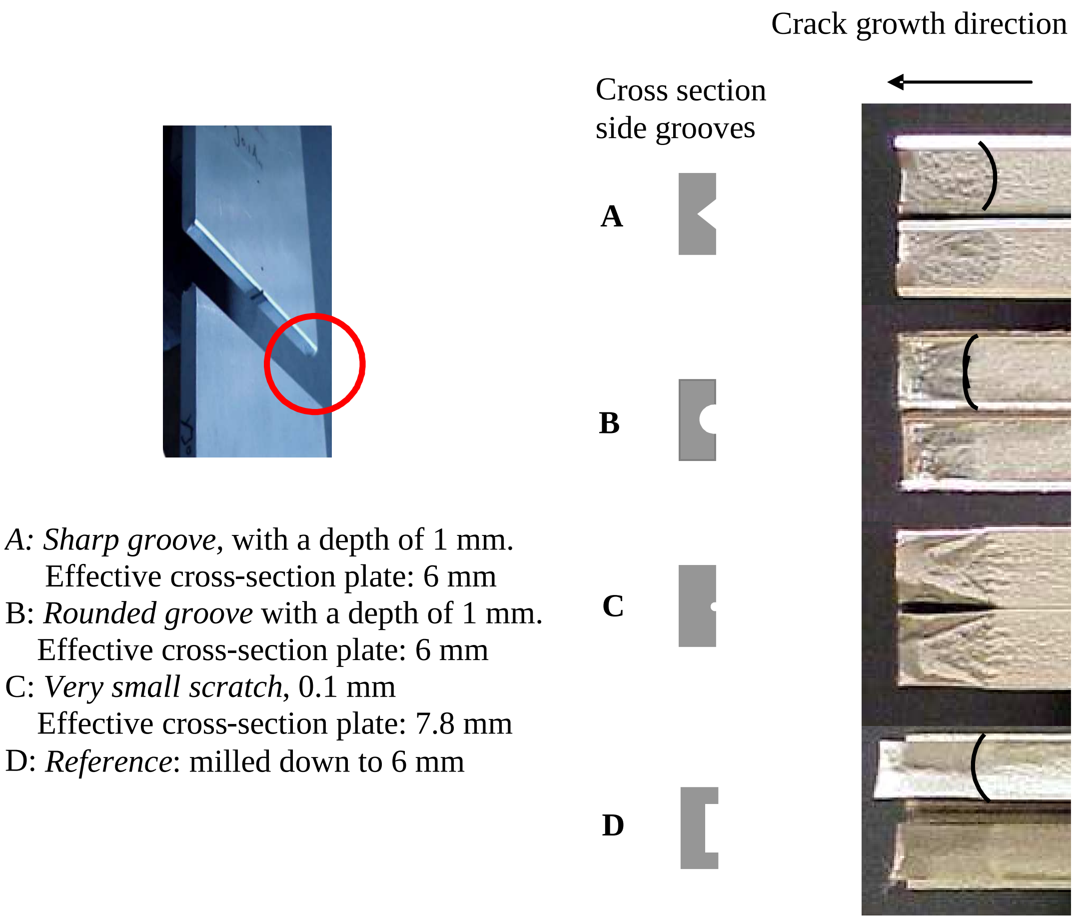

Figure 4.6. Different types of side grooves and tunnelling effect.

Figure 4.7 shows da/dN-ΔK plots for 4 different geometries at load ratios of 0.5 and 0.1. The different geometries A-D only have a small effect on the da/dN-ΔK results. This suggests that introduction of side grooves in this material does not influence crack growth rate significantly. For all geometries, except for type C, tunneling occurs. In geometries B and D the crack front at the surfaces lags behind relative to the centre, resulting in a convex crack front. For a sharp side groove, geometry A, this effect is reversed and a concave crack front is obtained, see figure 4.6.

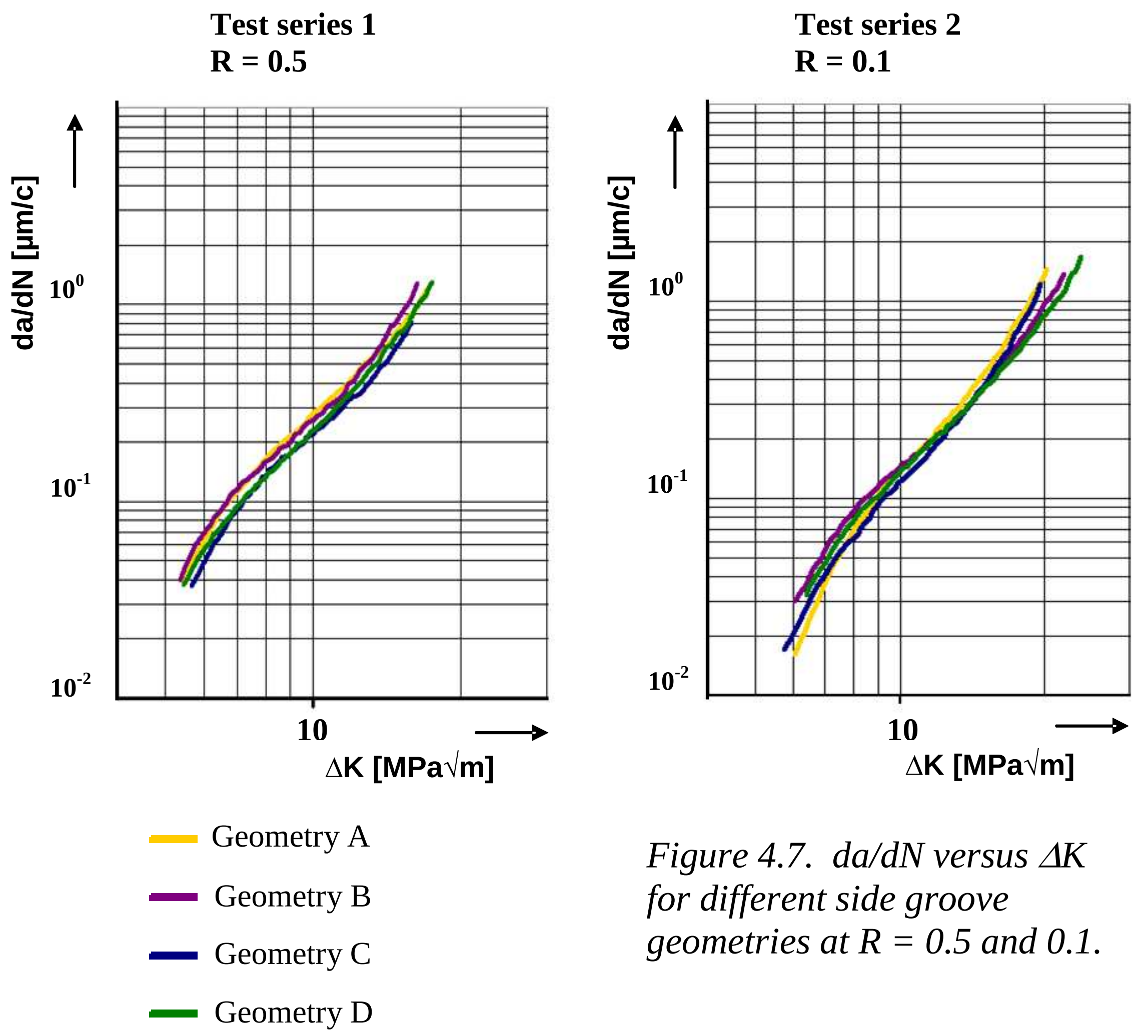

Figure 4.7. da/dN versus ΔK for different side groove geometries at R = 0.5 and 0.1.

Figure 4.8 shows results of test series 3, i.e. experiments with and without small side grooves, for two stress ratios. The crack growth rates da/dN for the series with scratches (side grooves type C), show no significant deviation from those for specimens without scratches. The latter specimens, however, did show the development of shear lips. Therefore, the assumption that shear lip formation is the cause for the transition phenomenon T3-T4 is not correct.

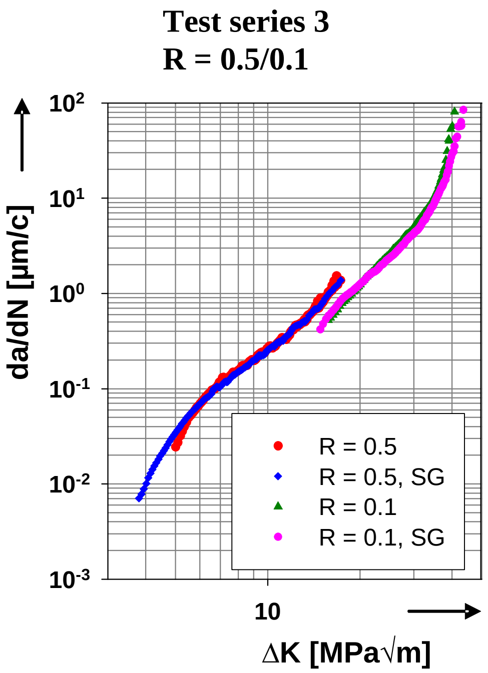

Figure 4.8 da/dN versus ΔK for R=0.1 and 0.5, with and without side grooves.

4.3 Linear side grooves in AA 2024

4.3.1 AA 2024: experiments with linear side grooves

Research on AA 5083 showed that suppression of shear lips, using linear side grooves, has no effect on the da/dN–ΔK relation, see section 4.2. For materials that form shear lips, a dependency of the forming of shear lips on the frequency was found. The transition from a tensile mode to a shear mode depends on the environment [2]. However, the frequency effect in AA 5083 is only small and the shear lips formed are smooth. For this reason the influence of linear side grooves is investigated in the more frequency-sensitive aluminium alloy AA 2024.

Two test series have been conducted, test series 4 and 5. They were performed on AA 2024 specimens, using 3 different frequencies, i.e. 1, 10 and 25 Hz. In test series 4 and 5 specimens without and with linear side grooves of type C, were examined respectively.

Test series 4 was performed to show the effect of the test frequency on the fatigue crack growth rate in AA 2024, while test series 5 was performed to investigate the effect of linear side grooves on da/dN–ΔK. Constant load amplitude tests were performed in normal laboratory air on centre-cracked tension specimens. Specimen dimensions were W = 100 mm, l = 340 mm and t = 6 mm. The details of the loads used are given in table 4.2.

Table 4.2: Parameters of test series 4 and 5

AA 2024	P_{max} [kN]	R	frequency [Hz]
Test series 4 no side grooves	30	0.1	1
	30	0.1	10
	30	0.1	25
Test series 5 with side grooves	30	0.1	1
	30	0.1	10
	30	0.1	25

4.3.2 AA 2024: results and discussion

Test series 4: AA 2024, different frequencies, no side grooves

In AA 2024 a different behaviour was observed compared to AA 5083. The results of tests at 3 different frequencies are shown in figure 4.9. Plots of da/dN versus ΔK using a load ratio of 0.1 and the corresponding fracture surfaces are shown. In contrast with the findings for AA 5083, shear lip surfaces are rough at higher frequencies (10 and 25 Hz) and smooth at the lower frequency of 1 Hz. This difference in shear lip roughness is suspected to be responsible for the difference in the crack growth rate.

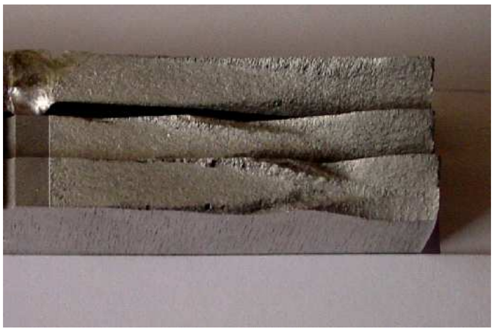

Test series 4

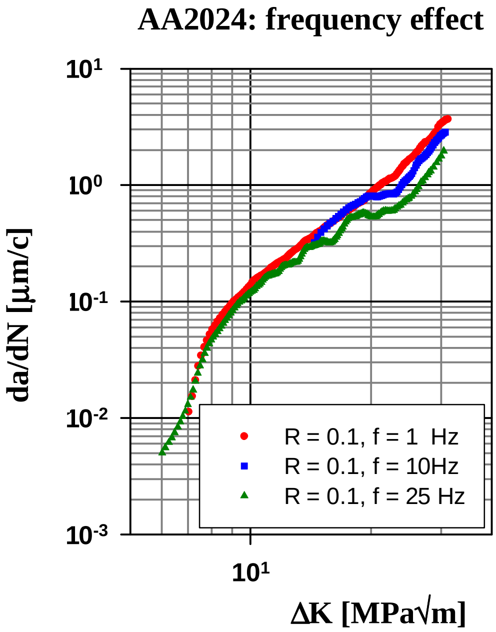

Figure 4.9. da/dN-ΔK relation for different frequencies. Three crack surfaces are shown, from top to bottom 1, 10 and 25 Hz respectively.

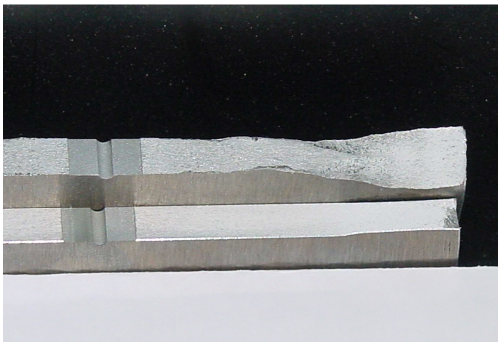

Test series 5

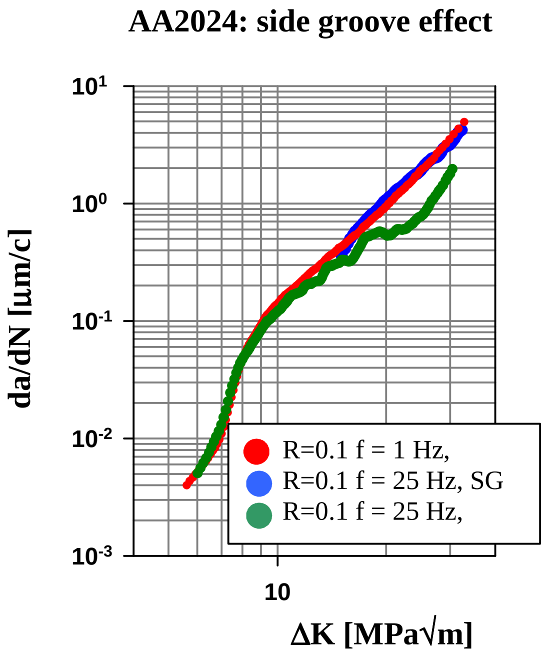

Figure 4.10. da/dN-ΔK relation for linear side grooved and non-side grooved specimens. The photo shows the crack surface for normal slant crack surface (top) and suppressed shear lips (bottom). The specimens were fatigued at a frequency of 25 Hz.

Test series 5: AA 2024, different frequencies, with linear side grooves

At all frequencies the results for tests using linear side grooves are the same as those for specimens tested without side grooves at 1 Hz (which have smooth shear lips). For clarity, only the effect of the linear side groove at 25 Hz is shown in figure 4.10. The same effect is found for the test at 1 and 10 Hz. The picture shows two fracture surfaces of AA 2024 samples. The fracture surfaces shown are the result of tests at a frequency of 25 Hz; the only difference is the presence or absence of side groove. Side grooves cause the crack to remain flat and eliminate the frequency effect by suppressing the formation of rough shear lips at higher frequencies.

4.4 Partial side grooves in AA 5083

In test series 6, see table 4.3, additional experiments were performed with side grooves along the full width on one side of the specimen, and with varying lengths of 0, 20 and 30 mm on the other side. Geometry C was used for the side grooves, see figure 4.6.

Table 4.3: Parameters of test series 6

AA 5083	P_{max} [kN]	R	frequency [Hz]
Test series 6 Partial side grooves	95	0.1	10

Figure 4.11 shows examples of fracture surfaces for specimens with varying side groove lengths. In specimen A there is only a side groove on one side; in specimens B and C there are also partial side grooves on the other side with lengths of 20 and 30 mm respectively. In specimen A shear lips develop

immediately on one side. The other side remains smooth and follows the side groove.

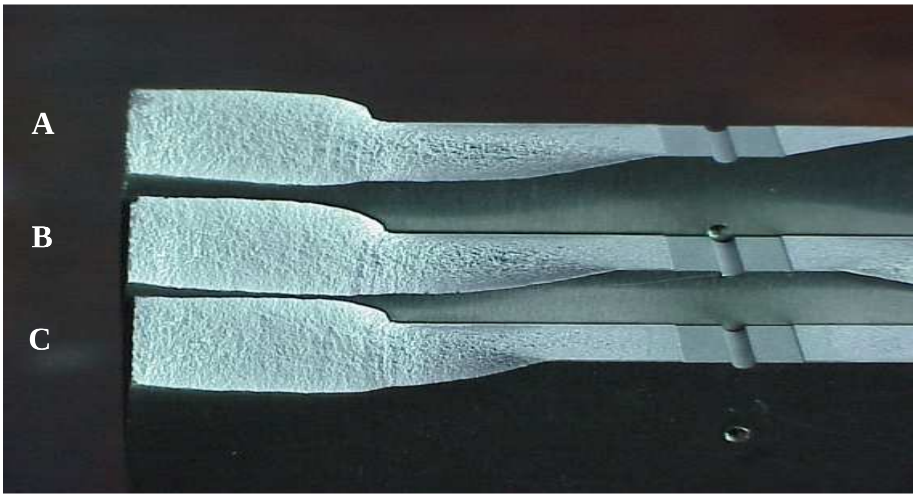

Figure 4.11. Side grooves, with varying length:
The shear lip is suppressed totally at one side, the upper side, and partial on the other side over respectively A: 0 mm, B: 10mm and C: 20 mm.

At the end of the partial side groove, in specimens B and C, the shear lip develops quickly until full shear is achieved. For a longer partial side groove, the shear lip develops faster: in specimen C the shear lip grows in a relatively short distance to the full specimen width.

Figure 4.12 shows three specimens with none, one and two linear side grooves over the full width, respectively. Despite the differences in the specimens, the crack growth rates are equal for all specimens.
The growth rate of the shear lip and shear lip width t_s can be predicted. [2, 3, 20, 21, 22]. The shear lip width t_s is chosen as a parameter to quantify slant growth. In [2] the shear lip width is defined as $t_s = (t - t_t) / 2$, where t = specimen thickness and t_t = width of tensile part of the crack surface, see figure 4.3. However, the shear lip width that covers more than half the specimen thickness, i.e. $2t_s > t$, cannot be obtained. It was thought [2, 3] that a larger shear lip width

could only be obtained in a thicker specimen. In test series 6, using partial side grooves, it is found that the shear lip can be suppressed on one side of a centre-cracked tension specimen. The growing shear lip on the other side of the specimen has the possibility to grow to more than half the specimen thickness. Thus the side groove technique enables one to find t_s also in (thinner) plates where $2t_s > t$. Moreover, the results from test series 6 prove clearly that t_s is not dependent on the specimen thickness as long as $t > t_s$.

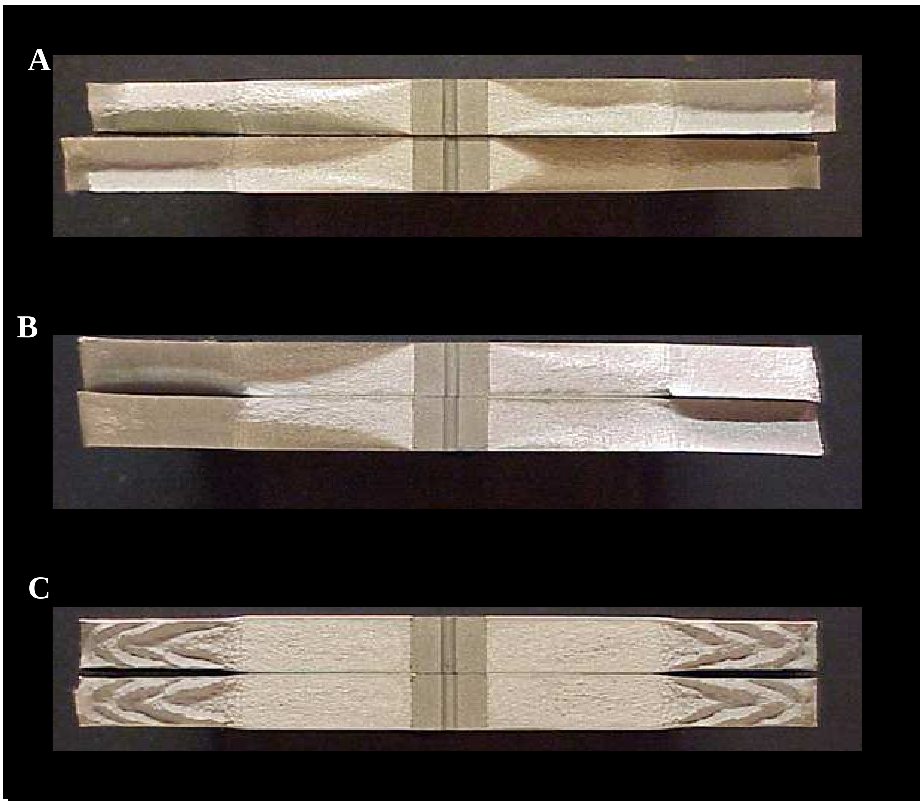

Figure 4.12. Effect of side grooves.
A: normal shear lip
B: suppressed on one side
C: suppressed on both sides

4.5 Influence of environment on transition point T3

4.5.1 Environment and transition point T3

Probably a number of crack growth mechanisms, operative at the crack tip, influence the crack growth rate. The elimination of one or more of these mechanisms can lead to another dominant crack growth mechanism. A change in slope of the log(da/dN)-log(ΔK) curve indicates a change in the dominant fatigue crack growth mechanism. At transition point T3, such a change takes place. After this transition the crack growth rate increases less rapidly with increasing ΔK than before, and there is a possibility for the formation of shear lips.

Several test series (see sections 4.2-4.4, test series 1, 2, 3, 5 and 6) were carried out in which the development of shear lips was suppressed by side grooves with different shapes and sizes, at one side or at both sides of centre-cracked tension specimens. The crack growth rates found in these series show no significant deviation compared to those of specimens without side grooves. Thus no causal relation exists between da/dN and shear lip development, but the shear lip width is indicative for da/dN. In other words, the assumption that shear lips are responsible for the T3 transition phenomenon is not correct, but if shear lips are not suppressed, the start of shear lip development can be associated with transition T3.

The change in slope at T3 in the log(da/dN)-log(ΔK) curve and the corresponding shear lip formation are probably not the result of a change in the stress situation, but they are both the result of another mechanism. A change in fatigue crack growth mechanism, represented by the T3 transition point, is probably due to the environment. If this assumption is true, the development of shear lips in an inert environment will be different from that in a corrosive / aggressive environment. To assess this hypothesis, two series of tests were performed in different environments (test series 7) and under different temperature conditions (test series 8).

4.5.2: Different environments

Test series 7: different environments

The influence of the environment on the T3 transition point was examined through a comparison of crack growth rates obtained in different environments, namely an aggressive environment (sea water), an inert environment (with dry argon as shielding gas) and a reference environment (normal lab air). Constant load amplitude tests were performed on AA 5083 specimens, using a frequency of 10 Hz. The test configuration was as described in Chapter 2, section 2.2.5. Results are shown in figure 4.13.

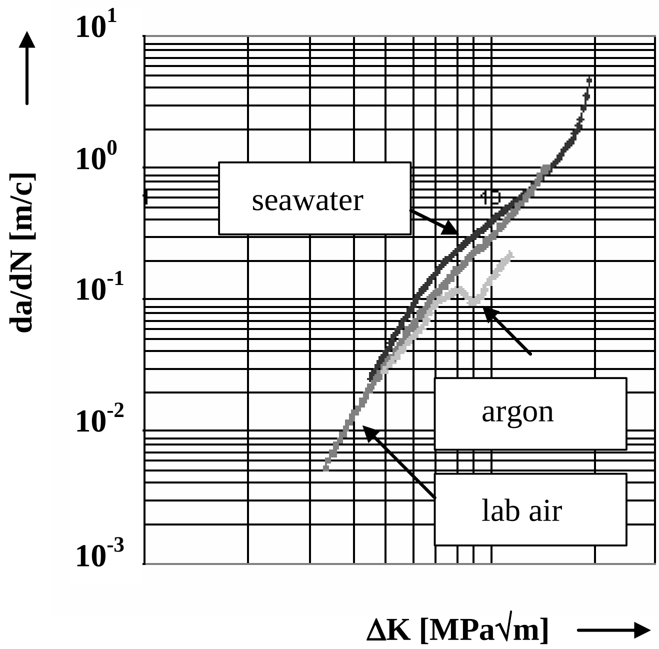

Figure 4.13. da/dN-ΔK curves for different environments, namely seawater, lab air and argon.

The transition point T3 in the case of seawater is shifted to a higher da/dN, compared to the reference curve. The formation of shear lips shows a corresponding shift; they are formed at a higher crack growth rate, compared to normal lab air. The effect of argon is that a dramatic change of crack growth is observed. Rough shear lips are formed immediately at the beginning of the test. Unfortunately, the airflow in the cell surrounding the crack was not completely turbulent, which is believed to be necessary to create a pure a argon environment. Rough shear lips were formed on the side of the specimen near the inlet of the clamped cell. On the other side, near the outlet, a smoother crack surface was formed, because some air remained present in the cell. This asymmetry resulted in asymmetric crack growth: the growing crack on the side of the rough shear lip lags behind. This demonstrates that even a small amount of disturbing lab air containing moisture can have a significant effect on the crack growth rate in this aluminium alloy.

Test series 8: different temperatures

The rate of a chemical (corrosion) reaction is strongly temperature dependent. In general, a corrosion reaction will be faster with increasing temperature. If a corrosion mechanism is involved in crack growth, a shift in T3 due to a change in reaction speed is expected at different temperatures. Environmental effects have been studied over a temperature range from +45 ºC to –20 ºC. Constant amplitude tests with P_{max} = 30 kN and R = 0.5 were performed on centre-cracked tension specimens, using a frequency of 10 Hz.

What has to be taken into account in these tests is that a change in temperature is accompanied by a change in relative humidity. A reference test series was made in normal lab air, at a temperature of 18 ºC and a relative humidity of 50%. The relative humidity decreases to 10% at higher temperatures, while it approaches almost 100% at temperatures below zero. However, the absolute amount of moisture in the air, expressed in mass per unit volume, is constant for higher temperatures, but becomes less for temperatures below which condensation occurs. Based on the specific combination of temperature and relative humidity of lab air, the point of condensation can be found at about 7 ºC. Below this temperature moister will condense easily inside the cooling system.

The effect of temperature on fatigue crack growth is shown in figure 4.14. The reference curve at a temperature of 18 °C and the curve of 45°C gave the same result and are shown in this figure as one curve.

A temperature of 45 °C did not result in a shift of the T3 transition point relative to 0 °C. It is a first indication that the amount of moisture, not temperature, is responsible for the change of slope near T3. A higher temperature will force a faster chemical reaction. However, probably the amount of humidity in the air rather than the reaction time determines the effect on da/dN.

For lower temperatures, 0 and –20 ºC, a shift downwards of T3 in terms of da/dN and a divergent curve compared to the reference curve is found, which can be explained as follows. At lower temperatures, the amount of moisture available to attack the fresh surface that is formed during each fatigue cycle, becomes less. However, even at low temperatures a small amount of water vapour is still present in the surrounding environment. With increasing crack growth rate, (> 0.1 μm/cycle) the influence of the corrosion mechanism decreases; the crack tip moves too fast for the corrosion mechanism to stay fully operative. This process is observed as a plateau in the log(da/dN)-log(ΔK) curve. Above a certain crack growth rate (about 0.8 μm/cycle), the influence of the corrosion mechanism on the crack tip can be neglected. The curve changes to the original slope at the end of this plateau, known as the T4 transition point. This is marked on the crack surface by the appearance of multiple shear lips.

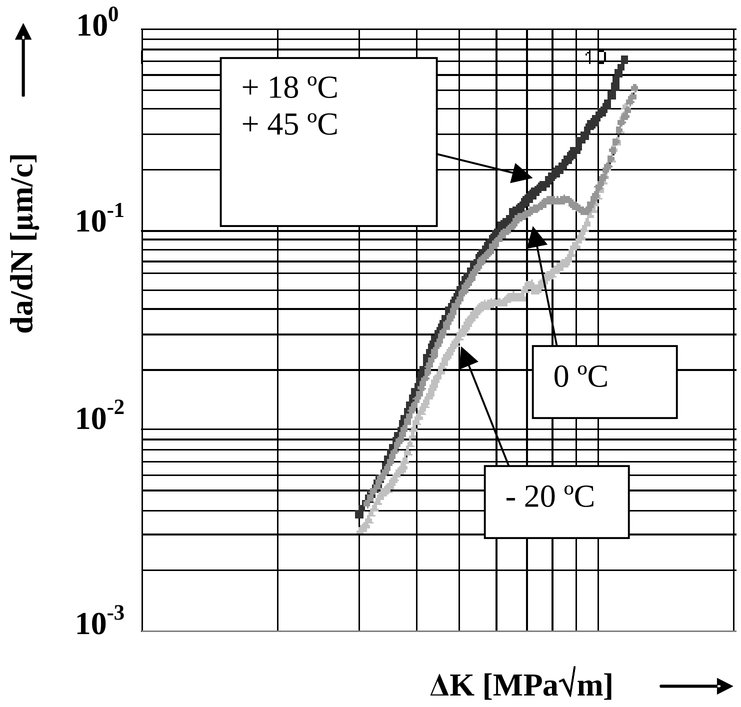

Figure 4.14. da/dN-ΔK curves for different temperatures.

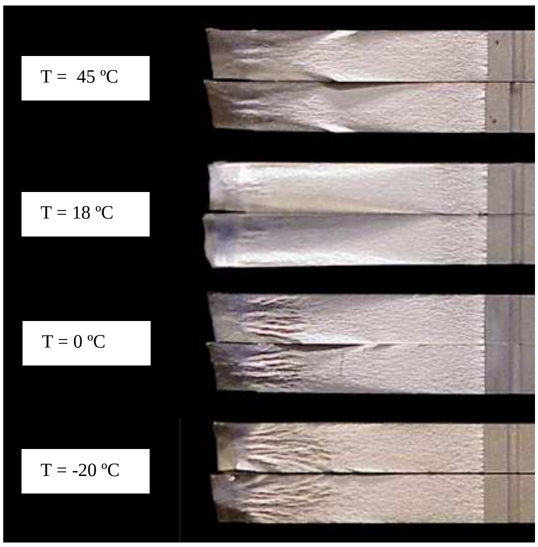

Figure 4.14b. Fracture surfaces of samples tested at different temperatures.

4.6 Summary, discussion and conclusions

In the present chapter the possibility of keeping a centre-cracked tension specimen in plane strain during a constant amplitude experiment by implementing side grooves has been investigated. A number of findings and experimental observations are summerized below.

1. If crack closure is caused by early contact of the crack flanks, which would be especially important near the plane stress edges of the specimens, a shift in the log(da/dN)-log(ΔK) curves at lower R values in tests with side grooves is expected. Test results however clearly showed that suppression of shear lips, using linear side grooves, has no effect on the da/dN–ΔK relation and no shift of crack crowth curves was observed.
2. Normally in lab air shear lips in AA 5083 have a smooth appearance. It is found that smooth shear lips can be suppressed, by making a scratch along the crack growth path. Different side groove geometries cause different tunneling behaviour: a sharp side groove promotes initiation of the crack in the flanks. All types of applied side grooves prevent the development of shear lips in AA 5083. A remarkable effect is found: constant amplitude tests on specimens with shear lips and suppressed shear lips show the same da/dN–ΔK results; i.e. the same transitions T3 and T4 are present. Thus the growing shear lip cannot be responsible for the slope change in log(da/dN)-log(ΔK) after T3. It can only be stated that shear lips start to grow near the slope change T3. The shear lip has no effect on da/dN, it can only be associated with da/dN. It seems that both the start of shear lips and the slope change are the result of another, yet unknown mechanism.
3. Since the development of shear lips is not the cause for the gradually changing slope of the log(da/dN)-log(ΔK) curve, transition point T3 can probably be attributed to an environmental assisted crack growth mechanism. To

assess this hypothesis, constant load amplitude tests were performed under different environmental conditions, namely seawater, lab air and argon. In normal lab air, no frequency effect in the range of 5 to 40 Hz on T3 was found in AA 5083 [16], however the effect of different environments on the fatigue crack growth in this material is evident. For AA 5083, it is not entirely clear why the mechanism of frequency dependent crack growth is not similar to the effect of different environments. Results of series made under different temperature conditions show a strong dependency on the absolute amount of moisture.

4. A series of experiments on specimens of AA 5083 with varying lengths of side grooves, shows that the development of shear lips is suppressed over the length of the partial side groove. At the end of the side groove, the shear lip develops quickly until full shear is reached. Almost no difference in crack growth rates is found between specimens of AA 5083 with scratches on both sides, where shear lips are fully suppressed, specimens with shear lips on one side, or specimens with full smooth shear lips.

5. In AA 2024, both plasticity-induced and shear lip-induced crack closure, the latter occurring at higher frequencies, have a significant effect on the fatigue crack growth behaviour. However, the da/dN-ΔK curves at higher frequencies with suppressed shear lips, are identical to those at a low frequency, i.e. with smooth shear lips. The results of test series 5, show that linear side grooves eliminate both shear lips and frequency effects in AA 2024. By suppression of rough shear lips, that are formed at higher frequencies, it becomes possible to separate the contributions of plasticity-induced and shear lip-induced closure.

The results obtained indicate that a corrosion mechanism is held responsible for the shear lip phenomenon and the associated crack growth rate behaviour.

It is thought that the corrosion mechanism gradually loses its influence at increasing da/dN from T3 to T4. This causes the slope change. At T4 no corrosion enhanced crack growth is left. The slope increases roughly to the value it had before T3. Thus: the lower slope in log(da/dN)-log(ΔK) between T3 and T4 is caused by a time dependent corrosion crack growth mechanism that gradually loses effectiveness because of a higher crack growth rate. Below T3 the corrosion mechanism is fully operative, while above T4 the enhanced mechanism no longer exists.

For AA 2024, a dependence of shear lip formation on the frequency is found, resulting from environmental effects. When the loading frequency is lowered (or the environment is made more aggressive, e.g. by change from air to salt water), it is found that the start of shear lip development is shifted to higher values of ΔK or da/dN, and flat tensile mode crack growth is favoured. A possible explanation can be that the more aggressive environment has an impeding effect on (the start of) dislocation movement along the slip systems near the plate surface.

There is a possible cause for the impending effect. The effect can be thought to result from foreign atoms or ions, products of a corrosion reaction near the surface, diffusing into the matrix. They settle near dislocation lines where the lattice spacing is higher than elsewhere. The settlement of foreign elements near the dislocation lines has a lowering effect on the total internal energy, i.e. it will require energy to move the dislocation lines out of this environment. The (start of the) movement of dislocation lines therefore becomes more difficult.

There probably has to be a little initial slant growth at the surface, before shear lips can grow to a larger width. If this initial shear lip growth is prevented by hindrance of dislocation movements near the surface, shear lips will only start to grow at higher ΔK_{eff}. Subsequent shear lip development will occur later. This explanation is consistent with the observation that in vacuum, shear lips develop almost immediately when the crack grows, even for a very low ΔK_{eff} and for a low frequency [26,27]. In the absence of contamination there are no obstacles for the dislocation movements needed for the start of shear lip growth.

References

[1] P. Paris and F. Erdogan, *A critical analysis of crack propagation laws*, Journal of Basic Engineering, Transactions of the American Society of Mechanical Engineers, pages 528-534, December 1963

[2] J. Zuidema, *Square and Slant Fatigue Crack Growth in Al 2024*, ISBN 90-407-1191-7, 177 pages, Dissertation, Delft University Press, Delft, The Netherlands, 1995

[3] F.A. Veer, *The effect of shear lips, loading transitions and test frequency on constant ΔK and constant load amplitude fatigue tests*, Dissertation, Delft University Press, Delft, The Netherlands, 1993

[4] R.W. Hertzberg, E.F.J. von Euw, *A note on the fracture mode transition in fatigue*, International Journal of Fracture Mechanics 7, pages 349-353, 1971

[5] C.M. Hudson, J.T. Scardina, *Effect of stress ratio on fatigue-crack growth in 7075-T6 aluminum-alloy sheet*, Engineering Fracture Mechanics, Volume 1, Issue 3, pages 429-446, April 1969

[6] D. Broek, P. De Rijk, P.J. Sevenhuijsen, Report NLR-TR M.2100, Nationaal Lucht- en Ruimtevaart Laboratorium, Amsterdam, 1962

[7] L.P. Pook, *Slant (45 Degrees) Crack Growth in Fatigue*, Metal Science 10, pages 334-335, 1976

[8] G. Marci and P.F. Packman, *The effects of the plastic wake zone on the conditions for fatigue crack propagation*, International Journal Fracture 16, pages 133-153, 1980

[9] R.O. Ritchie, R.F. Smith, J.F. Knott, *Effects of Thickness on Fibrous Fracture from a Notch and on Fatigue-Crack Propagation in Low-Strength Steel*, Metal Science 9, pages 485-492, 1975

[10] J. Zuidema, J.P. Krabbe, *The effect of Regular and Irregular Shear Lips on Fatigue Crack Growth in AA 2024*, Fatigue and Fracture of Engineering Materials and Structures 20, pages 1413-1422, 1997

[11] J. Zuidema, F.A. Veer and C. van Kranenburg (Invited lecture), *Square and slant crack growth in (thin) sheets*, Proceedings of the International Conference on Fatigue Crack Paths (FCP 2003), A. Carpinteri (Ed.), CD ROM, Parma, Italy, University of Parma, September 18-20, 2003

[12] F.A. Veer, J. Zuidema, P.A. Houdijk, *The effect of specimen thickness during constant fatigue testing of S 355 construction steel*, Volume 1/5, proceedings of ICF 8, Stockholm, 2002

[13] H.M. Nykyforchyn, *On the ambiguities of the parameters of fatigue crack growth and stress corrosion cracking,* Strength and Integrity of Materials, Fracture Mechanics, eds. O.M. Romaniv and S.Ya. Yarema, pages 84-94, 1996

[14] C. van Kranenburg, A.C. Riemslag, S. Benedictus-de Vries, J. Zuidema, F.A. Veer, *Plane stress and plane strain in side grooved centre-cracked tension specimens*, 10th International Conference on Fracture, Honolulu, USA, 2001

[15] ASTM E 647, *Standard test method for measurement of fatigue crack growth rates*, American Society for Testing and Materials, Philadelphia, PA USA, 2000

[16] A.P. Hascaryantono, *Effects of load frequency and stress ratio on corrosion fatigue crack growth of aluminium alloy 5083-H321*, Master Thesis, Delft University, The Netherlands, 2002

[17] J. Schijve, *Fatigue damage accumulation and incompatible crack front orientation*, Engineering Fracture Mechanics 6, pages 245-250, 1974

[18] D. Rhodes, L.E. Culver and J.C. Radon, *Analysis of combined static and fatigue crack growth data*, In: Proc. 3rd European Colloquium on Fracture, London, pages 287-296, 1980

[19] D. Broek J. Schijve, report NLR-TR M.2111, Nationaal Lucht- en Ruimtevaart Laboratorium, Amsterdam, 1965

[20] J. Zuidema, C. van Kranenburg, A.C. Riemslag, F.A. Veer and S. Boljanovic, *Anomalous fatigue crack growth behaviour in AA 2024 and AA 5083*, Proceedings of Materials Structures and Micro mechanics of Fracture, Brno, Czech Republic, 2001

[21] J. Zuidema, F.A. Veer and C. van Kranenburg, *Shear lips on fatigue fracture surfaces of aluminium alloys*, special Issue of “Fatigue and Fracture of Engineering Materials and Structures, 28, pages 159-167, 2005

[22] J. Schijve, *Shear lips on fatigue fractures in aluminium alloy sheet material*, Engineering Fracture Mechanics 14, pages 789-800, 1981

[23] S.R. Swanson, F. Cicci, W. Hoppe, ASTM STP 415, pages 312-362, 1967

[24] S. Benedictus-de Vries, *Corrosion fatigue of welded AA 5083 in seawater*, ISBN 90-771-7214-9, Dissertation, Delft, 2006

[26] M. Kanaar, Masterthesis, Delft, Februari 1992

[27] J.P. Krabbe, Masterthesis, Delft, May 1994

Chapter 5
Forced Crack Path Deviation

5.1 Introduction

Earlier investigations, reported in section 4.2.1, have shown that the introduction of linear side grooves with a depth of 100 μm over the full width of centre-cracked tensile specimens of AA 5083 suppresses the formation of shear lips during fatigue crack growth. This type of side groove however does not affect the crack growth rate [1] in this material.

It is well known from literature that in AA 2024 test frequency in combination with the environment have a significant influence on the morphology of shear lips and on the crack growth rate [2-4]. It was found that a flat fracture surface was promoted by an aggressive environment or by a low frequency in air. A higher da/dN is needed to develop shear lips in a more aggressive environment. Also the shear lip appearance is dependent on the frequency. In air smooth regular shear lips were found for low frequencies, while very rough shear lips were found at higher frequencies. For tests performed in vacuum, almost directly rough shear lips were formed at all ΔK levels. It was also found that rough shear lips had an enhancing effect on crack closure and that smooth shear lips had no effect [3, 12].

It was also shown in section 4.3.1, that the da/dN dependency in frequency-sensitive AA 2024 sheet found at higher frequencies with suppressed shear lips are identical to those found at lower frequencies with smooth shear lips. The results showed that linear side grooves eliminate both the shear lips and the frequency effect in AA 2024 [5].

It is of interest to try to force the crack path in a certain direction by introducing curved side grooves, to lengthen the crack path and possibly also the fatigue life. As shown in figure 5.1, the shear lip width in the z direction, $t_{s,z}$, is defined as: $t_{s,z} = (t-t_t)/2$, where t = specimen thickness and t_t the width of tensile part of the crack surface. When the shear lips are assumed to make an angle of about 45° relative to the surface, it follows that $t_{s,z} \approx t_{s,y}$

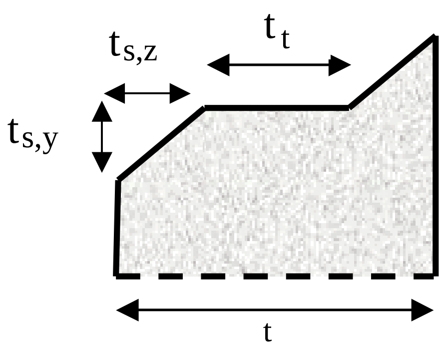

Figure 5.1. Schematic cross section of a centre cracked tension specimen containing a fatigue crack developing shear lips.

There are several methods to predict the development of shear lips in AA 2024 [6, 7]. A rough estimate, developed by Schijve [8], which is valid for constant amplitude testing, uses the following equations:

$$t_{s,z} = 2.85\times10^{-3}\Delta\mathrm{K}_{eff}^{2} \tag{5.1}$$

where $$\Delta K_{eff} = U\times\Delta K \tag{5.2}$$

and $$U = 0.55 + 0.35R + 0.1R^2 \tag{5.3}$$

These equations are used to predict the development of the natural shear lip width.

Side grooves along different curves where applied on centre- cracked tensile specimens of AA 2024, which were subsequently fatigue tested at a low frequency. Two curves are applied.

A curve with a large radius of 162.5 mm is chosen to follow almost the predicted development of the natural shear lip. The other one, a curved side groove with a smaller radius of 68.9 mm, causes an initial slant growth that has an angle larger than 45°. This curve forces the crack to grow at an angle higher than found in the natural shear lip.

The expected shear lip width $t_{s,z}$ and the forced shear lip width of the applied curves will be replaced from now on by $t_{natural}$ and t_{forced} respectively.

At a certain moment, in case of the curved side grooves with the smaller radius, t_{forced} becomes larger than $t_{natural}$. From this point forewards the crack will be forced out of the natural path and the forced path becomes larger than the natural path. This is called as “overdrawing”.

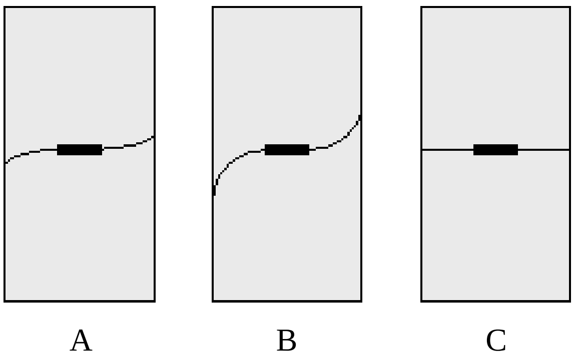

Figure 5.2. Side views of different side groove geometries
A: side groove along a curve with a radius of 162.5 mm
B: side groove along a curve with a radius of 68.9 mm and
C: linear side groove.

5.2 Experimental setup

Constant load amplitude tests were conducted in laboratory air on AA 2024 centre-cracked tension specimens. Specimen dimensions were W = 100 mm, l = 340 mm and t = 6 mm.

All side grooves have a depth of 0.1 mm and were created by putting a scratch on the surface using the edge of a chisel. Between the starter notch and the beginning of the curved groove, a linear side groove with a length of 10 mm was applied.

The details of the loads and side grooves used are given in table 5.1 and figure 5.2. da/dN-ΔK results from a linear side grooves represents the reference curve since the da/dN-ΔK relation for specimens tested at low frequency with and without linear side grooves is the same.

The crack length was measured using the pulsed direct current potential drop technique. All specimens were fatigue loaded until failure. The data were analyzed using the procedures given in ASTM standard E 647 [10].

Table 5.1. Load data

AA 2024 Frequency = 1 Hz	P_{max} [kN]	R	Side grooves
Test series 1	30	0.1	Curved; radius = 162.5 mm
Test series 2	30	0.1	Curved; radius = 68.9 mm
Reference curve	30	0.1	Linear side groove

5.3a

AA 20224
Curved side groove
Radius = 162.5 mm

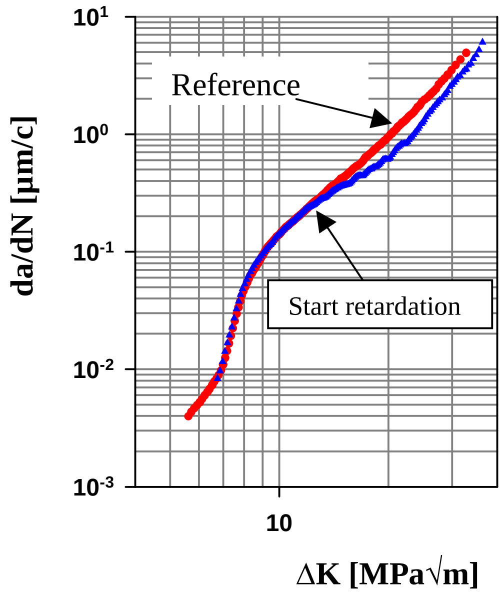

5.4a

AA 2024
Curved side groove
Radius = 68.9 mm

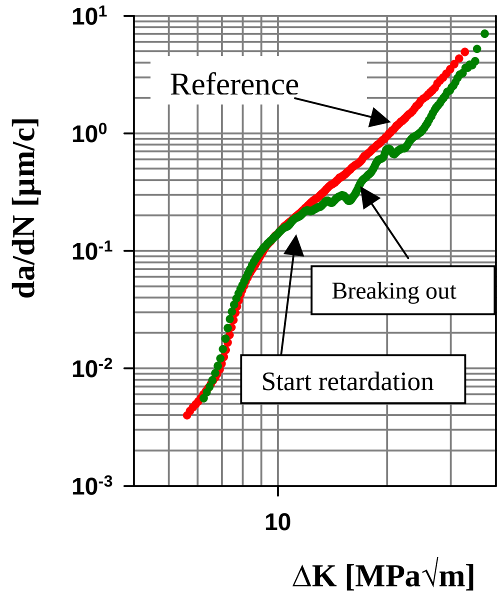

5.3b

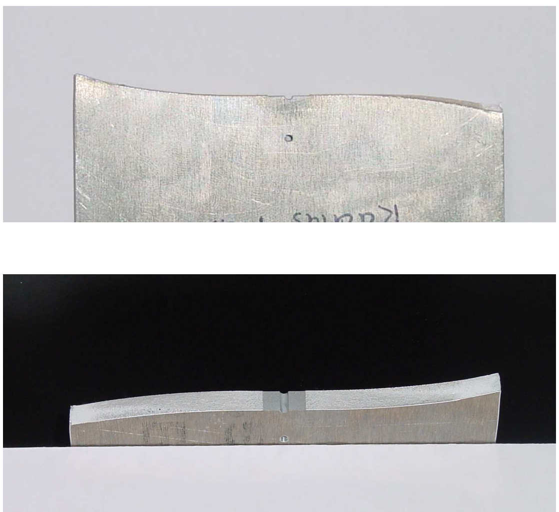

5.4b

Figure 5.3. Results for the linear side groove and the side groove with a radius of 162.5 mm.

Figure 5.4. Results for the linear side groove and the curved side groove with a radius 68.9 mm.

5.3 Results

Figures 5.3 and 5.4 illustrate the effect of the side grooves along a curve with a large and a small radius, respectively. In these da/dN-ΔK diagrams the measured fatigue crack growth rates are compared with reference data obtained at 1 Hz using a linear side groove.

5.3.1 Curved side grooves, large radius

Figure 5.3b shows a picture of the crack shape obtained in case of a radius of 162.5 mm. It can be seen that the crack, at least near the specimen surface, follows the prescribed path of the curved side groove. The side groove not only draws the crack down at the surface, but the whole crack front is drawn downwards. However, the degree of crack deviation in the middle of the specimen as a result of the forced path, is less than that at the surface.

Starting at a crack length of approximately 22 mm, which corresponds to a ΔK of 13 MPa√m, crack growth retardation is observed, see figure 5.3a, and a gain in fatigue life is obtained.

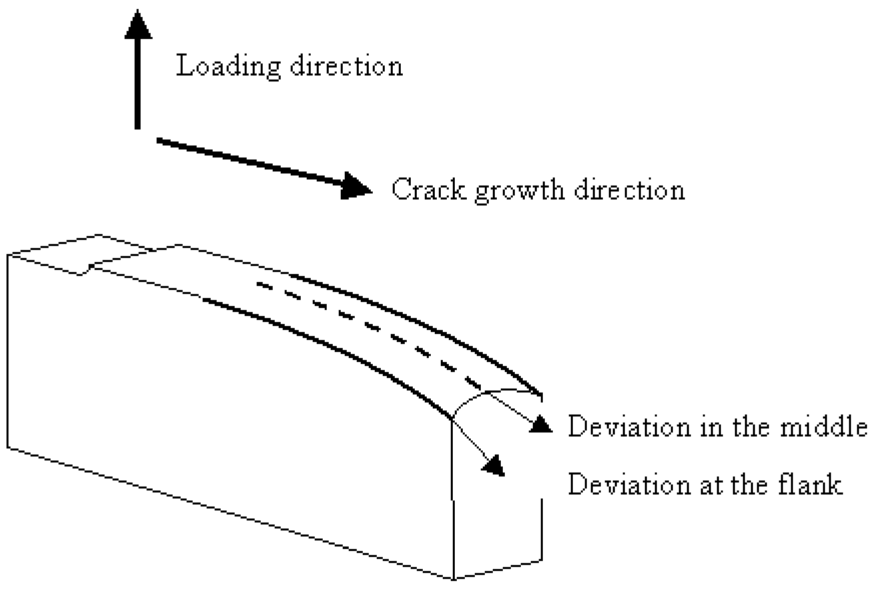

Figure 5.5. Forced crack path deviation. Degree of bending in the middle of the specimen differs from that at the flank.

5.3.2 Curved side grooves, small radius

Figure 5.4b shows some pictures of a specimen with side grooves along a curve with a radius of 68.9 mm. Again, retardation in crack growth is observed. The natural shear lip angle is now smaller than the angle the crack is forced into by the curved path. The crack breaks away from the side groove at a crack length of about 25.5 mm, which corresponds to a ΔK of 15.3 MPa√m. At this location several black spots are visible in the crack wake, which indicate crack surface fretting and thus increased crack closure, see figure 5.4b.

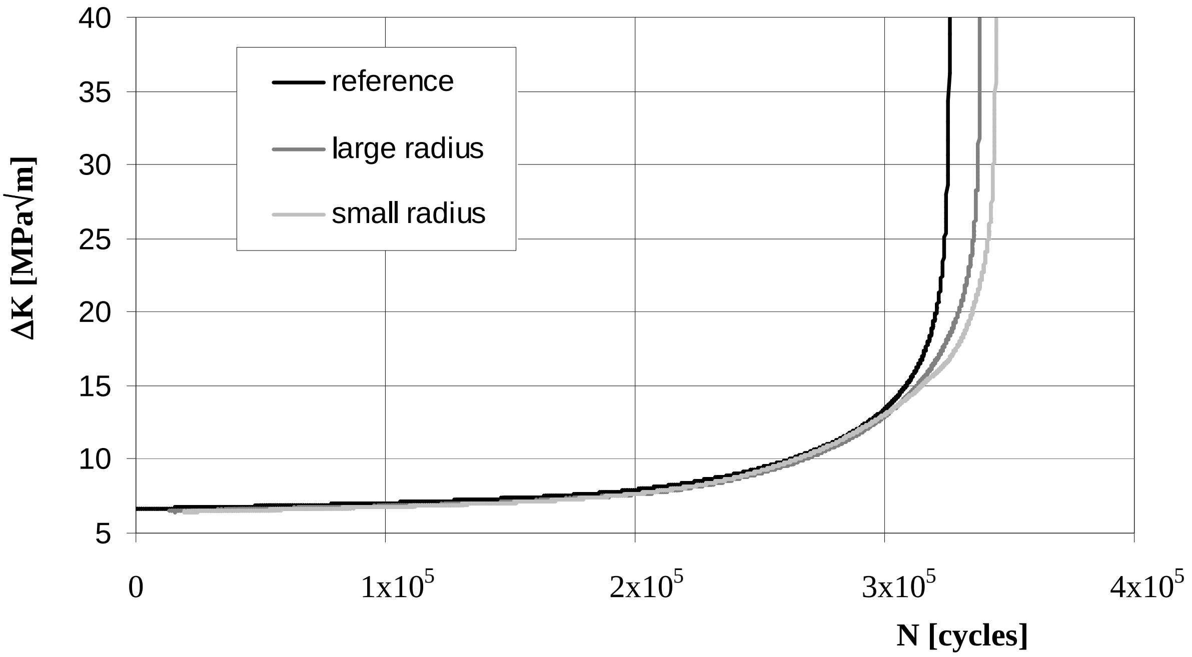

Specimen	**Total fatigue life** (cycles)	**11-25 MPa√m** (cycles)
reference	32.6×10^4	47.0×10^3
large radius	33.8×10^4	54.3×10^3
small radius	34.5×10^4	62.9×10^3

Figure 5.6. Fatigue life for different crack paths, expressed in cycles. Shown is the total amount of cycles and cycles spend in region ΔK 11-25 MPa√m.

5.4 Discussion and conclusions

5.4.1 Curved side groove with a large radius

Gain in cycles

Both plasticity induced crack closure and crack closure induced by rough shear lips can have a significant effect on the fatigue crack growth behaviour. In case of side grooves along a curve with a large radius, a gain of cycles is obtained over the ΔK range between 11-25 MPa√m. This is where the forced shear lip width is larger than the natural shear lip width, i.e. $t_{forced} > t_{natural}$.
The reference test spends 47.0×10^3 cycles over this range, the test with side grooves along the curve with a large radius 54.3×10^3 cycles, see figure 5.6. The gain in cycles is 7300, which corresponds to 15%. However, the absolute gain in fatigue life, expressed in cycles, is less important. More important is the mechanism underlying this behaviour.

Overdrawing effect

It can be calculated that the increase of crack surface area of the forced path for the large radius side grooves relative to the area formed during natural shear lip development is close to 5%. This indicates that the increase in cycles cannot be attributed to an increase of length of the forced crack path only.
For a better understanding (of this effect of “overdrawing”) crack growth rates must be compared between the natural and forced shear lip width. For this purpose, some factors are calculated as a function of crack length and plotted in figure 5.7.
Figure 5.7a shows the development of the forced and natural shear lip width as a function of crack length. Comparison between the natural and forced shear lip width is simply made by subtraction, see figure 5.7b. The difference in shear lip width (mm) is now defined as: $\Delta t_{sl} = t_{forced} - t_{natural}$.

The increase of the crack path is calculated as crack surface of the natural shear lip per mm crack length divided by the crack surface of the forced shear lip per mm crack length, see figure 5.7c.

Figure 5.7d shows the crack growth rate delay factor, defined as a ratio of crack growth rates, i.e. delay factor f_d = da/dN(reference) / da/dN(large curve).

As above mentioned, the prescribed path more or less follows that of the natural shear lip in case of the large radius side grooves, but there are some differences. From a crack length of about 22 mm, t_{forced} is larger than $t_{natural}$. This means that the amount of artificial shear exceeds the amount of natural shear from this point. As a result crack growth retardation is introduced, as shown in figure 5.3a.

If the overdrawing of the shear lip causes the observed increase in cycles, then there must be a relation between the amount of overdrawing, Δt_{sl}, and the change in crack growth rate, f_d.

From figure 5.7d it can be seen that the delay starts at about 22 mm ($f_d = 1$), rises to a maximum value of $f_d = 1.6$ at bout a = 37 mm and decreases from that crack length onwards.

The maximum of f_d appears at a slightly larger crack length than the maximum of Δt_{sl}. This observation is in agreement with [5.11]. It was shown there that the effect of a change in shear lip width on da/dN, in case of a relative large shear lip width, is only noticeable after a certain crack increment.

It can be concluded that there is a relation between on the one hand the degree of overdrawing and on the other hand the delay factor.

However, it is not clear why “underdrawing”, i.e. the suppressing of shear lip development or $t_{forced} < t_{natural}$, has no effect on crack growth rate, while “overdrawing” or $t_{forced} > t_{natural}$ leads to crack retardation.

a: Shear lip widths t_{forced} (grey line) and $t_{natural}$ (black line) are shown as a function of crack length a.

b: Difference in shear lip width:

$$\Delta t_{sl} = t_{forced} - t_{natural}$$

a = 22 mm: $\Delta t_{sl} = 0$
a = 33 mm: Δt_{sl} = maximum

c: Increase of crack surface area, calculated as:
crack surface t_{forced} per mm / crack surface $t_{natural}$ per mm.

d: Delay factor:
f_d = da/dN(reference)/da/dN(large radius)

a = 22 mm: $f_d = 1$
a = 37 mm: f_d = maximum

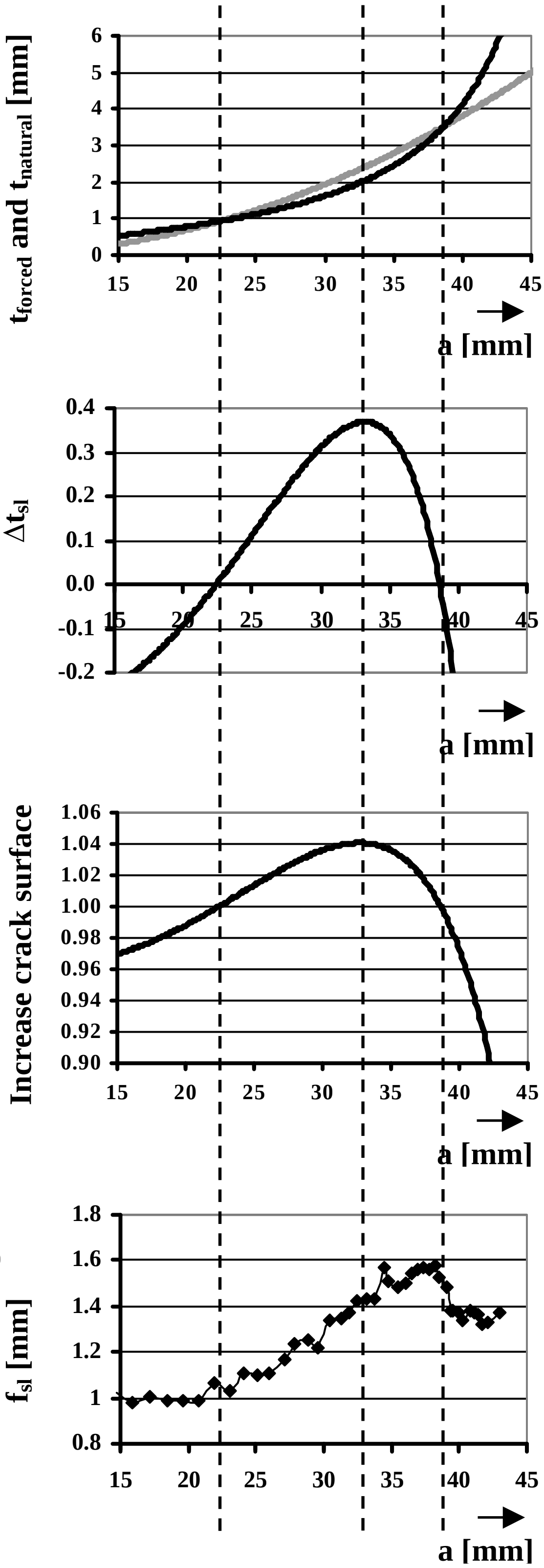

Figure 5.7. Development of shear lip widths (a), difference between the forced and natural shear lip width Δt_{sl} (b), increase of crack surface (delay factor f_d (c), d) and crack growth as a function of crack length in case of a large radius side groove.

5.4.2 Curved side groove with small radius

Breaking out effect

The development of the natural shear lip width $t_{natural}$, the forced shear lip width $t_{forced,}$ as a function of the crack length for the smaller radius side groove (= 68.9 mm) is shown in figure 5.8. From point 1 to point 2 the same situation exists as for side grooves with a radius of 162.5 mm: the artificial shear lip width exceeds the natural shear lip width. A small retardation in crack growth is observed as a result. However, after point 2, at a crack length of 25.5 mm and a ΔK of 15.3 MPa√m, the situation is different.

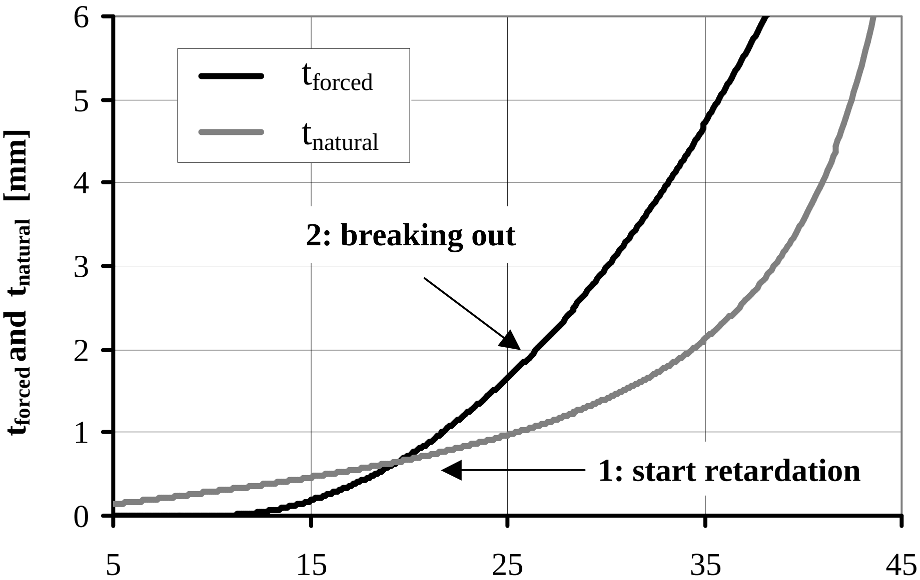

Figure 5.8. The forced shear lip width (t_{forced}) and the natural shear lip width ($t_{natural}$) as a function of the crack length in case of small radius side grooves.

Besides the effect of “overdrawing” there is another effect. The crack breaks away from the side groove. In terms of energy: it seems more efficient to change the cracking direction. During the process of breaking away from the side groove the crack reinitiates. This new direction is perpendicular to the previous shear lip crack growth direction because the two planes of maximum shear stress both make an angle of 45° relative to the loading direction, see figure 5.9.

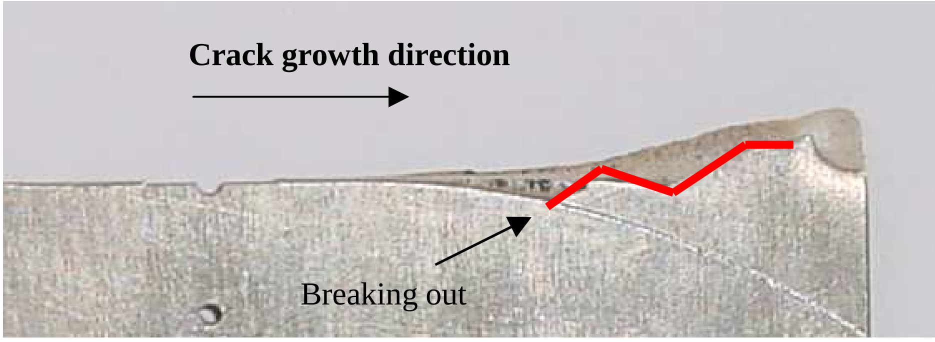

Figure 5.9. Reinitiation of the shear lips after breaking away from the side groove. This "zig zag effect" of the shear lips causes a significant closure effect.

This "zig zag effect" of the shear lips causes a significant closure effect. Thus breaking away at a low frequency leads to large shear lip-induced crack closure effects, comparable to those found at higher test frequencies in AA 2024. The da/dN-ΔK relation is similar to that found at 25 Hz for specimens without side grooves.

Plastic zone

Possibly a relation exists between reinitiation of shear lips and the size of the monotonic plastic zone, however this assumption is only supported by experimental results of a limited number of constant load amplitude tests [5.3]. It is observed that during the devolopment of the shear lips, the monotonic plastic zone at the tip develops in an asymmetric way [5.3]. Material above the direction in which the shear grows, is more plastically deformed, see figure 5.9. Plastic deformation leads to strain hardening which in turn generally leads to a higher fatigue crack resistance. If this asymmetric plastically deformed zone in the shear lip direction becomes too large, it is apparently "energetically" favorable to change the cracking direction. The crack thus reinitiates in the direction of undeformed material, see figure 5.10.

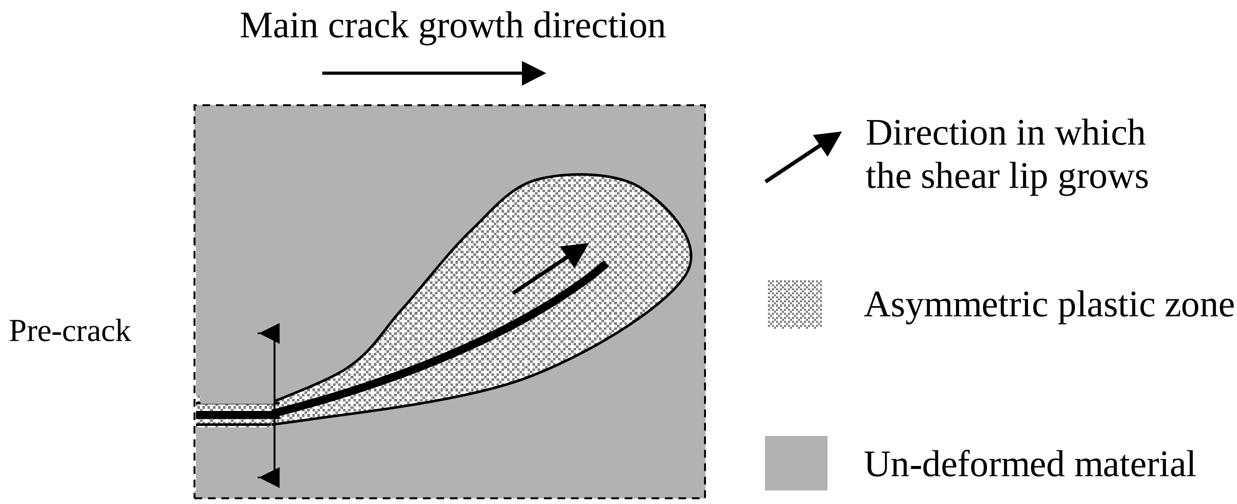

Figure 5.10. Asymmetric development of the plastic zone.

References

[1] C. van Kranenburg, A.C. Riemslag, S. Benedictus-de Vries, J. Zuidema, F.A. Veer, *Plane stress and plane strain in side-grooved centre-cracked tension specimens*, 10th International Conference on Fracture, Honolulu, USA, 2001

[2] F.A. Veer, *The effect of shear lips, loading transitions and test frequency on constant ΔK and constant load amplitude fatigue tests*, Dissertation, Delft University Press, Delft, The Netherlands, 1993

[3] J. Zuidema, *Square and Slant Fatigue Crack Growth in Al 2024*, ISBN 90-407-1191-7, 177 pages, Dissertation, Delft University Press, Delft, The Netherlands, 1995

[4] J. Schijve, W.J. Arkema, *Crack closure and the environmental effect on fatigue crack growth*, faculty of aerospace engineering, report vth-217, Delft, 1976

[5] C. van Kranenburg, J. Zuidema, and F.A. Veer, *Forced crack path deviation*, Proceedings of the International Conference on Fatigue Crack Paths, Parma, Italy, 2003

[6] J. Zuidema, C. van Kranenburg, A.C. Riemslag, F.A. Veer and S. Boljanovic, *Anomalous fatigue crack growth behaviour in AA 2024 and AA 5083*, Proceedings of Materials Structures and Micro mechanics of Fracture, Brno, Czech Republic, 2001

[7] J. Zuidema, F.A. Veer and C. van Kranenburg, *Shear lips on fatigue fracture surfaces of aluminium alloys*, special Issue of "Fatigue and Fracture of Engineering Materials and Structures, 28, pages 159-167, 2005

[8] J. Schijve, *Shear Lips on Fatigue Fractures in Aluminium Alloy Sheet Material*, Engineering Fracture Mechanics, 14, pages 789-800, 1981

[9] W. Elber, *Fatigue Crack Closure Under Cyclic Tension*, Engineering Fracture Mechanics, Volume 2, pages 37-45, 1970

[10] ASTM E 647, *Standard test method for measurement of fatigue crack growth rate*s, American Society for Testing and Materials, Philadelphia, PA USA, 2000

[11] J. Zuidema and M. Manesse, *A model for predicting slant fatigue crack growth in AA 2024*, Engineering Fracture Mechanics, 34, pages 445-456, 1989

[12] J. Zuidema and J.P. Krabbe, *The effect of Regular and Irregular Shear Lips on Fatigue Crack Growth in AA 2024*, Fatigue and Fracture of Engineering Materials and Structures 20, pages 1413-1422, 1997

Chapter 6
Fatigue Crack Growth in the Threshold Region

6.1 Introduction

The value of the threshold stress intensity factor range ΔK_{th} is defined in accordance with ASTM E 647 [1], meaning that this stress intensity factor range does not produce a fatigue crack propagation rate larger than 10^{-10} m per loading cycle. Near-threshold fatigue crack propagation rates generally are at the transition between fatigue crack growth regions I and II, see figure 1.8.

Fatigue crack propagation in the threshold region has become more and more important, since the focus of fatigue design has shifted from a defect-free material towards a defect-tolerant material. Whether a small defect or an already existing crack in a structural material will transform into a growing crack under fatigue loading, thus leading to material failure, is a question of great practical importance. Because most of the lifetime is spent in this range of very low crack growth rates, evidently near-threshold fatigue crack growth is one of the important factors in the development of materials and in design and lifetime assessment of structures.

Experiments in the past have shown that finding a fatigue crack growth threshold value ΔK_{th}, which is valid for a wide variety of loading situations, may not always be possible. Fatigue crack propagation near the threshold cannot simply be described as a function of the cyclic stress intensity ΔK and the stress ratio R. In many cases it is influenced by crack closure, although the mechanisms of crack propagation at the threshold are not exactly known yet.

There are three main aspects that influence the behaviour of fatigue crack propagation in the threshold region. The fatigue crack growth threshold value ΔK_{th} is not only a function of the material properties (e.g. the microstructure, grain size) [2-4], but also depends strongly on the type of loading, i.e. test frequency, wave form, stress ratio, variable or constant amplitude loading [5-7], and the environment (e.g. temperature and type of the surrounding) [8-11]. Besides these main aspects, fatigue crack growth data are not always geometry-independent since thickness effects sometimes occur. Fatigue crack growth rates over a wide range of ΔK have been reported to either increase, decrease, or remain unaffected as specimen thickness increases. Thickness effects can also interact with other variables, such as environment and heat treatment. This means that the influence of the thickness of a specimen on the fatigue crack growth rate is a mixed effect [6.1 section 5.1.3].
Obviously, fatigue crack growth in the threshold region is much more complicated than fatigue crack propagation at higher speed, for example in the Paris region where less material dependence is observed.

In this chapter two approaches are discussed first, namely the generally accepted crack closure concept and the new unified approach to fatigue crack growth. Subsequently, the experimental results of ΔK_{th} tests, obtained by using two different test methods, are presented. The methods chosen for this research are the ASTM E 647 procedure [1] and the constant K_{max}-increasing K_{min} test method. Finally, a comparison is made between these measurement methods. Both procedures are discussed and a possible explanation for the differences in the measured threshold levels is given.

6.2 The crack closure concept and the unified approach to fatigue

6.2.1 View on crack driving force

Although the vast majority of researchers accept crack closure as an important phenomenon affecting fatigue crack growth, a few skeptical papers have been published [12-15]. These papers question the importance of plasticity induced crack closure and suggest that fatigue crack growth should be described by K_{max} and ΔK instead of ΔK and R. The difference between these views focusses on the question of which parameters should be used as driving force for fatigue crack growth. The two views are further discussed in the following sections.

6.2.2 Description of fatigue crack growth threshold using plasticity induced crack closure

In the early 1970s Elber proposed that plasticity induced crack closure plays a significant role in fatigue crack growth [16]. He suggested that the crack growth rate is determined by the stress intensity range between a so-called closure stress intensity and the maximum stress intensity in each cycle, see figure 6.1a.

This traditional concept of crack closure is described by the parameter $U(R) = \Delta K_{eff}/\Delta K$, enabling the description of experimentally observed stress ratio effects.

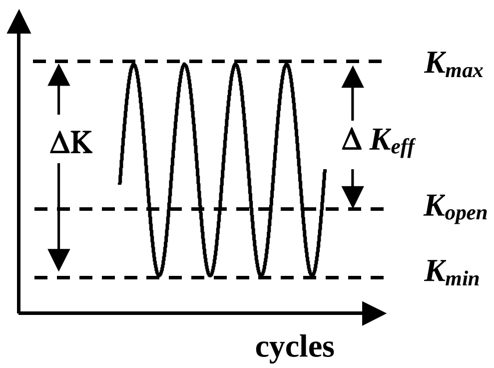

Figure 6.1a. Definition of the effective stress intensity range.

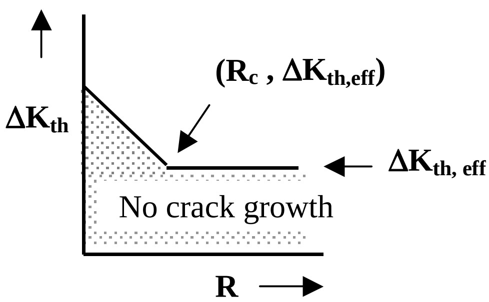

Figure 6.1b. ΔK_{th} as a function of R.

Also fatigue crack growth threshold values were found to depend on R. A common way to present the threshold data is a ΔK_{th}-R plot, see figure 6.1b. The intersection point of the two linear parts of this plot has the coordinates $\Delta K_{th,eff}$ and R_c. This $\Delta K_{th,eff}$ value is believed to be the effective ΔK_{th} for fatigue crack growth. The corresponding R_c value is the critical R above which ΔK_{th} is supposed to be independent of R and equal to $\Delta K_{th,eff}$, because of the absence of crack closure.

In general, crack closure is considered as an important feature for explaining the fatigue crack growth behaviour, however, there are some problems. Donald and Paris [17,18] proved experimentally that crack closure is only partial: measurements performed at locations remote from the crack tip show lower opening loads compared to measurements taken near the crack tip. Since crack opening and closure points depend on the location where measurements are performed, ΔK_{eff} cannot be determined unambiguously using this type of experiment.

6.2.3 The Unified Approach to Fatigue

The so-called unified approach to fatigue formulated by Vasudévan [19,20] uses two parameters to describe the driving force for fatigue crack propagation, namely ΔK and K_{max}. This avoids the complicated R effect caused by crack closure. Experimental results of fatigue crack growth threshold tests, carried out by Vasudévan and Sadananda [21], are explained by assuming that the fatigue crack growth rate is determined by both ΔK and K_{max}. They define two critical values at the threshold level, namely ΔK_{th}^* and $K_{max,th}^*$. Values of either ΔK or K_{max} below these critical values do not lead to crack growth, or more precisely, lead to crack growth rates below 10^{-10} m/c. The two parameter description for the fatigue crack growth threshold condition associated with ΔK_{th}^* and $K_{max,th}^*$ are schematically illustrated in figure 6.2 [22]. This ΔK-K_{max} plot gives the critical driving forces ΔK_{th}^* and $K_{max,th}^*$ needed for crack advance near the threshold value.

The idea behind this description is that the requirement $\Delta K > \Delta K_{th}^*$ ensures a sufficiently high cyclic load amplitude to induce a characteristic cyclic damage, while the requirement $K_{max} > K_{max,th}^*$ allows the peak load to break open the bonds in the cyclically damaged region [15, 22].

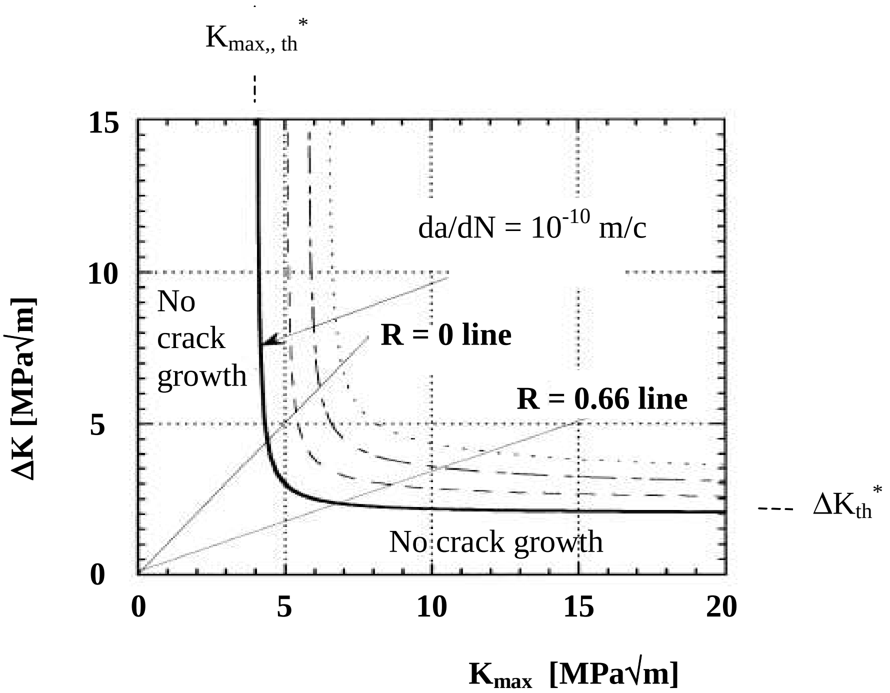

Figure 6.2. Two-parameter description using ΔK_{th} and $K_{max,th}$* for the threshold of fatigue crack propagation. Higher values for the crack growth rate are also shown. No crack growth means da/dN < 10^{-10} m/c.*

Consequently, there are two thresholds that must both be exceeded for a crack to grow. At low R values (and especially when R is negative), the threshold value for K_{max} (= $K_{max,th}^*$) limits the fatigue crack growth, while at high R, as R approaches 1, the threshold value of ΔK (= ΔK_{th}^*) limits the fatigue crack growth. In this description a possible crack closure effect on fatigue crack propagation is not taken into consideration.

6.3 The ASTM E 647 test method and the constant K_{max} - increasing K_{min} procedure

Threshold tests have been performed in two different ways on centre-cracked tension specimens of aluminium alloy AA 5083. The principle of the two threshold tests is shown in figure 6.3. The standardized ASTM test method, figure 6.3a, is compared with the constant K_{max} - increasing K_{min} method, figure 6.3b. Obviously, in both test procedures, ΔK decreases with increasing crack length.

The ASTM procedure recommends to start the test at a fatigue crack growth rate below 10^{-8} m/c, see section 8.6 of [6.1]. In general the fatigue crack growth rate is strongly influenced by the amount of plastic deformation near the crack tip. A disadvantage of the ASTM method, resulting from the fact that K_{max} decreases, is that both the plastic zone size and the average crack opening decrease with increasing crack length. To avoid effects on crack growth, K_{max} must be reduced in small steps. In view of this, section 8.6.2 of the ASTM standard [6.1] introduces the normalized K gradient, C, which is the relative rate of change of K (also called K shedding) with per unit crack growth, defined as C = (1/K) (dK/da). This normalized K gradient is limited to a numerical value equal to or greater than $-0.08\ \text{mm}^{-1}$. Since the load ratio R is kept constant, this means:

$$
\begin{aligned}
C &= \left(1/K_{\max}\right)\left(dK_{\max}/da\right) \\
&= \left(1/K_{\min}\right)\left(dK_{\min}/da\right) \\
&= \left(1/\Delta K\right)\left(d\Delta K/da\right) \qquad > -0.08\ \text{mm}^{-1}
\end{aligned}
\tag{6.1}
$$

Both K_{max} and K_{min} and thus ΔK are reduced at the same rate to keep the stress ratio R constant. ΔK_{th} values can be determined as a function of R, using this time consuming test procedure. The fatigue crack growth threshold, ΔK_{th}, is the asymptotic value of ΔK at which da/dN approaches "zero", see section 3.3.2 of [1].

For the constant K_{max} - increasing K_{min} procedure, the maximum stress intensity K_{max}, and thus the monotonic plastic zone size remains constant, while K_{min} increases with crack length. The speed of increase of the applied K_{min} will be further explained in section 6.5.1.

A disadvantage of this method is the variable stress ratio. R is not a fixed value for this type of experiment and increases as the crack grows.

In this test the crack grows until the driving force and the resistance to cracking of the material are in balance and crack arrest occurs. Crack arrest is assumed to be obtained when $da/dN \leq 10^{-10}$ m/c is reached. Now ΔK_{th} and the corresponding R_{th} are found.

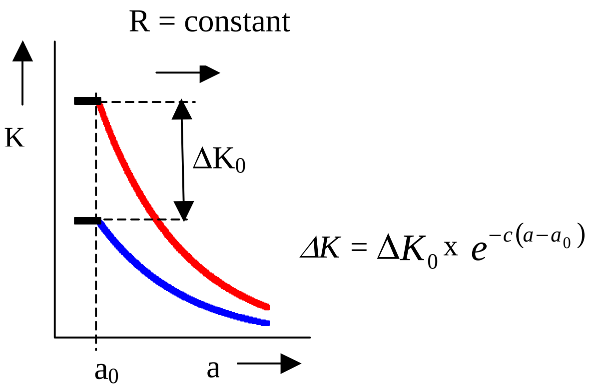

Figure 6.3a. ASTM E 647-method. ΔK_0 is the cyclic stress intensity at the beginning of the test.

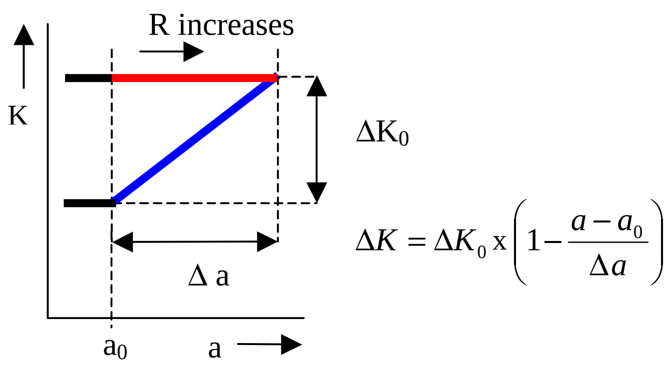

Figure 6.3b. Constant K_{max}-increasing K_{min} method.

6.4 Threshold measurements using the ASTM E 647 method

6.4.1 Experimental conditions

ΔK_{th} levels were measured according to the ASTM E 647 method. The dimensions of the specimen (AA 5083) were a thickness of 8 mm, a length of 340 mm and a width of 100 mm. The notch length was 5 mm. Measurements were performed using the test configuration described in Chapter 2. Tests were carried out at room temperature in a normal lab air environment using a constant load frequency. A number of different load frequencies were used in the range between 10 and 25 Hz. All tests were performed on a Schenck testing machine. For this test series, a C value of –0.06 mm^{-1}, was chosen, which leads to a lower K_{max} decrease rate compared to the maximum allowed C value of –0.08 mm^{-1}. The reason for this is to ensure that the influence of K shedding is minimized. All tests started after initial fatigue crack growth from the notch at a crack growth rate below 10^{-8} m/c. At the end of each test, once an average crack growth rate of da/dN ≈ 10^{-10} m/cycle (or lower) was obtained, the load was kept constant at P_{max} in order to prevent damage to the fracture surfaces. All specimens were broken after the tests and checked for crack length and asymmetric crack growth. A number of different, constant positive R values were used to find the corresponding ΔK_{th} value. The data were analyzed using the least square method, as described in Chapter 2.

6.4.2 Results found using the ASTM E 647 method

Results are presented in figure 6.4 and table 6.1.

The da/dN-ΔK curves for different R values, except for R = 0.4 and 0.86, are plotted in figure 6.4. From this figure it can be seen that the curves for R = 0, 0.1, 0.2 have lower crack propagation rates than the curves for R = 0.5 and 0.7. The curves for R = 0.5 and R = 0.7 almost coincide. The curve in case of R =

Table 6.1: ΔK_{th} and the corresponding $K_{max,th}$ at different stress ratios R for AA 5083.

R	ΔK_{th}	$K_{max,\ th}$
0	2.2	2.2
0.1	2.0	2.2
0.2	1.8	2.3
0.4	1.5	2.5
0.5	1.4	2.8
0.6	1.3	3.3
0.7	1.3	4.3
0.86	1.3	9.3

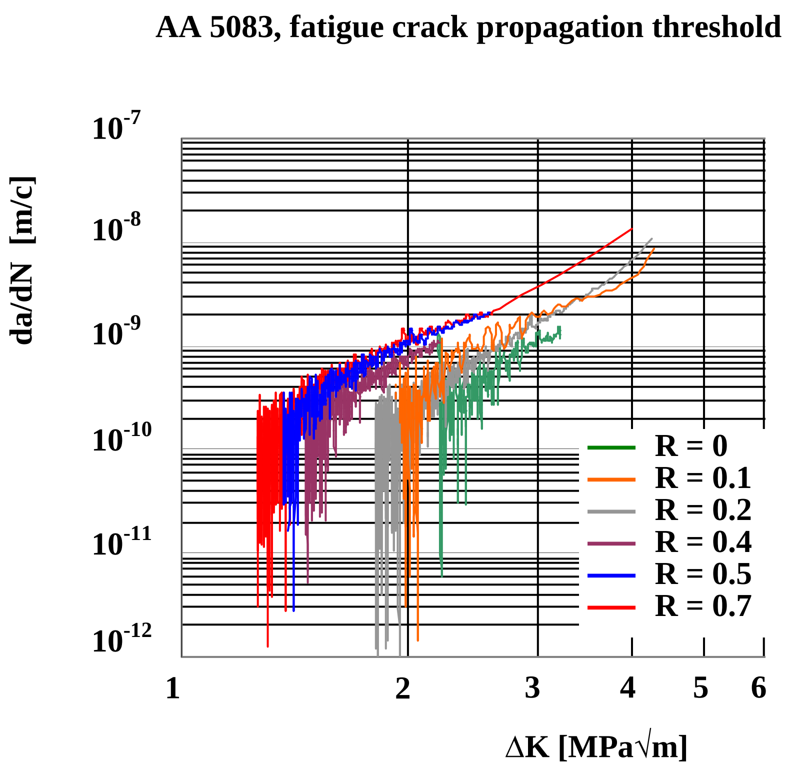

Figure 6.4. da/dN as a function of ΔK, tested with the ASTM E 647 method for different R values.

0.86 is not shown, because this curve is the same as for R = 0.7. Figure 6.5b shows the results of ΔK_{th} as a function of R. The ΔK_{th} value at the point of intersection of the two lines added, is believed to be the effective ΔK_{th} value for fatigue crack growth, denoted as the effective value $\Delta K_{th,eff}$. The R value at the intersection point is defined as R_c. ΔK_{th} has a constant value and is independent of R for $R > R_c$, because of the absence of crack closure.

A simple linear R dependent U function is calculated, see figure 6.5a, using a number of different threshold values taken from table 6.1 and figure 6.5b. This function takes the form of:

$$U = 0.59 + 0.67R \tag{6.2}$$

The assumption is made that $\Delta K_{eff,th} = U\Delta K_{th}$ (= 1.3 MPa√m) and that U = 1 for $R \geq 0.6$.

The two parameter description for fatigue crack growth in the threshold region, ΔK_{th}^* and $K_{max,th}^*$, found by using the ASTM E 647 method, are shown in figure 6.6. Crack growth only takes place when both threshold conditions are met.

6.5 Threshold measurements using the constant K_{max} -increasing K_{min} method

6.5.1 Experimental conditions

In case of a threshold test, using the constant K_{max} - increasing K_{min} method, the ΔK can be decreased over a shorter crack length, compared to a similar test in case of the ASTM procedure. For this reason the constant K_{max} - increasing K_{min} method can be a fast alternative for the latter method. Before the constant K_{max} - increasing K_{min} method can be accepted as an alternative to the ASTM standard

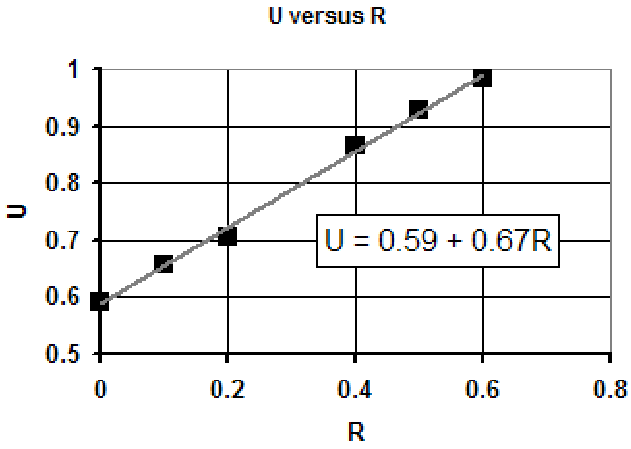

Figure 6.5a. U ($=\Delta K_{th,eff}/\Delta K_{th}$) versus R calculated using values taken from table 6.1. It is assumed that $\Delta K_{th,\ eff}$ = 1.3 MPa$\sqrt{}$m and U = 1 for R $\geq$ 0.6.

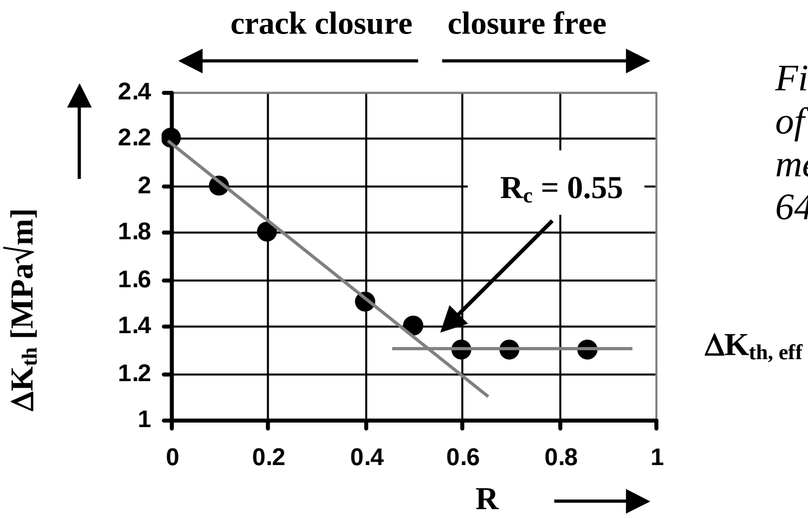

Figure 6.5b: ΔK_{th} as a function of R. Threshold values were measured using the ASTM E 647 method.

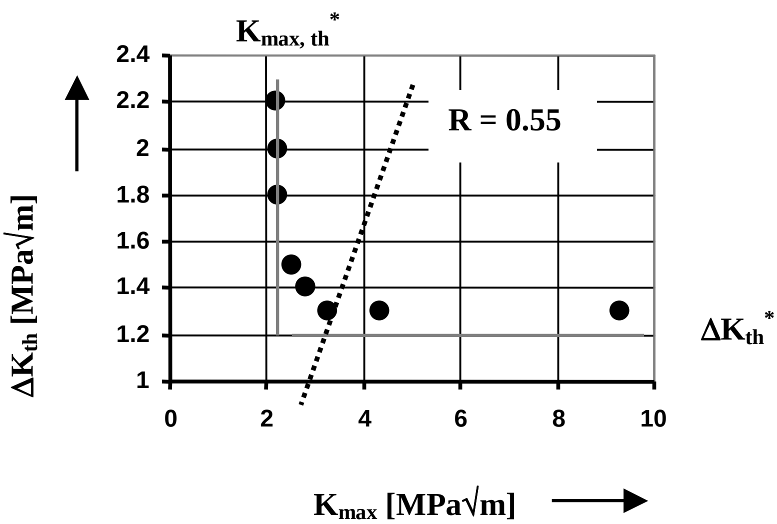

Figure 6.6: Unified approach concept. The two parameter description for fatigue crack growth are shown for the data from figure 6.5.

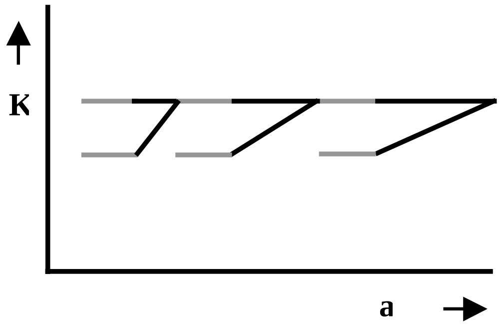

K_{max} = 6 MPa√m
R_{start} = 0.5

dK_{min}/da [MPa√m/mm]	R_{th}	ΔK_{th} [MPa√m]
0.25	0.8	1.1
0.5	0.8	1.2
1.0	0.8	1.1

Figure 6.7. Loading scheme and test results for test series 1. The influence of speed of increase of K_{min} (dK_{min}/da) is investigated. The resulting values for R and ΔK at the crack growth threshold are about the same.

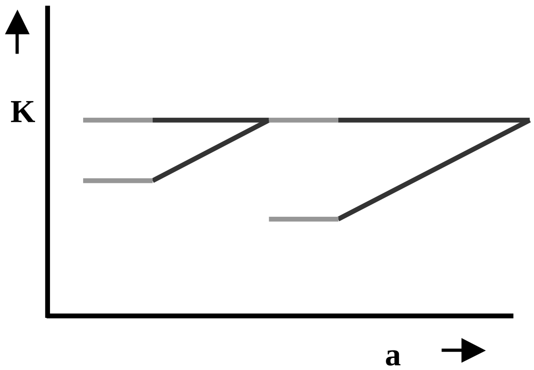

K_{max} = 6 MPa√m
dK_{min}/da = 0.5 MPa√m/mm

R_{start}	R_{th}	ΔK_{th} [MPa√m]
0.5	0.8	1.1
0.7	0.8	1.1

Figure 6.8. Loading scheme and test results for test series 2. The influence of R_{start} is investigated. The resulting values for ΔK_{th} and R_{th} are about the same.

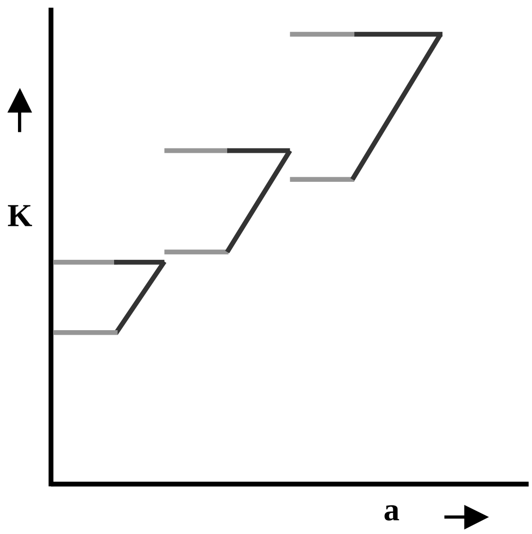

dK_{min}/da = 0.5 MPa√m/mm
R_{start} = 0.7

K_{max} [MPa√m]	R_{th}	ΔK_{th} [MPa√m]
6	0.80	1.1
12	0.90	1.1
18	0.93	1.1

Figure 6.9. Loading scheme and test results for test series 3. The influence of K_{max} is investigated. The resulting R_{th} values are different but the ΔK_{th} values are about the same.

method, a good understanding of the influence of the experimental conditions is important. The experimental conditions are defined by 3 parameters:

- the rate of increase of $K_{min,}$ (dK_{min}/da in MPa√m/mm),
- the initial R value
- the (constant) K_{max} value

Three tests series have been conducted in order to investigate the influence of the above-mentioned conditions on the results of this method and aluminium alloy. Tests have been carried out using the same specimen geometry and test configuration as described in section 6.4. The data were analyzed using a simple 'moving average' method; see Chapter 2, section 2.3.2.

Test series 1: dK_{min}/da is varied

In the first series, see figure 6.7, the speed of increase of the applied K_{min} is varied. K_{max} is kept constant at 6 MPa√m and all tests start at R = 0.5. The highest speed in test series 1 is limited to dK_{min}/da = 1 MPa√m/mm, due to the accuracy of the potential drop method in combination with the pre-stored load table.

Test series 2: R_{start} is varied

In the second series, see figure 6.8, the initial R value, R_{start}, is varied. K_{max} is kept constant at 6 MPa√m and in all tests the speed of increase of K_{min} is constant, namely 0.5 MPa√m/mm. In case of R_{start} = 0.5, the minimum stress intensity K_{min} is approximately equal to the opening stress intensity K_{op}, while for R = 0.7 this is higher than the opening stress intensity.

Test series 3: K_{max} is varied

In the last series, see figure 6.9, the K_{max} value is varied. All tests start at R = 0.5 and in all tests the speed of increase of K_{min} is constant, namely 0.5

MPa√m/mm. Note that in case of a relatively high K_{max}, the test starts at a crack growth rate larger than 10^{-8} m/c.

The da/dN-ΔK relations obtained for all these tests should be the same: if there is any difference in results, the experimental conditions are supposed to be responsible.

6.5.2 Results found using the constant K_{max} - increasing K_{min} method

The results are presented in three parts, series 1, 2 and 3 respectively. Figure 6.10 shows the results for the investigation of the speed of increase of K_{min}, figure 6.11 the influence of R_{start} and figure 6.12 the effect of K_{max}.
Results of test series 1, with the rate of increase of K_{min} as the variable, show no effect on R_{th} and ΔK_{th}, where R_{th} and ΔK_{th} are the R and the ΔK values at threshold respectively. This means that the influence of the rate of increase within the tested range is absent.
Results of test series 2 show that using either $R_{start} = 0.5$ or 0.7 does not result in a change in ΔK_{th} and R_{th}. This is what was expected, because both tests start almost in the absence of crack closure. However, test series 3 shows that the effect of K_{max} on R_{th} is significant. It is seen that R_{th} increases with increasing K_{max}. ΔK_{th} is found to be a constant value, which was expected for $R_{th} > R_c$, because of the absence of crack closure.
The relation R_{th} could be predicted with the following expression:

$$R_{th} = \left(1 - \frac{\Delta K_{th}}{K_{\max,th}}\right) \tag{6.3}$$

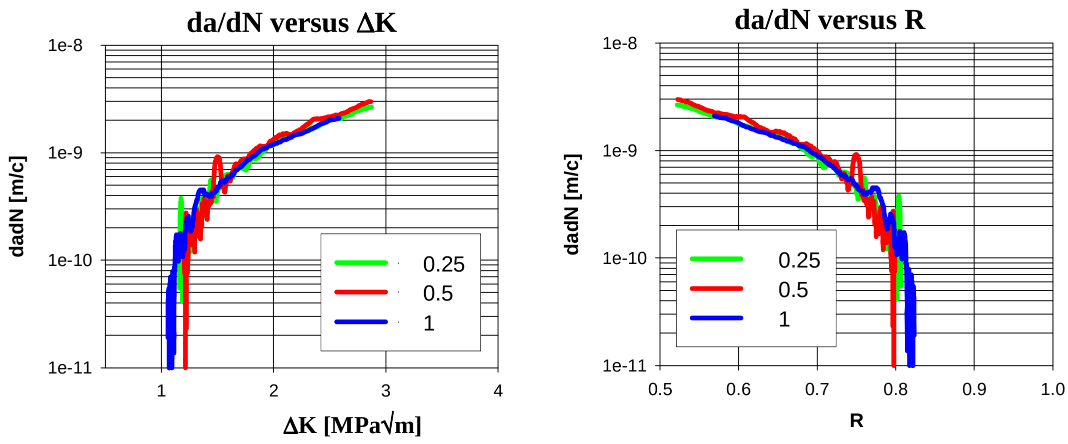

Figure 6.10: da/dN versus ΔK and R for test series 1. dK_{min}/da (0.25, 0.5 or 1 MPa√m/mm is variable. The resulting values for R_{th} and ΔK_{th} at the crack growth threshold are about the same, namely 0.8 and 1.1 MPa√m respectively.

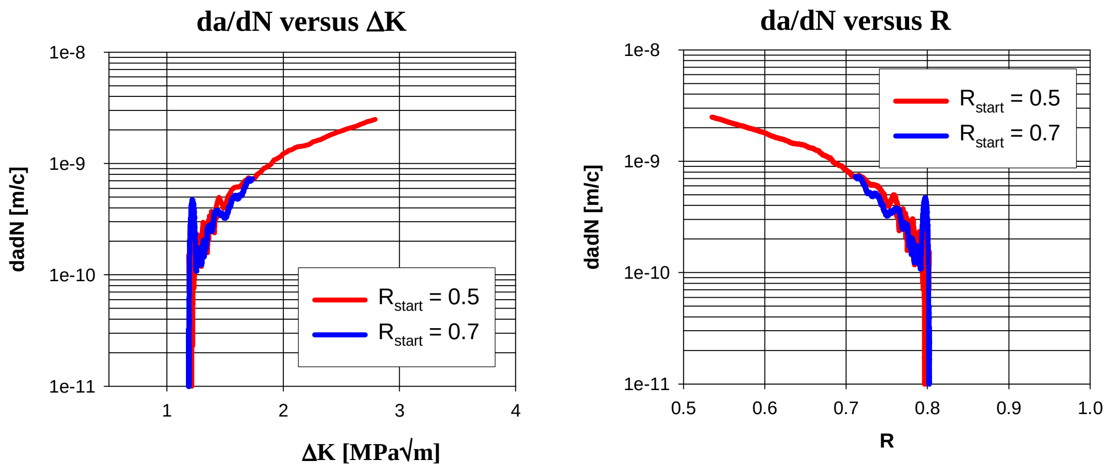

Figure 6.11. da/dN versus ΔK and R for test series 2. R_{start} is variable. The resulting values for R_{th} and ΔK_{th} at the crack growth threshold are about the same, namely 0.8 and 1.1 MPa√m respectively.

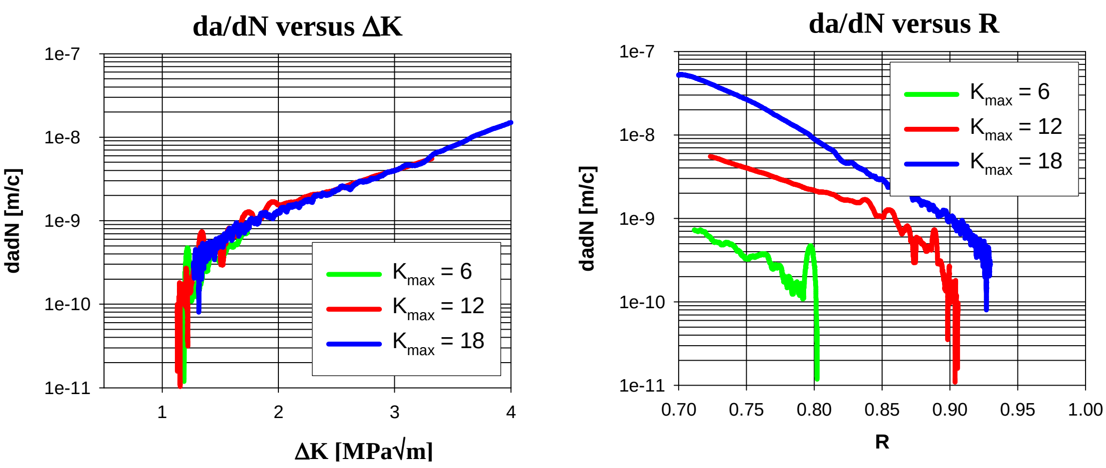

Figure 6.12. da/dN versus ΔK and R for test series 2. K_{max} is variable, namely 6, 12 and 18 MPa√m. The resulting values for R_{th} are 0.80, 0.90 and 0.93 respectively but the ΔK_{th} are about the same: 1.1 MPa√m.

Looking more closely at the results, it can be observed that the crack growth rate near the ΔK_{th}-value shows large fluctuations. An explanation is given in section 6.7.

In general a ΔK_{th} value of about 1.1 MPa√m is obtained, using this test method.

Some more experiments are performed, with R_{start} = 0 and 0.5 and a speed of increase of K_{min} = 0.5 MPa√m/mm using different $K_{max,start}$ values, see table 6.2. Crack propagation does not occur in all cases, see table 6.2.

The unified approach to fatigue defines two critical crack driving forces, namely ΔK and $K_{max,}$. It can be seen from figure 6.6 that at least values about 2.2 MPa√m and 1.3 MPa√m are required for K_{max} and ΔK respectively to obtain crack propagation. No crack propagation occurs at all when these two requirements are not satisfied, which agrees with tests results shown in table 6.2. A test using $K_{max,start} = \Delta K_{start}$ = 2.5 MPa√m leads to a combination of R_{th} = 0.41 and ΔK_{th} = 1.5 MPa√m. In case of a $K_{max,start}$ value of 9 MPa√m and ΔK_{start} = 4.5 MPa√m the crack grows until a threshold value of about 1.1 MPa√m.

Table 6.2. Measurement results using different Kmax start values, showing start conditions at the beginning of the tests, requirements, needed for fatigue crack growth and threshold values obtained. X indicates that no crack propagation has been observed.

start conditions			requirements		threshold values	
R_{start}	$K_{max,start}$	ΔK_{start}	K_{max} >	ΔK >	R_{th}	ΔK_{th}
0	2.0	2	2.2	1.3	XX	XX
0.5	2.2	1.1	2.2	1.3	XX	XX
0.5	2.4	1.2	2.2	1.3	XX	XX
0	2.5	2.5	2.2	1.3	0.41	1.5
0.5	9	4.5	2.2	1.3	0.87	1.1

6.6 Influence of load shedding

It is found in the constant K_{max} - increasing K_{min} tests, that, as long as K_{max} is larger than a critical threshold value K_{max}^*, variation in K_{max} values has no influence on ΔK_{th}, which is then about 1.1 MPa√m. The $\Delta K_{th,eff}$ obtained by using the ASTM standard test method has a value of about 1.3 MPa√m. The reason for this difference is not yet clear, but it should be due to differences in the test methods used. Three kinds of tests were carried out in order to find out if the prior loading history influences the value of ΔK_{th} in ASTM tests.

Experiments

Tests 4, 5 and 6 were conducted on AA 5083 centre-cracked tension specimens, using the decreasing ΔK procedure at fixed R, according to the ASTM. The loading schemes and the ΔK_{th} values found are given in Figure 6.13. All tests, except for one pre-crack procedure, are performed under crack closure free conditions, i.e. at R = 0.7. Test 4 starts with high values for K_{max} and $K_{min,}$, causing shear lips to develop, while test 6 starts at a ΔK too low to give rise to shear lip development. Test 5 is pre-cracked at R = 0.1. Under this condition shear lips also develop. After the pre-crack procedure, this test continues with R = 0.7 in order to propagate without crack closure. The load shedding value C is chosen as–0.06 mm^{-1}.

Results

Test 4 shows the transition point T2 at da/dN = 0.5×10^{-8} m/cycle, identical to what was found in earlier tests, see Chapter 4. A threshold value of 1.9 MPa√m was found in test 4, which is significantly higher than the value of 1.3 MPa√m that was measured in both tests 5 and 6.

Discussion: Remote crack closure

It is suspected that the high threshold value of about 1.9 MPa√m obtained from test 4 is the result of the large residual plastic deformation near the starter notch formed at the start of the test. It may be that this prevents the crack tip from completely closing at the end of the test. The term “remote crack closure” was introduced by Newman [6.23] and He [6.24] for this phenomenon.

	loading scheme	pre-crack	ΔK_{th} result
4	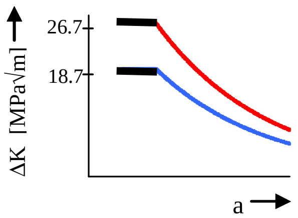	$R = 0.7$ $K_{max} = 26.7$ MPa√m $\Delta K = 8$ MPa√m	1.9 MPa√m
5	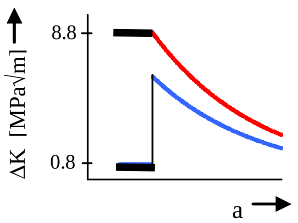	$R = 0.1$ $K_{max} = 8.8$ MPa√m $\Delta K = 8$ MPa√m	1.3 MPa√m
6	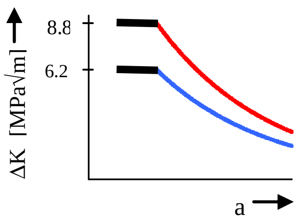	$R = 0.7$ $K_{max} = 8.8$ MPa√m $\Delta K = 2.8$ MPa√m	1.3 MPa√m

Figure 6.13. Loading scheme of tests 4, 5 and 6. Different pre-crack procedures are applied. After the pre-crack procedure all tests continue with R= 0.7 in order to propagate under a crack closure free condition. The load shedding value C is chosen as –0.06 mm^{-1}.

In order to understand the influence of the loading history that causes remote crack closure, the following parameters are calculated according to the equations given in [25]:

- the maximum and minimum vertical crack flank displacement (V_{max} and V_{min}) see equations 6.4 and 6.5.
- the monotonic plastic zone size ($2r_p$), see equation 6.6
-the maximum and minimum Crack Tip Opening Displacement ($CTOD_{max}$ and $CTOD_{min}$), see equations 6.7 and 6.8.

$$v_{\max} = \frac{2\sigma_{\max}}{E}\sqrt{a^2 - x^2} \tag{6.4}$$

$$v_{\min} = \frac{2\sigma_{\min}}{E}\sqrt{a^2 - x^2} \tag{6.5}$$

$$2r_p = \frac{1}{\pi}\left(\frac{K_{\max}}{\sigma_{ys}}\right)^2 \tag{6.6}$$

$$CTOD_{\max} = \frac{4}{\pi}\frac{K_{\max}{}^2}{E\sigma_{ys}} \tag{6.7}$$

$$CTOD_{\min} = \frac{4}{\pi}\frac{K_{\min}K_{\max}}{E\sigma_{ys}} \tag{6.8}$$

The V_{max} and the V_{min} indicate the maximum and minimum crack flank displacement at the crack centre, i.e. in the middle of the specimen, based on the applied stress and crack length, see figure 6.14 [25].

The monotonic plastic zone size can be used as an indication only of plastic deformation due to the loading history at the beginning of the test. The $CTOD_{max}$ and the $CTOD_{min}$ are an approximation for the maximum and minimum Crack Tip Opening Displacement respectively.

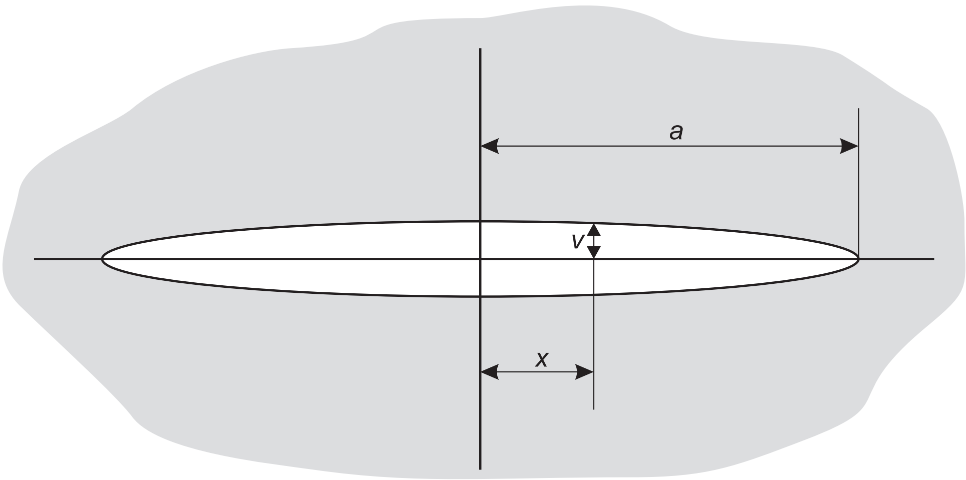

Figure 6.14. Crack flank displacement V at position x.

The values of these quantities for tests 4, 5 and 6 are given in table 6.3. At the moment the threshold condition is reached, the crack flank displacement *V* at the centre of the specimen, see equations 6.4 and 6.5, is calculated, using the applied stress σ and crack length *a* in combination with the starter notch length of x = 5 mm.

A much larger plastic zone size and CTOD is involved during pre-cracking of test 4, than of tests 5 and 6. Thus in test 4 much more residual deformation was induced along the flanks of the pre-crack compared to the other two tests. At the moment the threshold condition was reached in test 4, the crack opening at the centre should vary between 38 μm and 27 μm. These values are of the same order as the maximum CTOD at the moment the pre-crack was formed, i.e. 27 μm. It can therefore be imagined that the crack flank displacement at the threshold condition is not large enough to prevent crack closure in the middle of the specimen. This is the phenomenon of remote crack closure. The mechanism is schematically illustrated in figure 6.15.

Table 6.3. ΔK_{th}, [MPa√m], crack flank displacement at the centre *V* [μm] Crack Tip Opening Displacement *CTOD* [μm] and monotonic plastic zone size r_p [μm] for tests 4, 5 and 6.

	pre-crack load data	**ΔK_{th}** [MPa√m]	**$K_{max,th}$** [MPa√m	**$K_{min,th}$** [MPa√m]	**V** $V_{max, centre, th}$ $V_{min, centre, th}$ [μm]	**CTOD** $\delta_{max\ pre-crack}$ $\delta_{max\ th}$ [μm]	**r_p** $r_{p\ pre-crack}$ $r_{p,\ th}$ [μm]
4	ΔK=8 R=0.7 K_{max}=26.7 K_{min}=18.7	1.9	6.2	4.3	38 27	27 1.3	2232 18
5	ΔK=8 R=0.1 K_{max}=8.8 K_{min}=0.8	1.3	4.3	3.0	16 11	3 0.7	248 57
6	ΔK=3 R=0.7 K_{max}=8.8 K_{min}=6.2	1.3	4.4	3.1	18 13	3 0.7	248 57

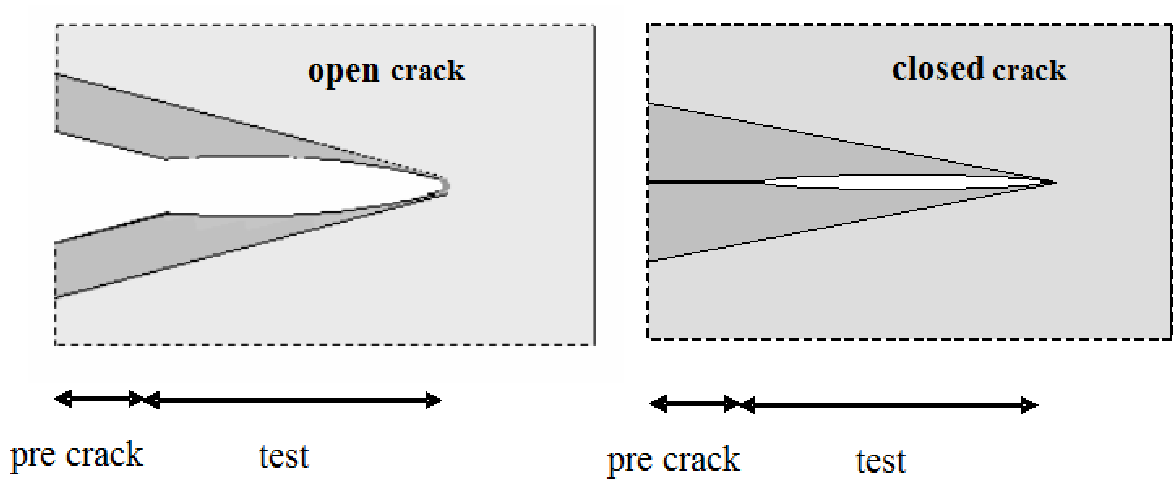

Figure 6.15. Remote crack closure. Large plastic deformation caused by a relative high K_{max} value at the beginning of the test leads to crack closure in the middle of the specimen at the threshold level and thus to a higher dK_{th}.

The CTOD values of test 5 and 6 during pre-cracking are quite low, namely 3 μm. At threshold level, V_{min} values in test 5 and 6 are large enough to prevent contact of the crack flanks in the middle of the specimen. Thus in these specific tests, if crack closure occurs, it does not occur in the middle of the specimen, but perhaps closer to the crack tip.

6.7 Comparison of the ASTM E 647 method and the Constant K_{max}-increasing K_{min} procedure

Fatigue crack propagation in the threshold regime is more complicated than that in the Paris regime. The fatigue threshold behaviour is not only sensitive to the material properties and the loading system, but also to the environment.

Figure 6.16 shows two da/dN-ΔK curves in the near-threshold area. They were found by using the ASTM method and the constant K_{max}-increasing K_{min} method respectively. The ASTM curve was performed with a high, constant R (0.86) with the expectation that $\Delta K = \Delta K_{eff}$, thus closure-free crack growth. In the second method, R increases.

In figure 6.16 four characteristic points (A-D) are shown:

A: start of the constant K_{max}-increasing K_{min} test. The test starts with R = 0.1 and K_{max} = 6 MPa√m, and the speed of increase of K_{min}, dK_{min}/da, is chosen as 1 MPa√m/mm.

A-B: this range shows a difference in the da/dN results found by both methods. The cause of this is that the constant K_{max}-increasing K_{min} method is influenced by crack closure leading to $\Delta K_{eff} < \Delta K$ at lower R. For the ASTM method at R = 0.86 it is expected that $\Delta K_{eff} = \Delta K$.

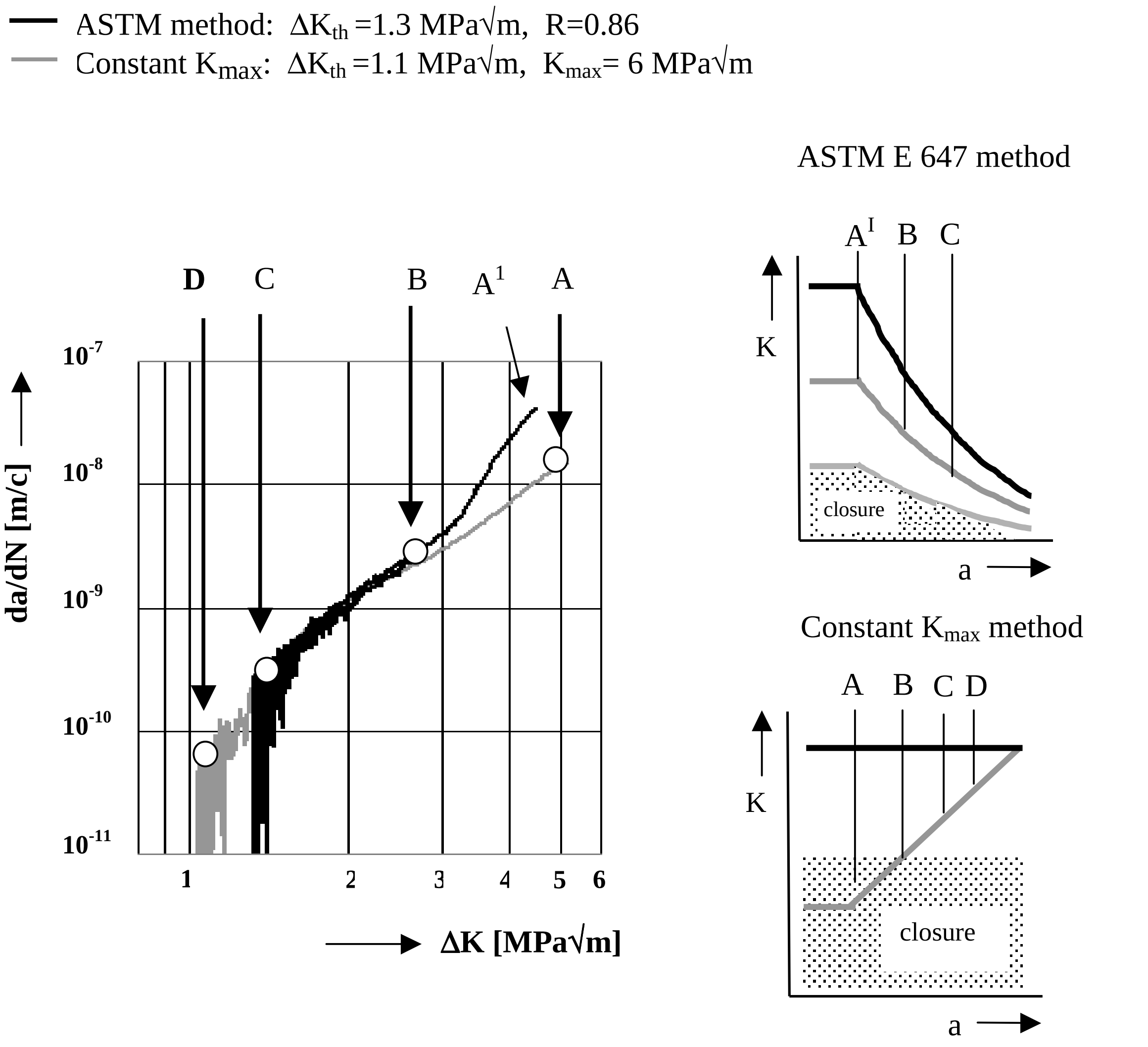

	ASTM E 647	constant K_{max} -increasing K_{min}
A/A[1]	$\Delta K_{eff} = \Delta K$	$\Delta K_{eff} = K_{max} - K_{closure}$
B	$\Delta K_{eff} = \Delta K$ (ASTM) $= \Delta K$ (CK_{max}) (for CK_{max}-method: $R \geq R_c$)	
C	$\Delta K = \Delta K_{th}$ $R=R_{th}$	$\Delta K_{eff} = \Delta K$
D	N/A	$\Delta K_{eff} = \Delta K = \Delta K_{th}$ $R=R_{th}$

Figure 6.16. da/dN versus ΔK with loading schemes for the ASTM E 647 and the constant K_{max}-increasing K_{min} methods.

B: at this point both curves coincide. R has grown now to about 0.6 in the constant K_{max}-increasing K_{min} method. This means that also here a crack closure free situation has been realized.

B-C: the results are the same for both test methods; for both $\Delta K_{eff} = \Delta K$.

C: the ASTM curve shows a sudden change in slope. It is suspected that from here crack closure starts due to the low load level, despite the high R-value. This is not observed in the other method, where K_{max} and R (about 0.8) are relatively high and a closure free situation is maintained.

D: here also the constant K_{max}-increasing K_{min} method shows a transition in crack growth rate. The ΔK value at this transition is lower than for the ASTM method. The crack growth now stops in a closure free situation, meaning that the corresponding ΔK_{th} may be a real intrinsic material property (with respect to the environment) that is not influenced by an extrinsic phenomenon such as crack closure. Note that following the ASTM definition ΔK_{th} is reached for da/dN = 10^{-10} m/cycle. In figure 6.16 it is shown that this definition can lead to problems if the constant K_{max}-increasing K_{min} curve is considered. The ASTM method has its transition point T1 above 10^{-10} m/cycle, while the constant K_{max}-increasing K_{min} method has its transition point below it.

Two different ΔK threshold values are found at 10^{-10} m/c. For this material a value of 10^{-11} m/cycle (which is much smaller than 2.5 x10^{-10} m, the order of the atomic spacing) probably would be a better criterion; however the physical meaning is less. On the other hand, fatigue crack growth at the threshold is not a stable, continuous process along the whole crack front. The fatigue crack growth rate is an average value over a number of cycles. The ASTM method has very low crack opening values at the threshold. This can lead to crack closure especially when rough crack flank surfaces are formed.

ASTM E 647

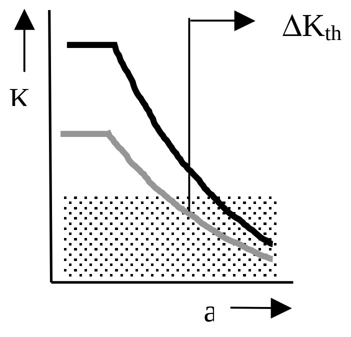

$\Delta K_{th\ eff}$ = ΔK_{th} – correction ΔK
due to: -surface roughness cc
-oxide induced cc
-load shedding

constant K_{max}-increasing K_{min}

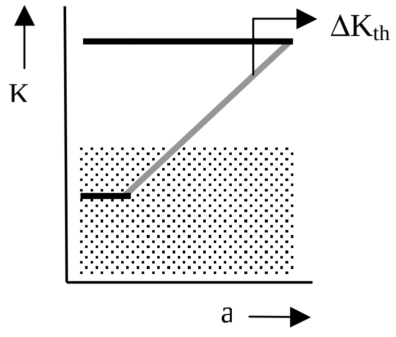

$\Delta K_{th,\ eff} = \Delta K$

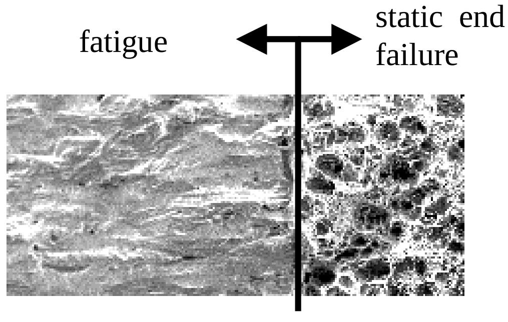

250 μm

- ΔK_{th} = 1.3 MPa√m, R = 0.86
- surface smoothed by friction
- not a “crack closure free” situation

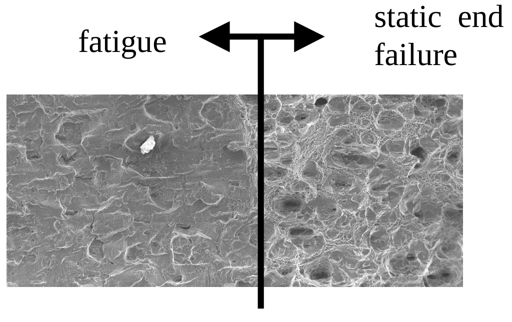

250 μm

- ΔK_{th} = 1.1 MPa√m, R_{th} = 0.83
- rough fracture surface
- a “crack closure free” situation ?

Figure 6.17. Fracture surfaces in the threshold region of an ASTM sample and of a constant K_{max}-increasing K_{min} sample.

Figure 6.17 shows micrographs of the fracture surfaces in the threshold region ($da/dN \approx 10^{-10}$ m/cycle). The fracture surfaces of samples resulting from both methods are observed. The fracture surface of the ASTM sample in the near threshold region, (C), is smooth, while the surface of constant K_{max}-increasing K_{min} method (D) is rough. The fracture surface of the ASTM sample is probably smoothed by contact between the fracture surfaces. It means that the ASTM method will not reach a crack closure free situation. This is in agreement with the higher ΔK_{th} compared with that of the constant K_{max} method, although the difference between these threshold values is small.

Note that a stepwise crack growth is observed in some parts of the fatigue curve for both methods. Crack propagation is probably delayed by grain boundaries. It takes about 30000 cycles to cross a boundary. The crack growth then restarts and grows over a distance in the order of 4 μm until the next boundary is reached, see figure 6.18. The material consists of grains with a length of 200 μm, a width of 80 μm (in crack growth direction) and a thickness of 20 μm, see figure 6.19 [26]. The observed stepped crack advance of 4 μm is much smaller than the grain width. The crack front does not grow in every cycle over the whole cross section, but grows locally, see figure 6.18. This stepwise crack growth behaviour differs from that in the Paris region.

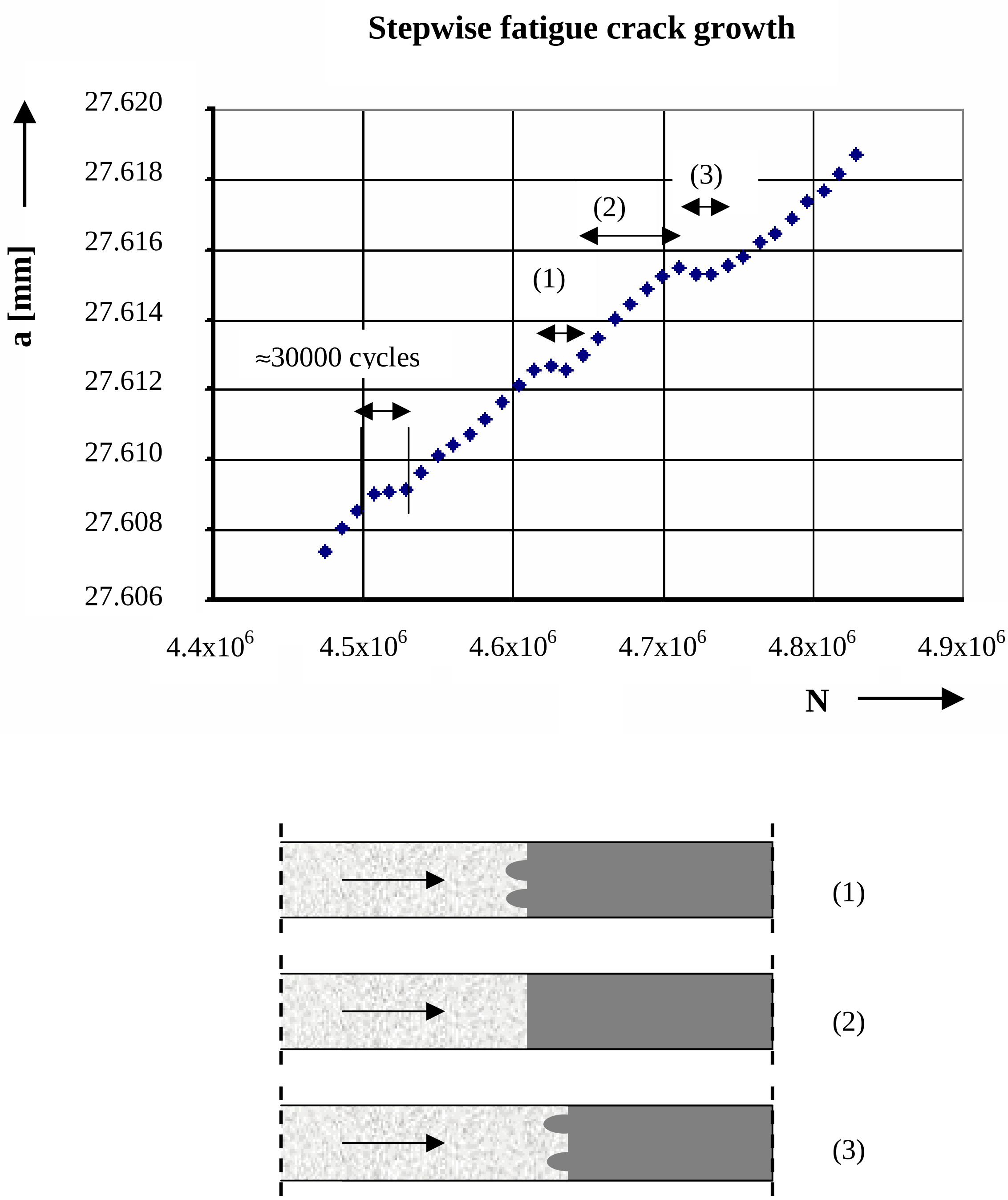

Figure 6.18. a-N plot showing plateaus at very low crack growth rates. Crack propagation is probably delayed by grain boundaries (1). It takes about 30000 cycles to cross a boundary (2). Crack growth then restarts until the next boundary is reached (3).

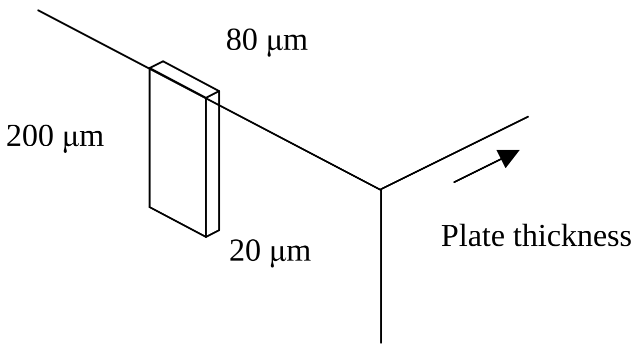

Figure 6.19: Grain size and orientation.

6.8 Discussion and conclusions

Two threshold parameter requirements

In the unified approach to fatigue it suffices to use two threshold parameters, i.e. K_{max}^* and ΔK_{th}^*. The two threshold parameter requirements can be simply calculated from the measured combinations of ΔK_{th} and R. It is shown that if these requirements are not satisfied, no crack propagation will occur in AA 5083.

Only two tests are enough to find the parametric thresholds below which no crack propagation takes place. The K_{max}^* requirement, with a value ≥ 2.2 MPa√m, is found using the ASTM procedure at R = 0 (i.e. $\Delta K = K_{max}$). The other requirement, the ΔK_{th}^* with a value ≥ 1.1 MPa√m, is found using the constant K_{max}-increasing K_{min} method.

ASTM threshold values affected by crack closure

Threshold values have been measured by means of the ASTM method and the constant K_{max}-increasing K_{min} procedure. Results found by using the ASTM method at higher R values, do not agree with data generated by the constant K_{max}-increasing K_{min} method. The difference in threshold values obtained is believed to be the consequence of crack closure near the crack tip. Scanning electron microscopy is used to study the resulting near threshold crack surfaces for both testing methods. The observed smooth fracture surface, obtained in the ASTM specimen, contrasts with the rougher crack surface for the constant K_{max}-increasing K_{min} method sample. A smooth fracture surface suggests contact between crack surfaces, whereas a rough surface indicates a crack closure free situation. This strongly supports the assumption that the ASTM threshold values are affected by some form of crack closure, even at high load ratio.

Two methods: dissimilar conditions near the crack tip

An important question at this point is whether crack growth in the threshold region for an ASTM test at higher R values is limited by the applied ΔK. If this is so, the question arises what is causing the crack closure at high R?

Two options are examined in the following section: the influence of the environment and crack opening values near the threshold.

Measurements in the Paris region, made under varying environmental conditions, demonstrate the sensitivity of crack growth to the environment, see Chapter 4. Results of test series made in the threshold region, using the constant K_{max}-increasing K_{min} method with dK_{min}/da as a variable, showed no difference in the resulting combination of R_{th} and ΔK_{th}. Environmental influence in the tested range (dK_{min}/da = 0.25-1 MPa$\sqrt{m}$/mm) is unlikely. The environmental effect is either the same or absent, since tests with different K_{max} values and different increasing rates of the K_{min}, result in identical threshold values. In case of the ASTM procedure, the crack tip is exposed to the environment for a longer period of time, compared to the faster constant K_{max} - increasing K_{min} method.

For example the ASTM method needs $25 \cdot 10^6$ cycles while the K_{max} - increasing K_{min} method spends $5 \cdot 10^6$ cycles to find the same ΔK_{th}. Presumably, a time-dependent, but a K_{max} independent mechanism, is involved. This time dependent mechanism may be more pronounced in the ASTM method, considering the different crack surfaces of the ASTM- and the constant K_{max} - increasing K_{min} samples.

The possibility of contact between two fracture surfaces, due to for example surface roughness, depends on the degree of closing of the crack. The possibility of contact in case of a low crack tip opening value is larger than in case of a high opening value. The difference in threshold values of the two applied test methods can probably be explained by a difference of crack tip opening values. For this reason the $CTOD_{min,ASTM}$ and $CTOD_{min,CKmax}$ values near the threshold value are calculated, using equation 6.8. The absolute values are small: the $CTOD_{min}$ values are about 0.5 and 1 µm for the ASTM procedure and the K_{max} - increasing K_{min} method respectively.

This means that the crack tip opening in case of the ASTM method is almost half of that of the constant K_{max} - increasing K_{min} method. Due to a constant K_{max} and an increasing K_{min}, the $CTOD_{min}$ value in case of the K_{max} - increasing K_{min} method increases during crack propagation. This value decreases in case of the ASTM procedure because of a gradual decrease of both K_{max} and K_{min}.

The ASTM E 647 procedure versus the constant K_{max} - increasing K_{min} method

An advantage of the time consuming ASTM procedure is the possibility to measure threshold values for a range of fixed R values, which is impossible in case of the constant K_{max} - increasing K_{min} method. However, in case of the ASTM method, crack arrest occurs not simply as a result of the low ΔK, but probably by a crack closure mechanism.

The constant K_{max} - increasing K_{min} method is suitable to measure crack closure free and thus possibly the true effective threshold value. However, the test method is not able to determine threshold values at lower R. Crack arrest occurs when the crack driving force ΔK becomes equal to ΔK^*. At higher K_{max} values, a crack closure free situation can be realized. Consequently, in contrast to the ASTM procedure, threshold values at higher R are not sensitive to the method of testing.

Probably in the threshold region a combination of mechanisms is operative in the damaged zone around the crack tip, depending on the interaction between loading system, material properties and environmental conditions. Even a combination of both testing procedures and two fatigue approaches are not sufficient to understand the fatigue crack growth in the threshold region properly, due to a lack of observable evidence. Which testing procedure is better is not a question of judgment since only partly comprehended mechanisms are involved.

References

[1] ASTM E 647, *Standard test method for measurement of fatigue crack growth rates*, American Society for Testing and Materials, Philadelphia, PA, USA, 2000

[2] M. Skorupa, *Load interaction effects during fatigue crack growth under variable amplitude loading – A literature review.* Part I: Empirical trends, Fatigue and Fracture of Engineering Materials and Structures, Volume 21, pages 987-1006, 1998

[3] G.H. Bray, *Effect of artificial aging on the fatigue crack propagation resistance of 2000 series aluminium alloys*, International Journal of Fatigue, Volume 23, pages 265-276, 2001

[4] J. Petit, *Some aspects of near-threshold crack growth: Micro-structural and environmental effects*, Proceedings of the international symposium on fatigue crack growth threshold concepts, Pennsylvania, October 3-5, 1983

[5] M.A. Moshier, T. Nicholas, B.M. Hillberry, *Load history effects on fatigue crack growth threshold for Ti-6Al-4V and Ti-17 titanium alloys*, International Journal of Fatigue, Volume 23, pages 253-258, 2001

[6] S.E. Stanzl-Tschegg, H. Mayer and A. Stich, *Variable amplitude loading in the very high-cycle fatigue regime*, Fatigue and Fracture of Engineering Materials and Structures, Volume 25, pages 887-896, September 2002

[7] M. Papakyriacou, H. Mayer, U. Fuchs, S.E. Stanzl-Tschegg, R.P. Wei, *Influence of atmospheric moisture on slow fatigue crack growth at ultrasonic frequency in aluminium and magnesium alloys*, Fatigue and Fracture of Engineering Materials and Structures, Volume 25, pages 795-804, September 2002

[8] S. Suresh, *Fatigue of materials*, Cambridge University press, first edition, ISBN 0521578477, 1991

[9] B. Lü, X. Zhen, *Predicting fatigue crack initiation life of an aluminium alloy at low temperatures*, Fatigue and Fracture of Engineering Materials and Structures, Volume 15, pages 1213-1221, 1992

[10] R.I. Stephens, *Fatigue at low Temperatures*, ASTM STP 857, American Society for Testing and Materials, Philadelphia, PA, USA, 1985

[11] J. Petit, C. Sarrazin-Baudoux, G. Henaff, *An overview on environmentally-assisted fatigue crack propagation,* Proceedings of the 7th International Fatigue Congress, Beijing, China; 8-12 June 1999, pages 2221-2228, 1999

[12] R.W. Hertzberg, C.H. Newton, R. Jaccard, *Crack closure: correlation and confusion*, Mechanics of Fatigue Crack Closure, ASTM STP 982, Philadelphia, PA, USA, pages 139-48, 1988

[13] A.K. Vasudevan, K. Sadananda, N. Louat, *A review of crack closure, fatigue crack threshold and related phenomena*. Materials Science and Engineering, A1888, pages 1-22, 1994

[14] D. Kujawski, *A new* $(\Delta K^{+}\Delta K_{max})^{0.5}$ *driving force parameter for crack growth in aluminum alloys*, International Journal of Fatigue, Volume 23, pages 733-740, 2001

[15] C.R. Krenn, J.W. Morris Jr., *The compatibility of crack closure and* K_{max} *dependent models of fatigue crack growth*, International Journal of Fatigue, Volume 21, pages 147-155, 1999

[16] W. Elber, *Fatigue Crack Closure Under Cyclic Tension*, Engineering Fracture Mechanics, Volume 2, pages 37-45, 1970

[17] J.K. Donald, P.C. Paris, *An evaluation of* ΔK_{eff} *estimation procedure on 6061-T6 and 2024-T3 aluminum alloys*. International Journal of Fatigue, Volume 21, pages 47-57, 1999

[18] P.C. Paris, H. Tada, J.K. Donald, *Service load fatigue damage - a historical perspective*, International Journal of Fatigue, Volume 21, pages 35-46, 1999

[19] A.K. Vasudevan, K. Sadananda, N. Louat, *Reconsideration of fatigue crack closure,* Scripta Metallurgica et Materialia, Volume 27, pages 1673-8, 1992

[20] K. Sadananda, A.K. Vasudevan, *Analysis of fatigue crack closure and thresholds,* Fracture Mechanics, Volume. 25, pages 484-501, 1993

[21] A.K. Vasudevan, K. Sadananda, N. Louat, *Two critical stress intensities for threshold fatigue crack propagation*, Scripta Metallurgical et Materialia, Volume 28, pages 65-70, 1993.

[22] L. Lawson, E.Y. Chen, M. Meshii, *Near-threshold fatigue: a review,* International Journal of Fatigue, Volume 21, pages 15-34, 1999

[23] J.A. Newman, *The effect of load ratio on threshold fatigue crack growth of aluminium alloys*, Dissertation, Blacksburg, Virginia, 2000

[24] W. He, *Fatigue crack growth threshold behaviour of Aluminium Alloy 5083*, Master Thesis, TU Delft, Delft, 2004

[25] M. Janssen, J. Zuidema and R.J.H. Wanhill, *Fracture Mechanics*, ISBN 90-407-2221-8, Second edition, 2002

[26] S.M. Benedictus-de Vries, *Corrosion Fatigue of Welded AA 5083 in Seawater*, ISBN 90-771-7214-9, Dissertation, Delft, 2005

Chapter 7
General Discussion and Conclusions

7.1 Introduction

This dissertation deals with fatigue crack growth of aluminium alloys: from threshold to instability. The main objective of this research is to contribute toward a deeper understanding of the fatigue phenomenon.

Extensive investigations have been performed in order to find R dependent closure functions, see Chapter 3. The formation of shear lips has been manipulated (Chapter 4). In Chapter 5, fatigue crack paths have been forced in a pre-described direction and threshold values are measured using the standard method and an alternative test procedure, see Chapter 6. The main findings are presented separately in these chapters.

The outcomes of some experimental results are in contradiction with the conventional fatigue concept. Therefore a general discussion and some conclusions are presented in this chapter covering the following themes: crack closure, shear lips and ΔK-threshold.

7.2 Crack Closure

7.2.1 The classic fatigue approach and stress ratio effects

In the classic fatigue approach, the cyclic stress intensity range ΔK is considered to be the most important fatigue driving force. A major advance in understanding stress ratio effects was made by Elber's introduction of the crack closure concept in 1971. Crack closure rationalizes load ratio effects by allowing for the effects of residual plastic deformation and the resultant residual compressive stresses acting on the crack flanks near the tip of a growing fatigue crack. In this approach, the shift of fatigue curves to higher ΔK levels for lower R values is the result of crack closure.

Crack closure has generally been accepted for more than thirty years as a crucial retardation mechanism in fatigue crack growth, and the concept is successful applied to a wide range of fatigue data. It has become the customary interpretation of stress ratio and transient loading effects and has been applied to many fatigue life prediction models. However, some results found in this research, cannot be explained or are even in contradiction with the crack closure theory.

7.2.2 Fundamental problems with crack closure

Plasticity induced crack closure

In Chapter 3, crack closure relations for AA 5083 were discussed. The U formulae for the regimes investigated, namely the tensile mode regime and the growing shear lip regime, are about the same. Because of this, the difference in slope in log(da/dN)-log(ΔK) indicates that the different crack growth behaviour in the tensile and shear lip regimes cannot be explained from a different crack closure behaviour. However, the stress situation tends to change from plane strain to plane stress with increasing ΔK. It seems that the larger amount of plastic deformation in the wake of the crack has no influence on crack closure levels for this material.

It has been shown in Chapter 4, that introduction of (sharp) side grooves has no effect on the fatigue crack growth curve. da/dN-ΔK results obtained from tests on AA 5083 specimens with or without side grooves are about the same. Also a partial side groove does not lead to a change in the fatigue crack growth curve. It means that elimination or removal of a substantial part of the plane stress plasticity induced crack closure, namely at the crack surfaces , does not lead to any effect on da/dN or ΔK_{eff}. However, based on the crack closure approach, a change in the fatigue crack growth behaviour is to be expected.

Shear lips

Shear lips are usually associated with plane stress conditions at the surface and are thought to introduce large surface roughness effects. The plastic deformation is larger for the shear lip part of the fatigue crack than for the tensile mode part in the middle of the specimen. In the unloading part of the fatigue cycle, shear lips are supposed to be the first part where matching crack surfaces will touch causing crack closure. It has been shown in Chapters 4 and 5, that side grooves suppress the development of shear lips. However, this have no effect on the da/dN-ΔK relation. In lab air, transition point T3, see figure 4.7, takes place at about the same crack growth rate for all measured R values, thus with and without side grooves.

Roughness induced crack closure, found in AA 2024 at higher frequencies, can also be prevented by side grooves, see Chapter 5. However the T3 transition takes place at the same crack growth rate and no shift of the fatigue curve is observed. This means that rough shear lips formed on the fracture surface of AA 2024 add extra crack closure without any effect on R.

Direct crack closure measurements

Crack closure levels have been measured by using two methods, namely: 1) direct crack closure measurements and 2) the crack growth rate method on centre-cracked tension, compact tension and single edge-notched bend specimens, see Chapter 3.

In the case of direct crack closure measurements, a series of centre-cracked tension specimens were pre-fatigued until a certain crack growth rate was reached and subsequently compact tension and single edge-notched bend specimens were cut out of the original centre-cracked tension specimens. By doing this, the loading history and thus the crack tip conditions are largely the same for all geometries. Direct crack closure measurements were performed on each geometry, while specimens were prevented from fatigue crack growth. In spite of differences in geometry, the same closure point was expected for all tested geometries because of the same loading history. However, these measurements showed different crack closure points in the (stabilized) shear lip regime for centre-cracked tension and single edge-notched bend specimens. This means that crack closure is not well defined and the results of measurement depends on the place of measurement and the specimen geometry.

Besides these direct crack closure measurements, fatigue tests were performed on each geometry. Different U values were found for centre-cracked tension and single edge-notched bend specimens. This difference in U can be explained by crack opening angles: crack opening angles are different for different geometries. Since the faces have contact at a finite distance from the crack tip, the part of the loading cycle at which the crack is opened, is larger for a specimen with a larger compliance, i.e. a larger crack opening.

Two driving forces: ΔK and K_{max}

The classic crack growth rate method essentially compares the ΔK values for different R-values at corresponding crack growth rates. ΔK values, i.e. the driving forces for fatigue crack growth, are fitted into one scatter band using an R-dependent U formula, where $\Delta K_{eff} = U\Delta K = UK_{max} - UK_{min}$. A major limitation is the impossibility to account for the observed role of K_{max}. The influence of K_{max} is not taken into account since U works on both K_{max} and K_{min} in this formula.

However, according to the unified approach described in Chapter 6 crack advance only occurs for $\Delta K > \Delta K^*$ and $K_{max} > K_{max}^*$. Some cracking mechanisms are directly K_{max} dependent. It is found in the constant K_{max} - increasing K_{min} tests that as long as K_{max} is larger than a critical threshold value K_{max}^*, variation in K_{max} has no influence on ΔK_{th}. Therefore a better approach for the threshold region would be: $\Delta K_{eff} = K_{max} - UK_{min}$. Then, the effective crack tip opening can be calculated from the real applied K_{max} and UK_{min}, which is $K_{closure}$, and U attains a physical meaning.

Similitude approach

Fatigue crack growth data for AA 5083 specimens with and without side grooves are comparable, which means that in both cases, according to the similitude approach, a "similar" ΔK_{eff} was applied. However, different crack fronts were observed: a straight line in the case of side grooved specimens and a growing shear lip for specimens without side grooves. The crack tip conditions are evidently dissimilar. In addition, a different plane strain-plane stress situation can be expected. The growing shear lip leads to a mismatch between the two crack surfaces and thus to crack closure caused by surface roughness effects. In spite of this, the same fatigue crack growth curve is measured for AA 5083 specimens with suppressed and normal growing shear lips.

Direct crack closure measurements on three different geometries with similar crack tip conditions proved that even these similar conditions are not sufficient for measuring unique closure points close to the crack tip.

It seems that there are some fundamental problems: a stress state which is more plane strain does not lead to a difference in measured da/dN-ΔK, the fatigue crack growth curves of specimens with dissimilar crack tip conditions in case of (partial) suppressed shear lips are the same and direct crack closure measurements on specimens with unique crack tip conditions, show different closure points. Because of these uncertainties in conventional models, da/dN-Δ

K_{eff} relations found in laboratories on standard specimens, cannot apply directly to lifetime prediction models for actual structures.

7.3 Shear Lips: an environmental effect?

The start of the shear lip in normal lab air, at transition point T3, takes place at about the same crack growth rate for all measured R values, thus with or without closure, see Chapter 4.

It is remarkable that shallow scratches are sufficient to suppress the development of shear lips. Furthermore, the change in crack growth rate as a function of ΔK at transition point T3, which is normally coupled to the start of the shear lip development, occurs even when the shear lip is (partially) suppressed. Since the da/dN-ΔK relation for a suppressed shear lip does not differ from that of a developing smooth shear lip, the change in slope of the fatigue crack growth rate curve, can no longer be attributed to the start of the growing shear lip.

The effect on the da/dN-ΔK relation in the Paris region of different environments is known. A more aggressive environment, e.g. seawater, leads to a shift of T3 to a higher ΔK, while an opposite effect is observed for experiments performed in an inert shielding gas such as dry argon. This means that an environmental effect must be involved and only this environmental effect is responsible for the transition point.

Tests on specimens with and without side grooves and experiments in different environments and at different temperatures indicate that the shear lip development is the result of an environmental effect.

7.4 ΔK-threshold

7.4.1 ASTM threshold values affected by crack closure

Threshold values have been measured according to ASTM standard E 647 and to the constant K_{max}-increasing K_{min} method. Results found by using these two methods do not agree. The difference in threshold values is believed to be the consequence of dissimilar conditions near the crack tip.

Scanning electron microscopy has been used to study the resulting crack surfaces formed near threshold for both testing methods. The observed smooth fracture surface, obtained in the ASTM E 647 specimens, contrasts with the rougher crack surface for the constant K_{max}-increasing K_{min} sample. A smooth fracture surface suggests contact between crack surfaces whereas a rough surface indicates a crack closure free situation. The micrographs strongly support the assumption that some form of crack closure, even at high load ratio, is present in the ASTM specimen and affects the threshold values found.

The observed crack closure can probably be explained by a difference of crack tip opening values. The minimum CTOD values are small: 0.5 and 1 μm for the ASTM procedure and the K_{max} - increasing K_{min} method respectively. This means that the crack tip opening in case of the ASTM is almost half compared to the constant K_{max} - increasing K_{min} method.

7.4.2 The constant K_{max}-increasing K_{min} method versus the ASTM E 647 procedure

Crack arrest in the threshold region does not occur simply as a result of a low applied ΔK, but is probably influenced by a complex environmental/crack closure mechanism, see Chapter 6. Because of anomalous test results, the ASTM E 647 procedure for measuring threshold values is under debate. Since threshold values at high load ratio, where $R>R_c$ are sensitive to the method of testing, the

ASTM method can probably no longer be used to measure unique threshold values.

The constant K_{max}-increasing K_{min} method is suitable to determine crack closure free and thus possibly the intrinsic threshold value. However, the test method is not applicable to determine threshold values at lower R. Crack arrest occurs when the driving force represented by ΔK, due to a fixed K_{max} and increasing K_{min}, becomes less than the ΔK^* . At higher K_{max} a crack closure free situation can be realized. Consequently, in contrast to the ASTM procedure, threshold values at higher R are not sensitive to this method of testing.

However, even a combination of both testing procedures is not sufficient to understand the fatigue crack growth in the threshold region properly, due to a lack of observable scientific evidence. Which testing procedure is better cannot be judged, since only partly comprehended mechanisms are involved.

Defining an intrinsic threshold value is only possible with respect to the environment, since a combination of mechanisms is operative in the damage zone around the crack tip, depending on the interaction between loading system, material properties and environmental conditions.

7.5 Crack closure and environment

The appearance of a crack surface is, in general, affected by the environment and/or plasticity. For example, tests on AA 2024 proved clearly that the absence of lab air leads to a rougher crack surface and to a change in crack growth rate. This crack growth retardation is explained by the classic term “crack closure”: the crack closes due to the reduction in stress after maximum load, crack face contact occurs in the wake of the crack tip before zero load is reached, thus lowering the cyclic stress intensity by decreasing the interval where the crack tip feels tensile stresses. In this view, the shifting of fatigue curves to higher ΔK levels, i.e. the R effect, is the result of crack closure.

Crack closure is a general (mechanical) term, comprising effects on the material, in particular on the crack surface, like oxide formation, roughness effects, plastic deformations and phase transformations.

It is shown in Chapter 4 that reducing plasticity at the surface by implementing (partial) side grooves does not lead to a change or a shift in the fatigue crack growth rate curve. Furthermore, it has been shown that crack closure cannot be directly responsible for the transition points T3 and T4. The start of the shear lip, at transition point T3, takes place at about the same crack growth rate in lab air for all measured R values, thus with and without closure. A dramatic change in the environment leads to a large change of transition point T3 and only to a small shift of the whole fatigue curve. These changes are related to the impact of environment on the material.

Probably environmental mechanisms are responsible for the characteristic shape of, and R effects on, the fatigue curve for AA 5083. The appearance of the crack surface, normally identified as crack closure, is the result of these mechanisms. Therefore crack closure can be regarded as a second order effect. If so, the influence of crack closure on fatigue crack growth cannot be properly accounted for, unless these "supposed" crack closure effects and the associated appearance of the crack surface are explicitly recognized as the result of environmental impact on the material.

7.6 Conclusions

The main conclusions of this research are summarized below:

- The crack closure relations obtained by similitude for the tensile mode regime and the growing shear lip regime in AA 5083 are almost identical, namely $U=0.79+0.40\ R+0.04\ R^2$ and $U=0.81+0.37\ +0.02\ R^2$ respectively.

- Because the U functions are almost the same in both regimes, the differences in crack growth behaviour in the tensile and shear lip regimes cannot be attributed to differences in crack closure behaviour.
- Linear side grooves with a depth of 100 μm over the full width of centre-cracked tensile specimens suppresses the formation of shear lips during fatigue crack growth.
- Constant amplitude tests on centre-cracked tensile specimens of AA 5083 with shear lips and suppressed shear lips show the same da/dN–ΔK results. Therefore the growing shear lip cannot be responsible for the slope change in log(da/dN)-log(ΔK).
- The da/dN-ΔK curves in frequency sensitive AA 2024 at higher frequencies with suppressed shear lips, are identical to those at a low frequency.
- Since the development of shear lips is not the cause for the gradually changing slope of the log(da/dN)-log(ΔK) curve, transition point T3 can probably be attributed to an environmental assisted crack growth mechanism. Results show a strong dependency on the absolute amount of moisture.
- The lower slope in log(da/dN)-log(ΔK) between T3 and T4 is caused by a time dependent corrosion crack growth mechanism that gradually loses effectiveness because of a higher crack growth rate. Below T3 the corrosion mechanism is fully operative, while above T4 the enhanced mechanism is no longer effective.
- Tests on specimens with and without side grooves and experiments in different environments and at different temperatures indicate that shear lip development is the result of an environmental effect.
- Results found by using the ASTM method at higher R values, do not agree with data generated by the constant K_{max}-increasing K_{min} method.

The difference in threshold values obtained is believed to be the consequence of crack closure near the crack tip.

- The ASTM threshold values are affected by some form of crack closure, even at high load ratio.
- The constant K_{max}-increasing K_{min} method is suitable to determine the crack closure free threshold value.

7.7 Future development

Far-reaching changes have taken place in the last few years in the field of fatigue at the level of materials, measurement techniques and computer simulations. This progress has led to a deeper understanding of the fatigue process. As a consequence some standard testing methods are under pressure, because experimental results are inconsistent with established theories.

New or highly improved applications demand the development of economically attractive new engineering materials and processing technologies; examples include the development of complex laminated structural materials such as Glare and Zappi. Another example of a new category of materials is self-healing materials, using advanced (chemical) mechanisms to reduce microscopic damage in case of cracking. The general appearance of fatigue and failure mechanisms of these materials differs from “classic” material behaviour.
Advanced Finite Element Method calculations are used to determine the material response on cyclic loading and to simulate crack advance.
Advances in existing measurement techniques and development of new characterisation technology have led to a better understanding of the sensitivity of materials to damage under cyclic loading. However, the experimentally observed correlation between crack growth rate da/dN and cyclic stress intensity

ΔK cannot yet be adequately reproduced over a larger stress intensity range by FEM models.

Fatigue approach

For environmental, safety and economical reasons, the development of accurate fatigue life prediction models is essential. However, the fatigue process from initiation to failure is not completely understood. Even advanced parameters, theories and computer simulations are not able to describe the complex process properly. Since the fatigue process is not completely understood from a theoretical point of view, it cannot be modelled in a physically relevant manner.

New damage parameters need to be found in order to characterize the fatigue behaviour of structural materials adequately. Evidently, the development of new and improved measurement techniques is a key component of the strategy to increase the knowledge of the cyclic damage process. Some effects on fatigue cannot be properly accounted for unless the contribution of the environment is explicitly recognized as a driving force. A reformulation of the fatigue process, probably in terms of a "damage zone" including environmental effects, is needed to describe the fatigue process more accurately.

In general, well-formulated theories provide unification and show how apparently unrelated phenomena are aspects of the same effect. In spite of this, no theory by itself can prove anything. The final proof comes from the combination of experiment and observation. Theory should make sense of the experimental data.

Evidently, the development of new and improved measurement techniques is a key component of the strategy to increase the knowledge of the cyclic damage process. This demands the development of new tests.

The proposed tests must allow measuring of a number of (partly new) parameters in a configurable test environment. Parameters and measurement techniques should include: crack length (potential drop, laser technique, optical scanning); failure characteristics (acoustic emission, heat dissipation, infrared technique); stresses, displacement (extensometers); temperature, humidity, pressure (environment control system); load and frequency (mechanical control system).

This innovative and exceptional test will involve high experimental demands. An extensive range of measurement equipment must be available in order to monitor several parameters at the same time within one cycle during non-standard test scenarios. The mechanical control system must offer a smooth control, sensors and software must support a high accuracy, and fast data acquisition and processing is required to manage acquired signals simultaneously. Monitoring all parameters at the same time is important because changing one parameter will often lead to changes in others.

In addition, the development of a cycle-by-cycle approach instead of considering average crack growth over a range of cycles, is an important challenge facing fatigue research and engineering practice in the near future.

Dankbetuiging

Dit proefschrift was er nooit gekomen zonder de hulp en support van collega's, studenten, vrienden en familie. In de loop van de tijd zijn er heel veel mensen betrokken geweest bij het onderzoek, waarvoor dank.

Er zijn een aantal personen die ik speciaal wil bedanken.
In de eerste plaats Jan Zuidema, voor zijn dagelijkse begeleiding en optreden als copromotor. Bedankt voor alle jaren van coaching en begeleiding, voor alle discussies, zowel vakinhoudelijke als politieke, en voor de talloze malen dat je publikaties en concepten hebt doorgenomen en deze even zovele malen hebt voorzien van commentaar.
Daarnaast Fred Veer, die in hoge mate heeft bijgedragen aan het proefschrift. Fred, de afgelopen 15 jaar waren enerverend en leerzaam. Ik heb je eerst leren kennen als docent, daarna als afstudeerbegeleider, vervolgens als initiator en medebegeleider van het onderzoek. En later, op de faculteit Bouwkunde, een aantal jaren als collega en leidinggevende. In al die jaren heb ik veel van je geleerd, niet alleen in wetenschappelijk opzicht, maar ook op het gebied van lesgeven, publiceren, presenteren, toetsen, coaching, organisatie en dan heb ik nog niet alles genoemd. Bedankt hiervoor, het was een prachtige tijd die en te kort duurde en bovendien veel te snel voorbij is gegaan.
Verder dank aan Theo van Soest, voor zijn niet aflatende hulp bij het oplossen van onmogelijke technische problemen. Theo, je enthousiasme en humor waren ongeëvenaard, waardoor het uitvallen van een vermoeiingsmachine soms zelfs iets feestelijks kreeg.
Ook Weihong He, die als afstudeerderster bij het onderzoek betrokken is geweest, wil ik bedanken. Ik heb meer van jou geleerd dan andersom. Bedankt voor de prettige tijd.

Ad Bakker die aanvankelijk als promotor heeft opgetreden en Ian Richardson, die in de finale fase promotor is geweest, wil ik bedanken.
Michael Janssen dank ik voor alle discussies en zijn bijdrage in de laatste fase van de totstandkoming van het proefschrift. Ton Riemslag bedank ik voor de begeleiding aan het begin van het onderzoek. Alle practikanten die hebben meegedraaid in het onderzoek: bedankt voor jullie bijdrage.
Mijn kamergenoten Nancy Kuipers en Mariya Lonyuk, jullie bedankt voor alle gezelligheid. Anneke van Veen bedank ik voor al het secretariële werk en alle leden van de vakgroep waarin ik werkzaam ben geweest bedank ik voor jullie collegialiteit.
Ook ben ik dank verschuldigd aan iemand uit de bouwkundetijd die niet bij dit onderzoek betrokken is geweest: Rien van der Voorden. Onder zijn leiding kreeg ik de kans ervaring op te doen met natuurwetenschappelijk onderzoek en hij heeft mij de liefde voor de bouwfysica bijgebracht, iets wat nooit meer is overgegaan.

De kinderen Arie, David en Esther: ik vond het fijn dat jullie af en toe de computer aan mij afstonden om aan het proefschrift te werken. Maar ook zag ik in jullie ogen hoe teleurgesteld jullie waren als ik in vakanties weer aan het proefschrift ging werken, in plaats van met jullie wat te gaan ondernemen. Hierbij een belofte, zwart op wit: dit gaan we inhalen.
Beste Karin, dame, je was vaak ongeduldig maar altijd vol vertrouwen. Jij zag het onderzoek als een project, ik zag het meer als een levenswijze. Later draaide dit om: ik zag het als een project en jij had je neergelegd bij de levenswijze. Bedankt voor je soms ongebreidelde commentaar maar ook voor je niet aflatende support, het was me een waar genoegen!

List of relevant publications

Journal papers

F.A. Veer, J. Zuidema, A.C. Riemslag, and C. van Kranenburg, *Mode II fatigue failure in transparent adhesive joints*, Physicochemical mechanics of materials, Volume 38, Jan-Feb 2002

C. van Kranenburg, A.C. Riemslag, J. Zuidema, S. Benedictus-De Vries and F.A. Veer, *Crack closure and fatigue threshold of AA5083 in air and seawater by two determination methods*, Physicochemical Mechanics of Materials, Volume 37, no 6, National Academy of Sciences of Ukraine, Ukraine, Nov-Dec 2001

J. Zuidema, F.A. Veer and C. van Kranenburg, *Shear lips on fatigue fracture surfaces of aluminium alloys,* Special Issue of “Fatigue and Fracture of Engineering Materials and Structures” (FFEMS), Volume 27, issue 7, pages 15, Prof. Andrea Carpinteri, University of Parma, Parma, Italy, 2004

Conference proceedings

C. van Kranenburg, A.C. Riemslag, S. Benedictus-de Vries, J. Zuidema, and F.A. Veer, *Plane stress and plane strain in side-grooved CCT-specimens*, 10th International Conference on Fracture, Honolulu, USA, Dec 2001

J. Zuidema, C. van van Kranenburg, A.C. Riemslag, F.A. Veer and S. Boljanovic, *Anomalous fatigue crack growth behaviour in AA 2024 and AA*

5083, Proceedings of Materials Structures and Micromechanics of Fracture, Brno, Czech Republic, 2001

F.A. Veer, S. Benedictus-de Vries and C. van Kranenburg, *Fracture control of glass through lamination*, 10th International Conference on Fracture, Honolulu, USA, Dec 2001

C. van Kranenburg, J. Zuidema, Y. Uematsu, H.M. Nykyforchyn and F.A. Veer *Crack closure in AA 5083*, Proceedings of the Eighth International Fatigue Congress, vol. IV, pages 2353-2360, Stockholm, Sweden, June 2002

J. Zuidema, C. van Kranenburg, Y. Uematsu and F. Veer *A Crack Closure Correction Model for Restoring Similitude between the Increasing Load Amplitude Test and the Conventional Constant Amplitude Test*, 14th European Conference on Fracture, vol. III, pages 649-656, Krakow, Poland, September 2002

F.A. Veer, A. Van den Berg, M.M.A. van der Sluijs, J. Zuidema and C. van Kranenburg, *The strength of glass,* 14th European Conference on Fracture, vol. III, pages 503-510, Krakow, Poland, September 2002

C. van Kranenburg, J. Zuidema, B. Lonyuk, B and F.A. Veer, *Fast delta threshold measurement: Investigation of boundary conditions*, In Bodner, SR (Ed.), Proceedings of the 9th International Conference on the Mechanical behaviour of Materials, ICM9, Geneva, Switzerland, May 25-29, 2003

J. Zuidema, C. van Kranenburg, H.M. Nykyforchyn, B. Lonyuk and F.A. Veer, *Effect of specimen geometry on fatigue crack growth in Al alloy AA 5083,* In Bodner, SR (Ed.), Proceedings of the 9th International Conference on the

Mechanical behaviour of Materials, ICM9, Geneva, Switzerland, May 25-29, 2003

C. van Kranenburg, J. Zuidema and F.A. Veer, *Forced crack path deviation,* In Carpinteri, A (Ed.), Proceedings of the International Conference on Fatigue Crack Paths (FCP 2003), (CD ROM), pages 1-6, Parma, Italy: University of Parma, September 18-20, 2003

J. Zuidema, F.A. Veer and C. van Kranenburg (Invited lecture), *Square and slant crack growth in (thin) sheets,* In Carpinteri, A (Ed.), Proceedings of the International Conference on Fatigue Crack Paths (FCP 2003), (CD ROM), pages 1-15, Parma, Italy: University of Parma, September 18-20, 2003

C. van Kranenburg, W. He, J. Zuidema and F.A. Veer; *Influence of measurement method on fatigue crack growth threshold,* Proceedings of The 15th European Conference of Fracture (ECF 15), (CD ROM), Stockholm, Sweden, August 11-13, 2004

C. van Kranenburg, F.A.Veer, and J. Zuidema, *Threshold measurements,* In Carpinteri, A (Ed.), Proceedings of the International Conference on Fatigue (ICF 9), 9th International Fatigue Congress, Atlanta, USA, May 14-19, 2006

C. van Kranenburg, F.A.Veer, and J. Zuidema, *The relation between shear lips and crack closure,* Proceedings of the International Conference on Fatigue (ICF 9), 9th International Fatigue Congress, Atlanta, USA, May 14-19, 2006

Symposia

C. van Kranenburg, A.C. Riemslag, J. Zuidema, S. Benedictus-de Vries and F.A. Veer, *Crack closure dependence of long crack fatigue thresholds of AA5083 in air and seawater using two delta thresholds measurement methods*, Actual problems of materials mechanics: physicochemical aspects and diagnostics of materials properties, Materials of International Symposium, Lviv, Ukraine, June 2001

J. Zuidema, C. van Kranenburg, F.A. Veer, A.C. Riemslag, *A calculation of fatigue crack growth in all alloys after blocks of underloading*, Actual problems of materials mechanics: physicochemical aspects and diagnostics of materials properties, Materials of International Symposium, Lviv, Ukraine, June 2001

F.A. Veer, J. Zuidema, A.C. Riemslag, C. van Kranenburg, *Mode II fatigue crack growth of transparent adhesive joints*, Actual problems of materials mechanics: physicochemical aspects and diagnostics of materials properties, Materials of International Symposium, Lviv, Ukraine, June 2001

Reports (in Dutch)

F.A. Veer, J. Zuidema, C. van Kranenburg , Y. Franchimon , J.B. Scheepmaker, *Onderzoek naar Crack Closure bij vermoeiing van aluminium 5083*, rapport aan derden (CORUS), Delft, oktober 2000

F.A. Veer, J. Zuidema, C. van Kranenburg, J.M. Heijnis, S. Verweij, *Onderzoek naar de verschillende invloeden op de scheurgroeisnelheid bij vermoeiing van AA 2036 T4*, rapport aan derden (NIMR), Delft, mei 2001

J. Zuidema, F.A. Veer, M.J. Tenpierik, C. van Kranenburg, *Onderzoek naar verschillende invloeden op de scheurgroeisnelheid bij vermoeiing van AA 2024*, rapport aan derden (CORUS), Delft, oktober 2001

J. Zuidema, F.A. Veer, C. van Kranenburg, C. Rietdijk, M. Den Boon, *Onderzoek naar de invloed van corrosie op de scheurgroeisnelheid bij vermoeiing van AA5083*, rapport aan derden (CORUS), Delft, januari 2002

J. Zuidema, F.A. Veer, C. van Kranenburg, R. Van der Linden, D.I. Zwaal, *Onderzoek naar vermoeiing van AA2024 en AA5083,* rapport aan derden (CORUS), Delft, mei 2002